3D NAPHTHALENE AND PERYLENE DIIMIDE DERIVATIVES AS NON-FULLERENE ACCEPTORS FOR ORGANIC SOLAR CELLS

A Thesis

Presented to

The Academic Faculty

by

Xiaochu Ba

In Partial Fulfillment

of the Requirements for the Degree

Master of Science in the

School of Chemistry and Biochemistry

Georgia Institute of Technology

December 2016

3D NAPHTHALENE AND PERYLENE DIIMIDE DERIVATIVES AS NON-FULLERENE ACCEPTORS FOR ORGANIC SOLAR CELLS

Approved by:

Dr. Seth R. Marder, Advisor
School of Chemistry and Biochemistry
Georgia Institute of Technology

Dr. John R. Reynolds, Advisor
School of Chemistry and Biochemistry
Georgia Institute of Technology

Dr. Stefan France
School of Chemistry and Biochemistry
Georgia Institute of Technology

Date Approved: December 9th, 2016

To my family

ACKNOWLEDGEMENTS

Throughout the two years and half graduate study at Georgia Tech, I was very fortunate to be co-advised by Professor Seth Marder and Professor John Reynolds. I really thank their supports and advices during my graduate career. I was lucky to have the opportunity to work between two groups, it was great time.

I had the best mentors, Dr. Kostiantyn Ziabrev for my thesis projects and Dr. Reddy Dasari for the rotation program at Marder group during my first year. I have learned advanced organic chemistry techniques from them, and I was so lucky to have the opportunity to closely work with these two experienced synthetic chemists, to learn how they handle difficulties during synthesis. I thank Dr. Yadong Zhang and Dr. Junxiang Zhang for helpful discussions and comments on synthetic chemistry. I also thank Dr. Stephen Barlow and Dr. Tim Parker for their help and support during the years.

I was fortunate to work with Dr. Kostiantyn Ziabrev, Rylan Wolfe, and Yeli Fan as a team on these 3D conjugated molecules. We not only shared materials, but also thoughts, skills, and tricks on how to synthesize and purify these molecules. I thank my collaborators, Dr. Shruti Agarkar and Dr. Marcel Said for their hard work on device fabrication and characterization, and Dr. Zilong Zheng and Dr. Veaceslav Coropceanu from Brédas group for density functional theory calculations.

Finally, I thank everyone else in Marder and Reynolds research group, we had good time. Especially to Kin Lo, Dr. Anna Österholm, Dr, Eric Shen, Matthew Cooper, Rebecca Hill, Dr. Hayden Black and Dr. Denise Bale. I appreciate the funding for this project from Office of Naval Research, and thank all members from Center for Advanced Organic Photovoltaics.

TABLE OF CONTENTS

LIST OF TABLES

LIST OF FIGURES

LIST OF SCHEMES

LIST OF ABBREVIATIONS

NFA	Non-fullerene acceptor
BHJ	Bulk heterojunction
$PC_{61}BM$	Phenyl-C_{61}-butyric acid methyl ester
$PC_{71}BM$	Phenyl-C_{71}-butyric acid methyl ester
D	Donor
A	Acceptor
DFT	Density functional theory
HOMO	Highest occupied molecular orbital
LUMO	Lowest unoccupied molecular orbital
vis.	Visible
NIR	Near infra-red
UV	Ultra-violet
OSCs	Organic solar cells
PCE	Power conversion efficiency
EQE	External quantum efficiency
J-V	Current density-voltage
EA	Electron affinity
IE	Ionization energy
CV	Cyclic voltammetry
CS	Charge separated
CT	Charge transfer
PDI	Perylene diimide
NDI	Naphthalene diimide
FF	Fill factor
ICT	Intermolecular charge transfer
Calc.	Calculated
HRMS	High resolution mass spectrometry
NMR	Nuclear magnetic resonance
DCM	Dichloromethane
DMF	*N*,*N*-Dimethylformamide
THF	Tetrahydrofuran
DSC	Differential scanning calorimetry
TGA	Thermogravimetric analysis
h	Hour
min	Minute
s	Second
mol	Mole
mmol	Millimole
g	Gram
mg	Milligram
PL	Photoluminescence
Abs.	Absorbance
equiv.	Equivalents
rt	Room temperature

eV	Electron volt
cm	Centimeter
cm^{-1}	Wavenumber
ITO	Indium-Tin oxide
nm	Nanometer
vs.	versus
LDA	Lithium diisopropylamide
M	mol/L
L	Liter
mL	Milliliter
NBS	*N*-Bromosuccinimide
BuLi	Butyl lithium
Hz	Hertz
TLC	Thin layer chromatography
SEC	Size exclusion chromatography

Other abbreviations are explained in the text.

LIST OF SYMBOLS

P_{in}	Incident power
P_{max}	Maximum power point
V_{OC}	Open-circuit voltage
J_{SC}	Short-circuit current
ε_{max}	Extinction coefficient at maximum absorption
λ	Wavelength
λ_{max}	Wavelength at maximum absorption
λ_{onset}	Wavelength at the onset of absorption
$E_{1/2}$	Half-wave potential
E_{opt}	Optical gap
E_{redox}	Redox potential
^{o}C	Degrees Celsius
Å	Angstrom
V	Volts
W	Watt
q	Elementary charge
e	Electron
δ	Chemical shift

Other abbreviations are explained in the text.

SUMMARY

Non-fullerene acceptor (NFA) have great potential to replace fullerene materials and overcome their limitations such as relatively weak light absorption, poor morphological stability, and synthetic complexity of introducing structural diversity to fine tune energy levels. A series of naphthalene and perylene diimide (NDI and PDI, respectively) based 3D-shaped non-fullerene acceptors were synthesized and their optical and electronic properties were studied as described in this thesis. Chapter 2 focuses on four NDI-based NFAs with different non-planar central core units. It was found that these materials have broader absorptions compared to typical fullerenes, and the strong tendency of planar NDIs to aggregate was hindered by the non-planar structure that arises when four naphthalene diimides are connected to a core. These materials have comparable estimated reduction potentials to $PC_{61}BM$, and exhibit multi-electron reductions. Upon blending with a low optical gap crystalline donor polymer, these materials are electron acceptors and produce average device efficiencies, specifically PCEs, between 1.3-2.6 %. In chapter 3, an analogue of the best performing NFA in chapter 2 was synthesized in which NDIs were replaced by PDIs. These PDI-based NFAs have broader and stronger light absorptions in the visible region of the spectrum in comparison with NDI analogs, while maintaining similar electrochemical properties. Device fabrication and optimizations of these PDI materials is ongoing.

CHAPTER 1 INTRODUCTION

1.1 BULK HETEROJUNCTION ORGANIC SOLAR CELLS

1.1.1 Organic solar cell operation mechanisms

Organic solar cells (OSCs) potentially offer some advantages over their inorganic counterparts because they can be light-weight, flexible, and offer the possibility to be fabricated on an industrial scale by roll-to-roll production techniques. Unlike the immediate generation of free electron and hole carriers in conventional inorganic solar cells, in OSCs light absorption results in formation of spatially localized electron-hole pair, which is referred to as exciton.[1] Due to the excitonic nature of OSCs, their operation mechanism involves five processes: (i) exciton formation, (ii) exciton migration, (iii) exciton dissociation, (iv) free charge carrier migration to the collecting electrodes, and (v) charge collection.[1]

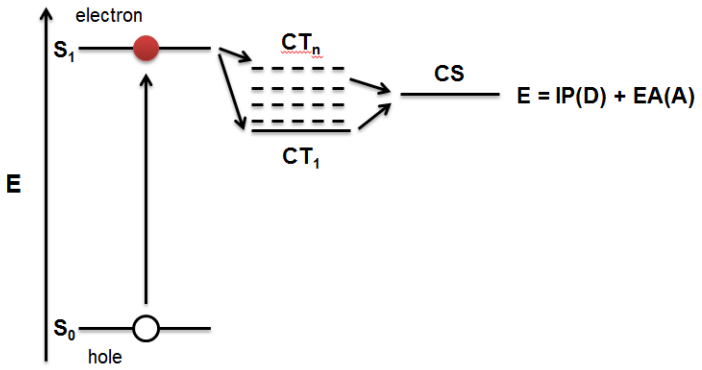

Figure 1.1 Electronic state diagram in organic solar cell.

In process (i) (Figure 1.1), photo-induced excitation followed by relaxation of π-system to the bottom of the potential energy surface of the lowest excited state generates the singlet exciton.[1] This electron-hole pair has a binding energy of about 500 meV, which is large relative

to thermal energy at room temperature, which is about 26 meV.[2] In order for excitons to dissociate to free charge carriers, the electron-hole pair needs to migrate to the donor/acceptor interface.[1] Since the exciton has a finite lifetime due to the possibility for radiative and non-radiative decay, it is necessary for it to diffuse to the D/A heterojunction before it decays back to its ground state. This process is limited by exciton diffusion length, which is:

$$L = (D\tau)^{\frac{1}{2}} \qquad \text{Eq. (1)}^{1}$$

where D is the diffusion coefficient and τ is the exciton lifetime. Therefore, a comparable film thickness of the absorber layer to exciton diffusion length is important (especially for bilayer device) for exciton migration. For OSCs, typical thickness of the active layer is relatively thin (about 100-200 nm).[2] The active layer thickness is critically related to exciton diffusion length in bilayer OSCs, but no longer true for bulk heterojunction OSCs (more detail in the following paragraph).[2] After reaching the heterojunction, the exciton dissociation in process (iii) is often described as a two-step processes: formation of the charge-transfer (CT) state followed the charge-separated (CS) state (this process compete with relaxation back to the ground state).[1] In the CT state, electron and hole are still bound to each other. The CS state is defined as the case where electrons and holes are completely free from each other (*i.e.* experience essential no coulomb attraction to each other). The details of the charge separation process is still debated in the literature, two cases have been developed to describe the transition from exciton state to CT state in process (iii): (a) the CT state is in the lowest energy state in which the hole sits on the donor and the electron is located on the acceptor, and the dissociation of this strongly coulombically bound electron-hole pair can be assisted by disorder or dipoles at the heterojunction; (b) the CT state is in high-lying energy state, in which the electron-hole pair are loosely bound to each other and easy to separate from each other.[2,3] After dissociation, charge

carriers need to move toward their corresponding electrodes, this process (iv) mainly depends on charge carrier mobilities of the materials. The charge-carrier mobility of organic materials is much lower than in inorganic semiconductors; the latter is typically in the range of 10^2-10^3 $cm^2V^{-1}s^{-1}$.[1] The mobility of organic semiconductors in the blend depends on intrinsic mobility of the material as well as the efforts of morphology and mixing, which varies between 10^{-6} to 1 $cm^2V^{-1}s^{-1}$ from amorphous to highly ordered materials.[1] The last process of charge collection at electrodes depends on alignment of materials frontier energy levels to Fermi levels of corresponding electrodes.[1] Conducting oxide electrodes are often used for great compatibility with organic semiconductors.[1]

Due to the fact that excitons need to migrate to the donor/acceptor interface to dissociate, the concept of bulk heterojunction (BHJ) OSC was introduced by Yu *et al.* in 1995.[4] Compared to conventional bilayer device, BHJ solar cell has interpenetrated donor and acceptor materials that forms bicontinuous phases (Figure 1.2)[5]. In Yu's work, a 10-fold increase in electron conversion efficiency was observed in a BHJ OSC blended with (poly(2-methoxy-5-(2'-ethyl-hexyloxy)-1,4-phenylene vinylene)) (MEH-PPV) and C_{60} acceptor, compared to bilayer device fabricated with same semiconductor materials.[4] The increase in performance was attributed to increased interfacial area of the donor and acceptor materials.[4] Since experimental measurements indicated that exciton diffusion length *L* is in the range of 10 nm for many prototype devices, an ideal BHJ organic solar cell should have domain size around a few tenths of nanometers.[5]

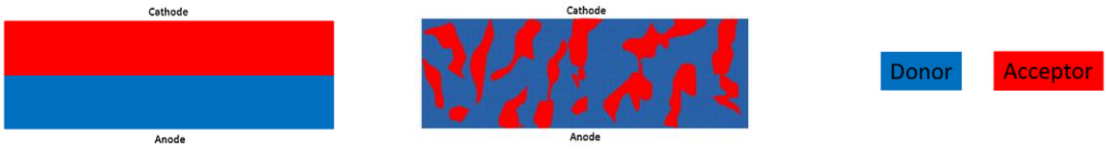

Figure 1.2 Bilayer (left) and bulk heterojunction (right) device architectures for organic solar cells.

1.1.2 Power conversion efficiency in OSCs

The device performance of OSCs is usually tested under standardized illumination air mass (AM) conditions, which defines as the path length that light path through the atmosphere to the shortest possible path lengh.[6]

$$AM \approx \frac{1}{\cos\theta} \qquad \text{Eq. (2)}$$

where θ is the angle between incident light to vertical. The two popularly used AM conditions are AM = 1 (sun directly above head without penetrating through the atmosphere) and AM = 1.5 (where $\theta \sim 48^{o}$ - 49^{o}), and the AM 1.5 condition is equivalent to a maximum current density of 46 mA/cm^2, if every photon is successfully converted to an electron.[6]

The overall device power conversion efficiency (PCE) is defined as the ratio of power output from the solar cell device to power input from the sun, which expresses as:

$$\eta = \frac{J_{\max} V_{\max}}{P_{inc}} = FF \frac{J_{SC} V_{OC}}{P_{inc}} \qquad \text{Eq. (3)}$$

where P_{inc} is the incident power density, J_{sc} is the short-circuit current density; V_{oc} is the open circuit voltage, and FF is the fill factor.

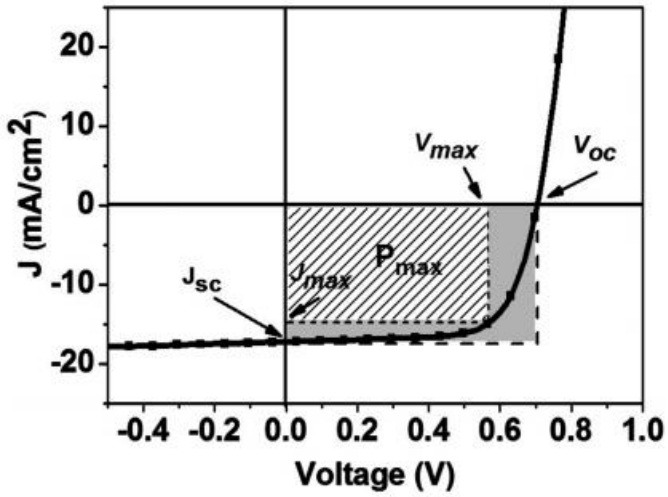

Figure 1.3 Current density versus voltage plot of organic solar cell. (adapted from[8])

The short circuit current density J_{sc} is defined as current per unit area that flows under illumination at zero bias.[6] This parameter depends on many factors that include the optical properties of the materials in solar cell, charge separation, and charge collection. For a device fabricated with the same absorbers, the most critical parameters that affect J_{sc} are exciton diffusion length and surface passivation.[6] Exciton diffusion length is related to J_{sc}:

$$J_{SC} = qG(Ln + Lp) \qquad \text{Eq. (4)}$$

where G is the exciton generation rate, Lp is the diffusion length.[6] The open circuit voltage V_{oc} is the voltage obtained from a solar cell when the net current through the device is zero; it depends on CT energy and the amount of recombination.[6] Empirically, the upper limit of V_{oc} increase as the difference between IE of the donor and EA of the acceptor increase; while J_{sc} decreases as the optical gap increases.[6] An ideal solar cell needs to maximize $V_{oc} \times J_{sc}$, which requires optimizing one parameter without substantially sacrificing the other. The last parameter, fill factor, measures the quality of the solar cell.[7] Graphically, it is the area of largest rectangle that

fits in the JV curve (Figure 1.3), the empirical expression of its upper limit is highly dependent on the IP and EA of the materials (hence V_{oc}), and it can be expressed as the following equation[2]:

$$FF = \frac{V_{OC} - \ln(V_{OC} + 0.72)}{V_{OC} + 1} \qquad \text{Eq. (5)}$$

The *FF* generally varies significantly from different materials, typical *FF* for solar cells ranges from 0.5 to 0.82.[7]

Another important parameter used to characterize solar cell device performance is the external quantum efficiency (EQE). Quantum efficiency is defined as the ratio of generated charge carriers to number of photons of a given energy incident on the solar cell, and it depends on the efficiency of light absorption, exciton dissociation, and charge collection.[6] This parameter depends on the efficiencies of light absorption, the exciton dissociation, and charge collection. The "external" quantum efficiency does not take into account loss from reflection or transmission of the light.[6]

1.2 CONJUGATED MATERIALS IN OSCS

1.2.1 Electron donors

Though the major part of this thesis covers electron acceptor materials, especially non-fullerene acceptors, the background of electron donors plays an important role in this thesis, and some state-of-art donor materials are mentioned and used throughout the thesis. In this section, representative electron donor materials will be briefly reviewed and their structure-property relationships will be described to provide an understanding of organic semiconductor design.

Since the introduction by Tang in 1986 used copper phthalocyanine (CuPc) as donor and perylene tetracarboxylic derivative (PV) as the acceptor to fabricate a planar heterojunction OSC

that achieved PCE about 1%[9], numerous efforts have been put into developing advanced electron donor and acceptor materials. The factors that need to be considered when designing a donor material include: absorption property, IPs and EAs, and morphological compatibility with acceptors to form a bicontinuous interpenetrating network. A good donor should absorb sunlight matching sizable portion of the solar spectrum (even extending to the high energy side of the near-IR region), and ideally it should complement the acceptor's absorption. A quantitative example that was provided by Nunzi demonstrates that a donor polymer with optical gap of 1.1 eV can absorb at most 77% of the solar energy, while a polymer with larger optical gap of 2.0 eV can only absorb 30% of the incident sun energy.[10] Factors other than absorption need also to be considered when engineering the optical gap, such as energy level alignment with the acceptor. It is believed that the upper limits of V_{oc} is determined by energy level differences between the IE of the donor and EA of the acceptor.[1,2] Both energy levels of the donor need to have sufficient energy offsets to provide the necessary driving force for electron-hole transfer. This minimum EA/EA offset (Δ_{EA}) value is often reported as 0.3 eV for fullerene based OSCs, which is often referred as ΔG_{CS}.[8, 11] An in depth investigation of OSCs performance on the IP/IP offset is still lacking in the literature, since fullerene acceptors generally do not contribute much in light absorption, but this will become increasing important to study with NFAs. The discussion of representative donor materials for OSCs is divided into two classes: polymeric donors and small conjugated molecule donors.

One early stage polymer donor investigated for organic solar cell is the poly(phenylenevinylene) (PPV, Figure 1.4) family.[4, 12] The first example using this type of polymer was reported by Heeger and co-workers with a BHJ OSC that blended with (poly(2-methoxy-5-(2'-ethyl-hexyloxy)-1,4-phenylene vinylene)) (MEH-PPV) and C_{60} as active layers to

achieve PCE about 2.9%.[4] However, it was found that frontier energy levels of MEH-PPV was too high for C_{60} acceptors (MEH-PPV has EA of 3.2 eV with ΔG_{SC} ~ 1 eV to C_{60})[12]. Later, Reynolds and co-workers developed a strategy utilizing cyano-substituted PPV backbones that increases both the IP and EA without changing the polymer optical gap.[12] The cyano-substituted PPV polymer (CN-PPV) had a much larger EA of 3.8 eV.[12] Not much more significant structural modifications were done on PPV family donors due to their large optical gap (> 2 eV), which is not optimal for light harvesting, thus low J_{sc} and V_{oc} are often observed for blends MEH-PPV with PCBM.

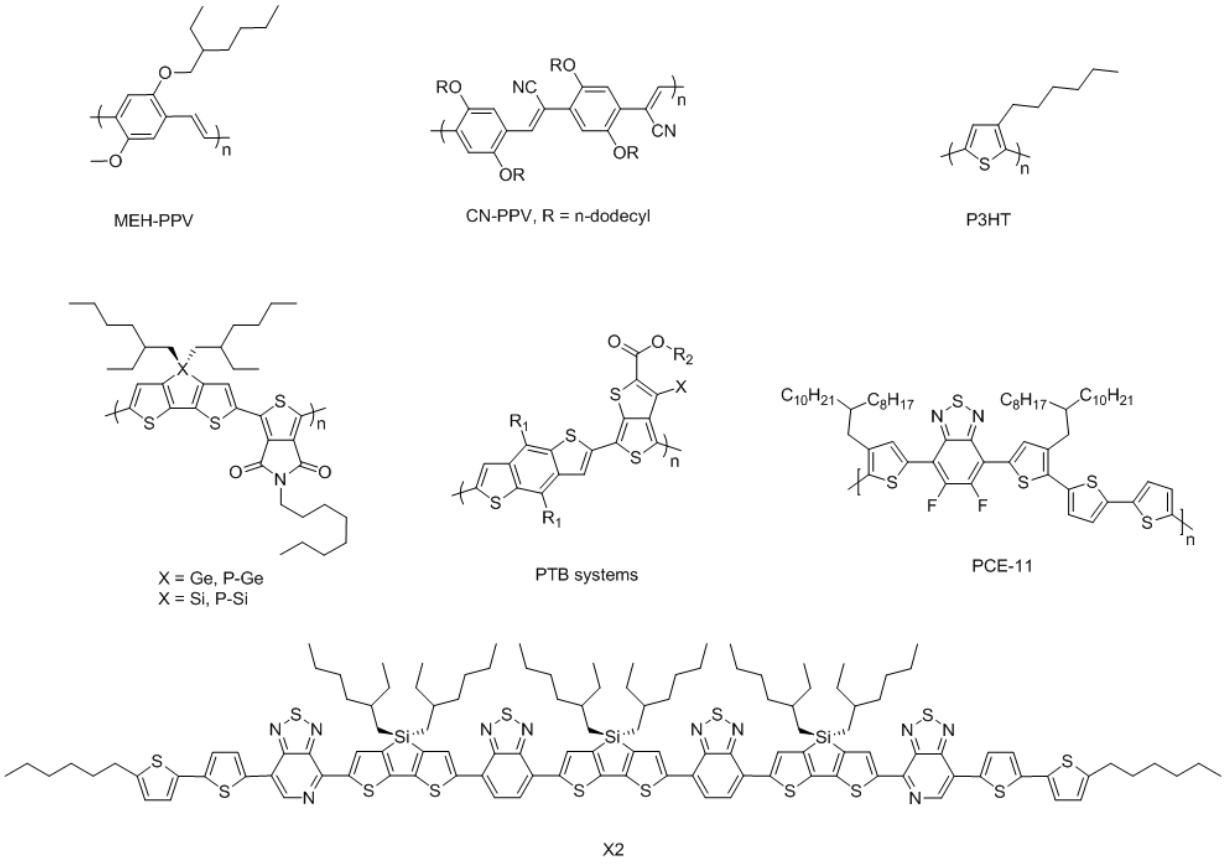

Figure 1.4 Molecular structures of representative polymer donors materials in this chapter.

Another donor polymer system that developed in early stages of BHJ development and still is in active use today is the poly(3-hexylthiophene-2,5-diyl) (P3HT, Figure 1.4). P3HT is one of the scalable polymer donors and is, therefore, an attractive candidate for OSC commercialization.[13] Another advantage of P3HT is the high achievable EQE, which was reported reach as high as 88%.[14] Much effort has been focused on optimizing the morphology of P3HT-containing solar cells, for example, by inkjet printing and spray coating.[15, 16] However as was the case with PPV, P3HT has a large optical gap (about 1.9 eV[17]) and small EA, which result in inefficient sunlight harvesting and insufficient driving force for exciton splitting. One solution to overcome this issue is to reduce the acceptor' EA.[13, 18] For example, Zhao *et al.* blended P3HT with a fullerene derivative indene-C_{60} bisadduct (ICBA)[18], which has an electron affinity about 0.2 eV lower than that of $PC_{61}BM$. A higher PCE of 6.5%[18] resulted from this donor/acceptor selection, which is significantly higher than for the device performance observed for P3HT:PCBM blends. Recently, a nonplanar rhodamine-flanked small molecule with smaller EA than $PC_{61}BM$ was reported by McCullough and coworkers to achieve PCE of 6.4% with P3HT.[13] These results demonstrated that P3HT solar cells still have room for further improvement by proper selection of the acceptor materials. Fullerene and non-fullerene acceptors will be discussed in detail in the following sections.

As mentioned earlier, the major disadvantages of the PPV and polythiophene donor polymers are their relatively large optical gap and difficulties of optical gap engineering through structural design. An alternative approach was made to use alternating donor-acceptor copolymers, which are often referred as "push-pull" copolymers.[8] The concept behind using alternating donors and acceptors in the donor polymer main chain is to decrease the optical gap of the material (as illustrated in molecular orbital diagram in Figure 1.5). In addition, the

approach simplifies optical gap engineering allowing for mixing and matching of a wide donor and acceptor units with different electronic properties. In some case, the "push-pull" copolymers can also benefits from the "quinodal effect", in which increase the planarity of the polymer backbone can enhance electron delocalization along the polymer chain and allow further narrowing of the optical gap.[8] It was reported in literature that the IP and EA of these copolymers are largely dependent on the strength of the donor and acceptor, respectively.[1] Recent advances in the design of these "push-pull" copolymers includes incorporation of heteroatoms such as silicon and germanium, polymer backbone structural variations, and morphology control through side-chain engineering.[19-25] One example of each will be introduced in the following paragraphs.

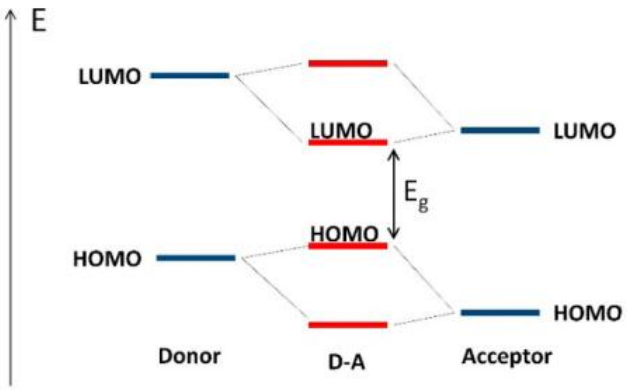

Figure 1.5 Molecular orbital theory explanation of narrow optical gap "push-pull" copolymer donors. (adapted from[8])

Heteroatoms are often incorporated in organic semiconductor materials.[19, 20] For example, in the work by Amb *et al.*[19], dithienogermole was first introduced as a fused electron donor units in conjugated polymers. The hypothesis of this work was that larger heteroatoms can push the solubilizing alkyl side chains further away from the polymer backbone and result in strong π-stacking interactions of the conjugated polymer backbone.[19] After copolymerization with the

electron-poor *N*-octyl-thieno[3,4-*c*]pyrrole-4,6-dione (TPD) units by Stille polycondensation, the resulting polymer P-Ge (Figure 1.4) achieved a superior device performance (PCE of 7.3%) compare to its dithienosilole analog P-Si. The improved device performance was attributed to red shift of P-Ge absorption compare to P-Si, as well as the possible different molecular packing structures after incorporating the germanium atom.[19]

One benchmark donor polymer that was designed to study the effect of different polymer backbones is the PTB family of polymers (Figure 1.4) developed by the Yu group.[21-23] The design of PTB polymers utilizes the "quinoidal effect" that can be observed in donor-acceptor polymers. As shown in Figure 1.6, the electron-poor unit may adopt quinoidal structure to achieve aromaticity in the thiophene ring. The quinoidal structure leads to a more planar and rigid structure which is favorable for π-stacking interactions, lowering the optical gap (PTB polymers have optical gaps between 1.6 – 1.8 eV) due to more efficient π-delocaliztion.[21] The alkyl ester functional group on TPD units help to increase the solubility of the polymer as well as its stability against oxidation.[21] Substantial structure engineering were done on PTB polymers, such as introduction of fluorine atoms to lower both IP and EA[22], or attachment of 2D aromatic groups to improve the coplanar structure of the polymer backbone for enhanced π-stacking interactions[24]. The PTB polymer backbone with a grafted thienyl group is named as PTB7-Th (where R_1 = ethylhexyl, R_2 = ethylhexyl, and X = F), which can achieve PCE up to 9.94% when blended with $PC_{71}BM$ acceptor.[24]

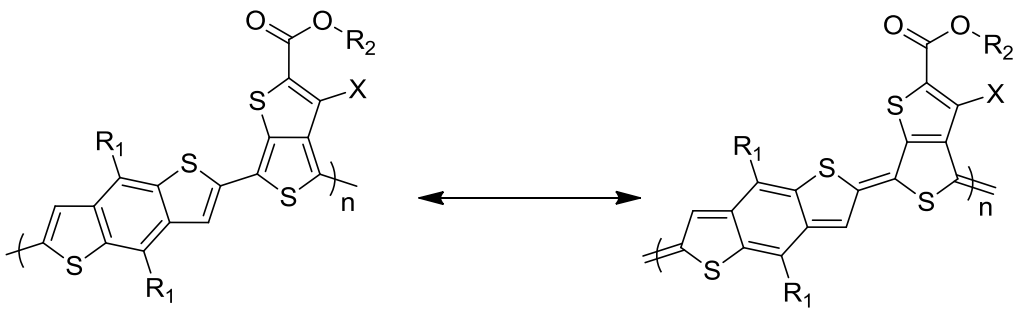

Figure 1.6 Quinoidal effect in PTB family of polymers.

A recent new class of polymer donor material is the PCE-11 (also called PffBT4T-2OD).[25] This polymer (Figure 1.4) allows morphology control through its temperature-dependent aggregation. The absorption of the polymer strongly red shifts as the temperature is decreased from 85 to 25 ^{o}C. During device fabrication, the PCE-11:fullerene composites were processed at high temperature, then allowed cool down and dried during the film-casting process which lock-in the length scale of the morphology.[25] The change in the optical spectrum as a function of temperature is known as thermochromism. The thermochromic behavior, specifically the temperature-dependent aggregation, helps to enable the formation of reasonably small and pure donor domains of the polymer, and the polymer itself is highly crystalline (favorable for achieving high hole mobility). The optimal aggregation behavior was developed by screening different branching positions and the lengths of the branched alkyl chains of a series of polymers.[25] Unlike previous work that focused on tuning the electronic properties of the donor polymer, the design of PCE-11 offers a new approach to improve OSCs device performance by controlling active layer morphology with highly temperature-dependent aggregation.

Small conjugated molecules can overcome the limitations of polymer materials, such as batch-to-batch variation, molecular weight distribution, and difficulties in purifications. The Bazan group has developed a structurally well-defined conjugated molecular systems with

donor-acceptor alternating structure D^1-A^1-D^2-A^2-D^2-A^2-D^2-A^1-D^1 (X2, Figure 1.4) that leads to appropriate absorption properties and energy levels.[26] Interestingly, relative to most polymer solar cell blends, the X2:fullerene device performances are less sensitive to the donor:acceptor ratio in the blends. The PCE remained around 6% for various ratios without any solvent additives.[26] However, the major drawback of this kind of system is the synthetic difficulties, which requires a tedious 10 steps of synthesis as reported by Bazan and coworkers.[26]

1.2.2 Fullerene acceptors

Since the first evidence of photoinduced electron transfer from a donor polymer MEH-PPV to C_{60} that introduced by Heeger and Wudl in 1992[27], soluble fullerene derivatives. such as phenyl-C_{61}-butyric acid methyl ester ($PC_{61}BM$) (**1**, Figure 1.8) and phenyl-C_{71}-butyric acid methyl ester ($PC_{71}BM$) (**2**, Figure 1.8), have been used as dominant electron acceptors for BHJ OSCs. The advantages of fullerene acceptors include the possibility of quasi-isotropic charge transport (since the LUMO of C_{60} is delocalized over the entire molecule), high electron mobility, and their ability to aggregate, which facilitates the formation appropriate morphology for BHJ OSCs device. However, significant limitations also exist in fullerene acceptors, which are their relatively poor light absorption that limits the harvesting of photons, as shown in Figure 1.7, and their morphological instability, as fullerenes tend to form aggregation domains over time.[28]

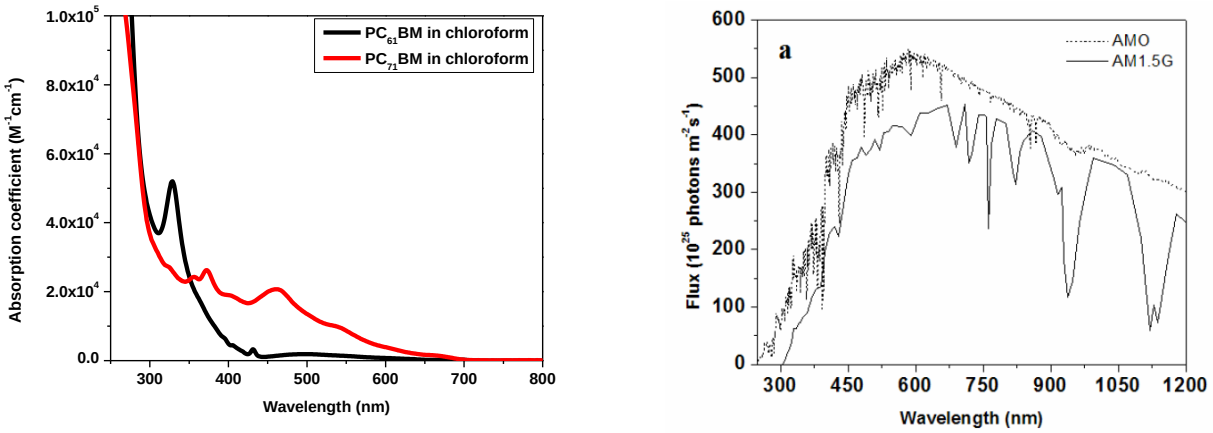

Figure 1.7 Absorption spectra of $PC_{61}BM$ and $PC_{71}BM$, and solar spectra under standard air mass (AM) conditions[29]

Tuning the electronic properties and absorption profiles of fullerene, through chemical modification is a relatively difficult and limited approach to modifying the electronic properties. Two common approaches for structural modification of fullerene acceptors include substitution of different groups on the C_{61} carbon methanofullerenes, and Diels-Alder cycloaddition reaction on the fullerene.[30-33] Popescu *et al.* introduced thienyl functional groups to replace phenyl group in $PC_{61}BM$ (**3**, Figure 1.8) that result in an improved PCE of 4% due to smaller EA of the thienyl-substituted methanofullerene (hence higher V_{oc}).[31] Another piece of work using the same concept involved substituting an electron donating triphenylamine for phenyl to $PC_{61}BM$, which also exhibited improved device performance (**4**, Figure 1.8) relative to $PC_{61}BM$.[32] This substitution approach only lead to small changes in the fullerene's electronic properties, as introduction of electron donating functionalities shift the fullerene's EA by only tens of meV.[30] The second approach is using Diels-Alder chemistry, where C_{60} behaves as a dienophile to react with *o*-quinodimethane to form a dihydronaphthyl bisadduct (**5**, Figure 1.8).[33] This fullerene bisadduct shows multiple advantages over $PC_{61}BM$, such as broader absorption, better thermal

stability, and smaller EA.[33] In addition to chemical functionalization of C_{60}, other fullerenes have also been actively explored for OSCs field. For example, $PC_{71}BM$ which has the same EA as $PC_{61}BM$, but a broader and stronger absorption profile (Figure 1.7). $PC_{71}BM$ often shows superior device performance compares to $PC_{61}BM$ under the same device conditions, but high costs limits its usage on industrial scales.

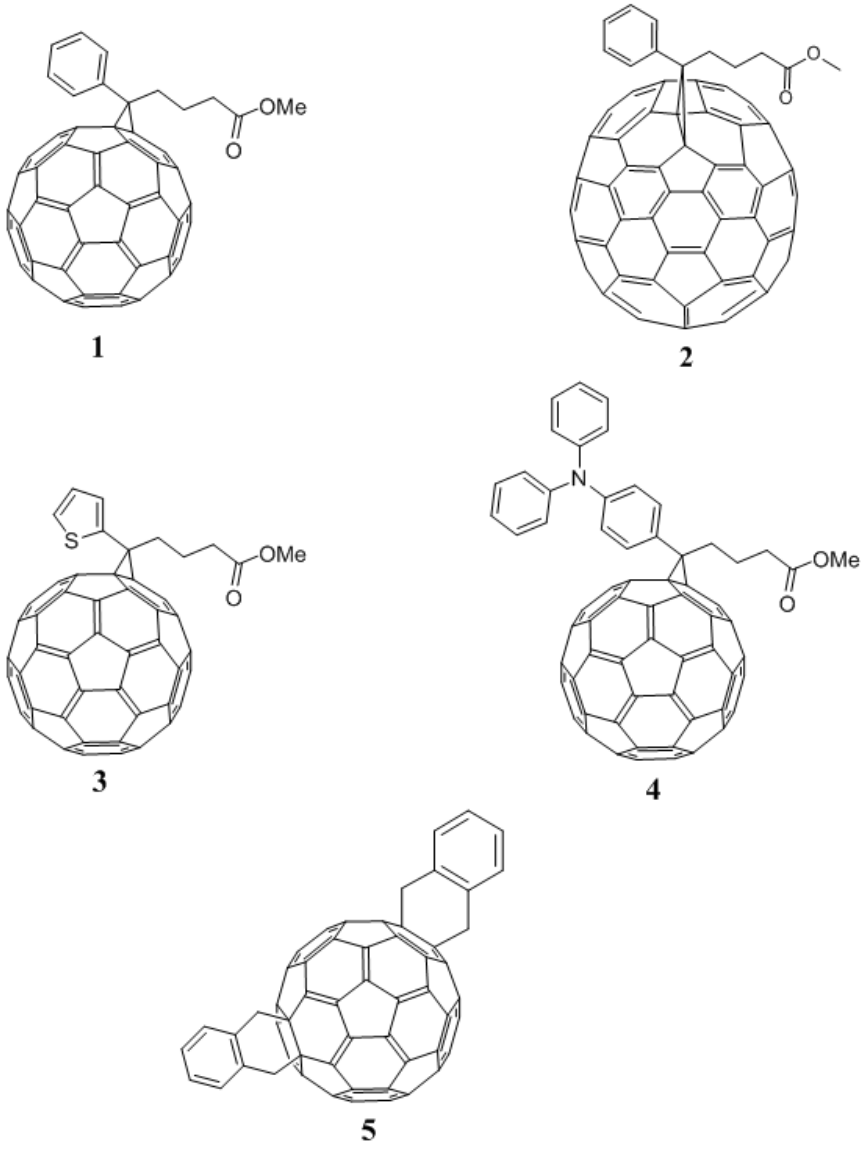

Figure 1.8 Molecular structures of fullerene acceptors described in this chapter.

1.3 INTRODUCTION OF NON-FULLERENE ACCEPTORS

Due to the relatively weak absorption and lack of structural versatility of fullerene acceptors, researchers in the OSC field are actively searching for alternative electron acceptors to replace fullerenes. Non-fullerene acceptors require careful structural design to maintain the advantages of fullerene acceptors, but also to overcome their limitations. Functions that non-fullerene acceptors need to have are: a) broader and stronger absorption in the visible and near-infrared regions compared to fullerenes; b) moderate electron mobility; c) ideally, fullerenes' ability for quasi-isotropic charge transport; and d) the ability to form appropriate morphology accompanied by careful selection of donor polymers. Literatures on high performance non-fullerene acceptors to date can be divided to two major classes: conjugated "push-pull" linear structures and 3D shaped structures.

By analogy to the "push-pull" approach of low optical gap polymers discussed in the donor section, conjugated "push-pull" linear structures have the advantage of providing for tunable structures for optical gap engineering. By replacing different donor and acceptor groups, these non-fullerene acceptors can be optimized to work with both low and high optical gap polymers. Zhan and coworkers developed one of the earliest efficient "pull-push-pull" linear non-fullerene acceptor, ITIC **1.13**.[38] ITIC has the structure of fused indacenodithieno[3,2-*b*]thiophene end capped with malononitrile groups. Hexylphenyl groups are substituted on indacenodithieno[3,2-*b*]thiophene core to increase solubility. ITIC has good IP/IP and EA/EA offset (0.24 and 0.28 eV) with PTB7-Th donor polymer, as well as high energy gap (1.37 eV) between the IP of PTB7-Th to EA of ITIC that ensures high open circuit voltage.[38] The appropriate energy level, broad and intense absorption, and good film formation of the active layer using ITIC results in a high PCE of 6.8%.[38] Another example of optical gap engineering of

"push-pull" linear non-fullerene acceptor is **1.14**, with has extended conjugation by introducing a second acceptor group benzothiadiazole between donor and acceptor units. The absorption of **1.14** at the low energy side of the visible spectrum is highly complementary to the absorption of P3HT.[39] The idea of designing the non-fullerene acceptor that will be paired to use with P3HT is that P3HT is the most scalable and the most well-understood donor polymer.[39] A high J_{sc} of 13.9 mA cm^{-2} and a high PCE of 6.30% were obtained from P3HT:**1.14** blend.[39]

On the other hand, the use of 3D-shaped non-fullerene acceptors seems intuitively reasonable, since they structurally mimic fullerenes. The 3D shape of non-fullerene acceptors has the potential of quasi-isotropic charge transport, which is thought to be one of the advantages of fullerene ball-shaped acceptors. This type of acceptor often uses electron-poor building blocks, often rylene diimides, twisted by steric repulsions or by introduction of twisted linkages between them. The drawback of rylene diimides family is tendency to form large crystalline domains, which possibly lead to trapped charge carriers and within crystallites in the blend. The twisted design of rylene diimide acceptor may hinder the formation of large crystalline domains, and increase the solubility of the rylene to aid in facile solution processing. One of the earliest and simplest 3D-shaped non-fullerene acceptor is the hydrazine-linked perylene diimide (PDI) **1.15**.[40] Two perylene diimides units are linked to each other through the *N*-terminal of imide groups. An average domain size of 10 nm was observed for blend of PBDTTT-C-T: **1.15**, and a high J_{sc} of 9.0 mA cm^{-2}.[40] Thanks to the synthetic flexibility of rylene diimides, this non-fullerene design was further utilized on PDIs by linking the PDIs through the *bay* position as in **1.16**, and fused PDI helices **1.17**.[41, 42] Other types of 3D-shaped non-fullerene acceptors that are twisted by introducing a nonplanar linker "core", like **1.18**, will be covered in detail in chapter 2.

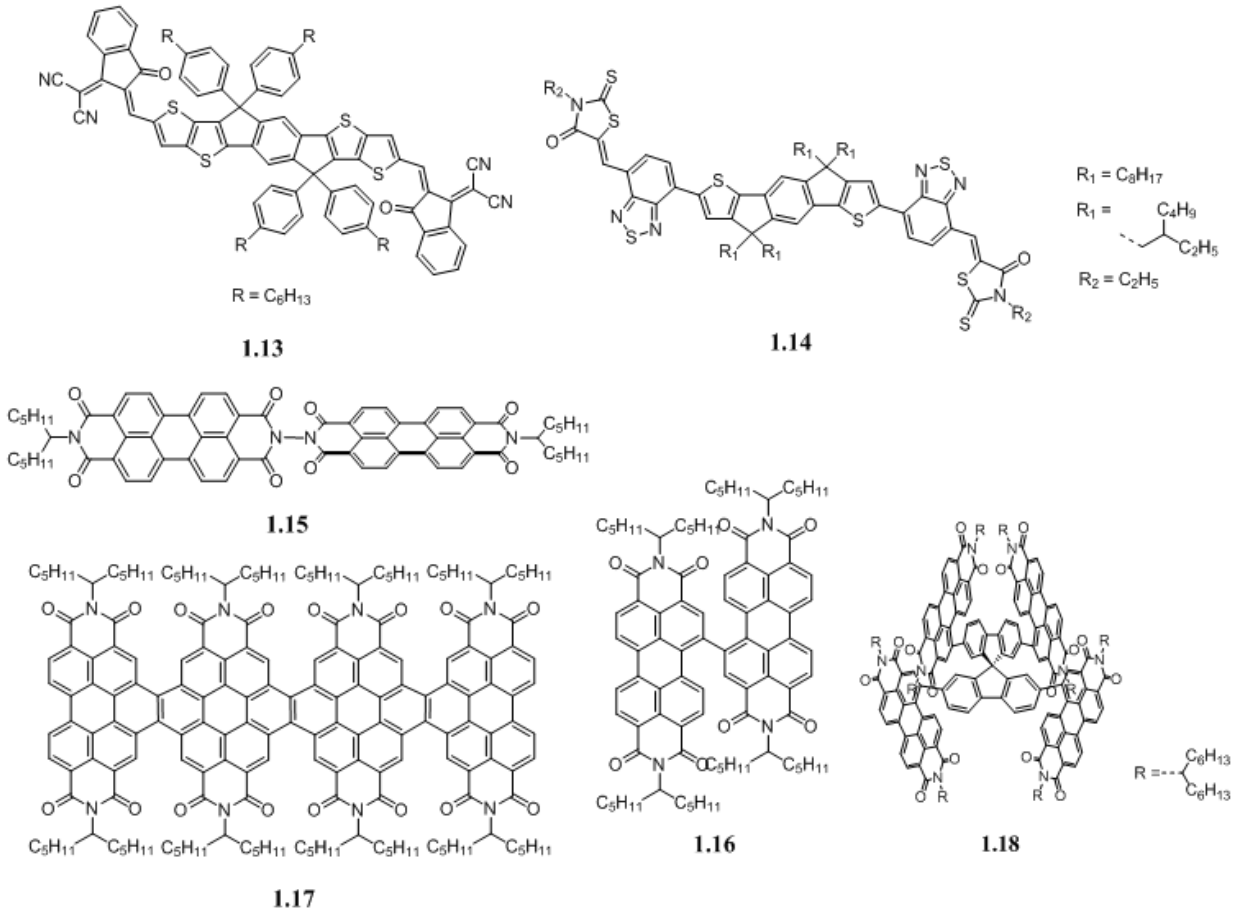

Figure 1.9 Molecular structures of non-fullerene acceptors described in this chapter.

1.4 ORGANIZATION AND OVERVIEW OF THE THESIS

Chapter 1 introduces the operation mechanism and characterization parameters of OSCs, and structure-property relationships behind modern electron donor and acceptors, to serve as background of the thesis. The next two chapters not only cover the synthetic aspect of these 3D shaped non-fullerene acceptors, but also fundamental properties such as optical properties, electrochemical properties, and thermal properties.

Six non-fullerene acceptors synthesized for this thesis project are divided into two groups (Figure 1.10). Chapter 2 covers four NDI-based non-fullerene acceptors with different central

core units: spiro, ethylene, and fulvalene (set #1 in Figure 1.10). The design, synthesis, fundamental properties, as well as device results will be discussed in this chapter.

For chapter 3, the electron-poor units of non-fullerene acceptors were replaced by perylene diimide (PDI) derivatives, while the central core units were maintained the same for comparison purpose (set #2 in Figure 1.10). Syntheses of perylene diimide non-fullerene acceptors, comparisons of optoelectronic properties, as well as initial device results will be covered in this chapter.

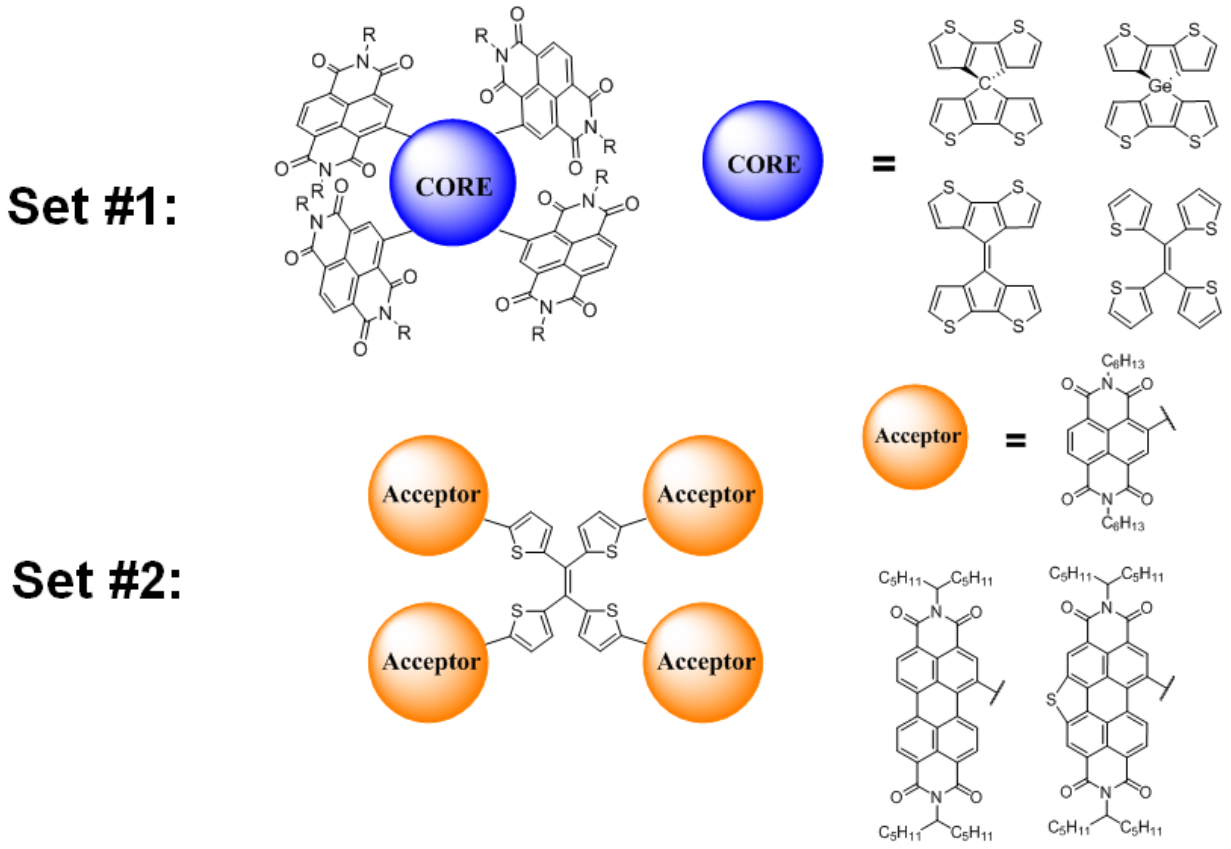

Figure 1.10 Molecular structures of non-fullerene acceptors studied in this thesis.

CHAPTER 2 NAPHTHALENE DIIMIDE-BASED NON-FULLERENE ACCEPTORS WITH DIFFERENT CORE UNITS

2.1 INTRODUCTION

Rylene diimides have been used actively in the field of organic electronics, due to their high electron affinity and electron mobility, their structural versatility, and their good thermal and photochemical stabilities.[43] The high electron affinity of rylene diimides originates from the two strong π-electron withdrawing imide functional groups. A variety of chemistries have been developed for rylene diimides, including extension and introduction of functional groups on the rylene core,[44, 45] and substitution on the *N*-terminal of rylene diimides.[46] The most commonly used rylene diimides are naphthalene diimide (NDI) and perylene diimide (PDI), shown in Figure 2.1.

One of the earliest works using rylene diimides as electron acceptor for OSCs was reported by Friend and coworkers, with a PCE of 0.25% being achieved by blending **2.1**:P3HT in the active layer.[47] The high crystallinity of **2.1** was evidenced and rationalized to cause electron trapping in the blend and hence inferior device performance.[47] Compare to PDI, the other rylene diimide family member NDI has been studied less extensively as an electron acceptor for OSCs. The first NDI-based conjugated molecule acceptor for OSCs was designed by linking two NDI units by a vinyl donor group **2.2**, and was reported by Russell and coworkers in 2015.[48] The concept behind this design is to extend the effective conjugation length through the vinyl linkage, and facilitate intermolecular π-π stacking.[48] By blending with the PTB7 donor polymer, a PCE of 2.41% was achieved.[48] This vinyl-linked NDI derivative also demonstrates the high charge-carrier mobility nature of rylene diimides; a high electron mobility of 0.365 $cm^2\ V^{-1}\ s^{-1}$ was reported as the thin film transistor mobility in ambient atmosphere.[48]

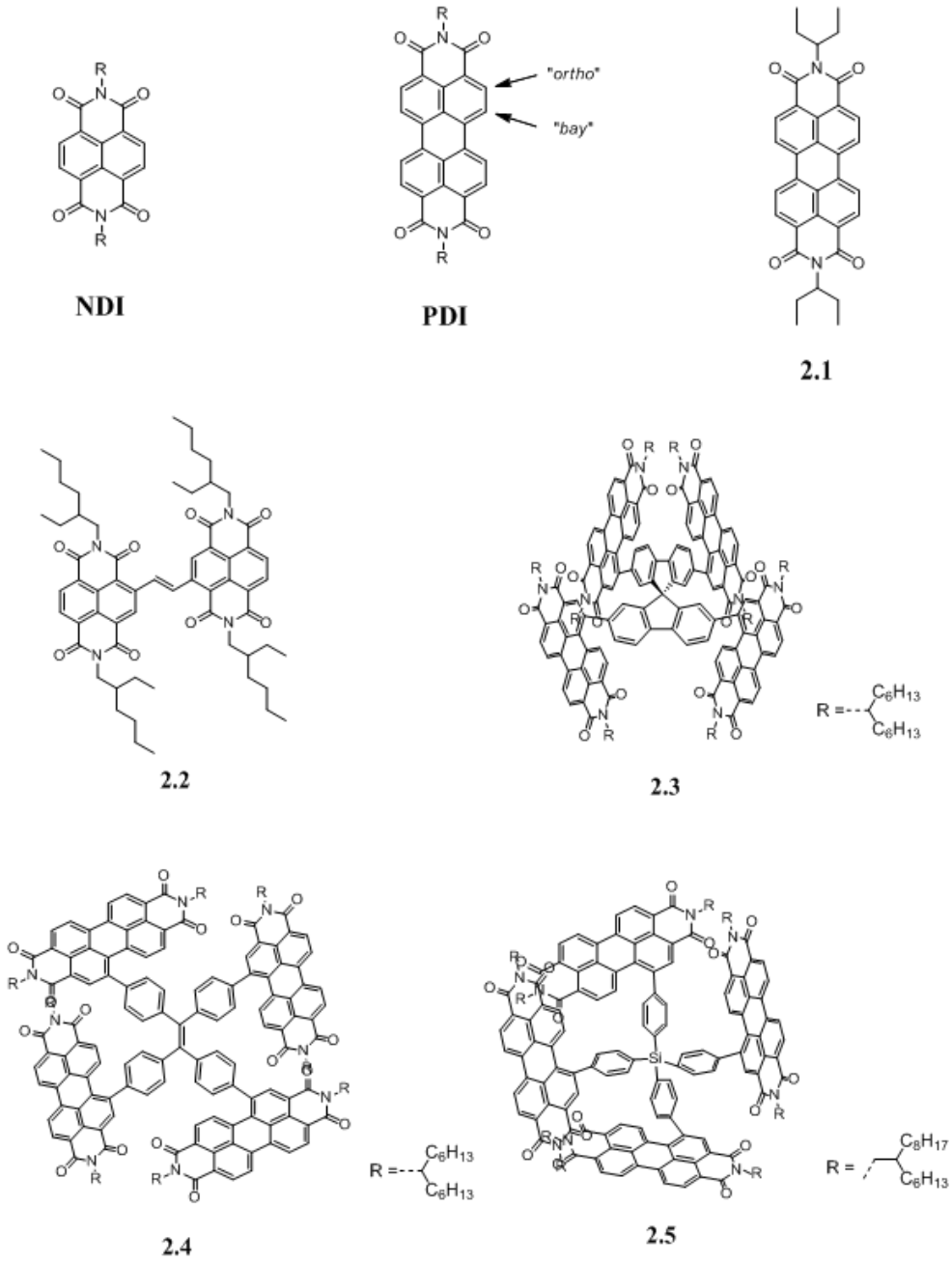

Figure 2.1 Molecular structures of rylene diimides described in this section.

The device performance of rylene diimides derivatives was dramatically improved by introduction of the 3D structural design of non-fullerene acceptors. One of the earliest examples was reported by Lee *et al.*; four PDIs were attached to a structurally twisted spiro-bifluorene core

through their *bay* positions (structure **2.3** in Figure 2.1).[49] Hindered crystallizations of PDIs are evidenced by atomic force microscopy (AFM) imaging. The author attributed the good device performance PCE of 5.82% to proper energy level alignment of **2.3** with the appropriate donor material, and formation of smooth, bicontinuous films with interpenetrating morphology.[49] This design was further utilized on other 3D structural systems with different donor core units, such as on tetraphenylethylene **2.4**,[50] and tetraphenylsilane **2.5**.[51]

To further explore structural-property relationship of 3D-shaped non-fullerene acceptors, a series of NDI-based acceptors have been synthesized in this thesis project (Figure 2.2). The acceptor unit of the "push-pull" structure remains unchanged for four acceptors, but different core donor parts are applied: spirobi(cyclopentadithiophene) (for **SCPDT-NDI$_4$**), spirobi(dithienogermole) (for **SDTG-NDI$_4$**), tetrathienylethylene (for **TTE-NDI$_4$**), and bi(cyclopentadithiophenylidene) (for **DCPT-NDI$_4$**). The aim of this chapter is to describe the syntheses and compare fundamental properties of four NDI-based non-fullerene acceptors with different core units, which includes optical properties, electrochemical properties, and solid-state properties.

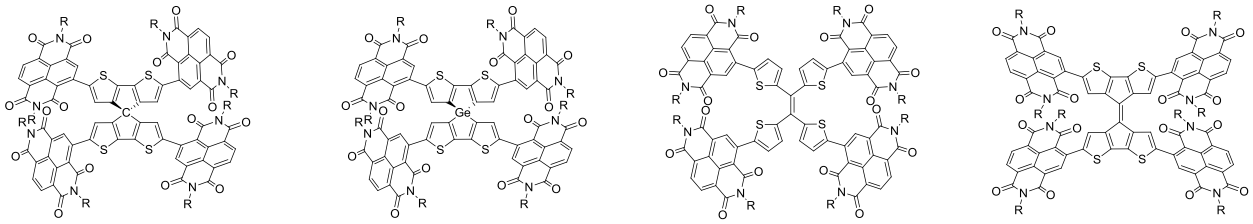

SCPDT-NDI$_4$ **SDTG-NDI$_4$** **TTE-NDI$_4$** **DCPT-NDI$_4$**

Figure 2.2 Molecular structures of NDI based non-fullerene acceptors studied in this chapter.

Heteroatoms have been used often in organic semiconductor materials.[52, 53] In this chapter the carbon center of SCPDT-NDI_4 was replaced to a germanium atom as different spiro linkages in SDTG-NDI_4 without significantly altering the structural conformation (section 2.2.1). The spiro-conjugation is defined as considerable overlaps of HOMO p-orbitals on atoms close to the spiro center, and quantum chemical calculations have shown the overlap integral between HOMO p-orbitals in the two planes is about 20% of the two p-orbitals in the same plane in spirobifluorene.[54] If there is any considerable electronic couplings between NDIs, the electronic couplings should happens through the LUMOs near the spiro center. In this case, there is neither net bonding nor antibonding interactions between the LUMOs near the spiro center. SDTG-NDI_4 will be compared with SCPDT-NDI_4 on fundamental optoelectronic properties.

In this chapter, SCPDT-NDI_4 is also compared with two other twisted systems, TTE-NDI_4 and DCPT-NDI_4. By density functional theory (DFT) calculations, these three acceptors have significantly different molecular conformations (section 2.2.1), hence possibly different solid-state properties. High performance polymer-fullerene bulk heterojunction organic solar cells contain three-phase morphology, which includes pure polymer domain, pure fullerene domain, and mixed polymer/fullerene domain.[55] Therefore, it is interesting to manipulate NFAs' amorphous nature/crystallinity through structural design. As an example of changing solid state properties of NFAs by varying the molecular structures in the literature, a strategy of rigidifying twisted non-fullerene acceptor to increasing crystallinity has been demonstrated on a cyclized PDI-thiophene-PDI system, and the superior performance of rigidified non-fullerene acceptor was attributed to increased aggregation of the acceptor in blend films.[56]

2.2 RESULT AND DISCUSSION

2.2.1 Density functional theory calculations (collaboration with Brédas group)

The frontier molecular orbital energies and geometries from density functional theory (DFT) calculations are summarized in Table 2.1 and 2.2. LUMOs of all four acceptors are comparable to LUMO level value of $PC_{61}BM$ in literature, which is -3.91 eV by the same method of DFT calculations.[57] Table 2.1 shown HOMO energy levels of these 3D-shaped NFAs are tunable via the different donor core units. Comparing the optimized molecular structures in Table 2.2, SCPDT-NDI_4 has no significant conformation changes in comparison to SDTG-NDI_4. However, changing the core units induced different degree of twisting for SCPDT-NDI_4, TTE-NDI_4, and DCPT-NDI_4. In comparison to TTE-NDI_4, acceptors SCPDT-NDI_4 and DCPT-NDI_4 have more twisted structures. NDI units on the TTE core are parallel to each other, which makes the entire molecule more planar and more likely to facilitate intermolecular π-π stacking. For SCPDT-NDI_4, orthogonal twisting by the spiro core provides more space between each NDIs, that might allow greater intermolecular π packing. Besides molecular conformations, the energy level distributions of these acceptors shown that the LUMO of these molecules are delocalized over four NDI units, while the HOMO is localized on each central core units, but there are small spatial overlaps between HOMO and LUMO in each molecule.

Table 2.1 Calculated HOMO and LUMO energy (in eV) at B3LYP/6-311G(d,p) level.

	HOMO	**LUMO**
SCPDT-NDI_4	-5.73	-3.73
TTE-NDI_4	-5.49	-3.69
DCPT-NDI_4	-5.85	-3.77
SDTG-NDI_4	-5.86	-3.74

Table 2.2 Structural optimizations and energy level distributions of NDI-based non-fullerene acceptors at B3LYP/6-311G(d,p) level.

	Front view	Top view	Side view	LUMO	HOMO
SCPDT-NDI_4			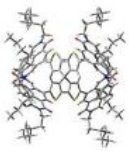	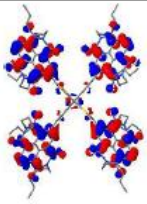	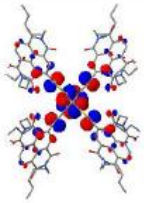
TTE-NDI_4				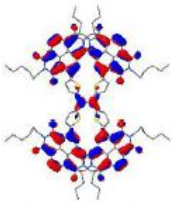	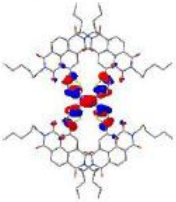
DCPT-NDI_4	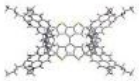	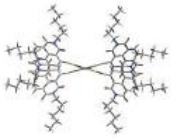	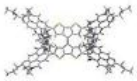	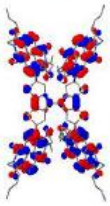	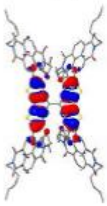
SDTG-NDI_4	-[a]	-[a]	-[a]	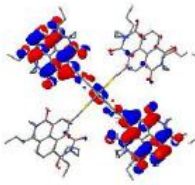	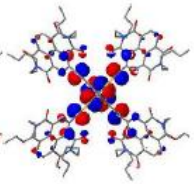

[a] Same configuration as SCPDT-NDI_4.

Charge transport properties of organic semiconductors are highly depend on electronic coupling, and the magnitude of electronic coupling is defined as the interaction of the wavefunctions of two charge-localized states.[58] The electronic coupling values of NDIs on four non-fullerene acceptors were calculated and summarized in Table 2.3. The second column of the table are electronic coupling values of each non-fullerene acceptors with all four NDI arms, calculated by half of maximum energy gaps in four degenerated LUMOs of NDIs. The three columns on the right are three different possible combinations of two NDIs on the same or

different side of the plane. Values in the third and fourth columns indicated that electronic coupling through spiro centers and double bond are relatively weak (for comparison, the calculated electronic coupling of pentacene dimers through space is about 84 meV by the same method[58]), and the major contribution of electronic coupling between four NDIs is from the coupling through the conjugated plane (in second column). In the fourth column, SCPDT-NDI_4 and SDTG-NDI_4 have comparable electronic coupling values, and this could be explained by the large germanium atom act as an insulting link, which pushed two cyclopentadithiophene planes away from each other, resulting in weak electronic coupling in SDTG-NDI_4 through space.

Table 2.3 Electronic coupling between different NDI groups (in meV) at B3LYP/6-311G(d,p) level.

	CoreX+4NDI[a]	CoreX+2NDI[b]		
CoreX	IDN, NDI, IDN, NDI	IDN, NDI	IDN, NDI	IDN, IDN
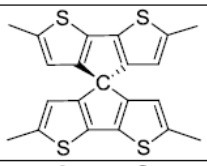	63	73	6	-
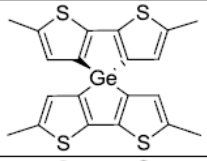	59	64	3	-
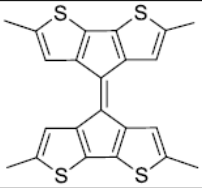	66	80	12	8
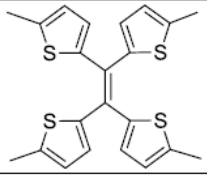	26	27	7	8

[a] Calculated by half of maximum energy gaps in 4 degenerate LUMOs

[b] Calculated by half of molecular orbital splitting energy

2.2.2 Synthesis of NDI based non-fullerene acceptors

DCPT-NDI_4 was synthesized by Kostiantyn Ziabrev (Marder group), and SDTG-Br_4 was prepared by and Rylan Wolfe (Reynolds group) as a collaborative synthesis project. The synthetic routes and detailed experimental procedures of these two compounds will not be included in this thesis.

The preparation of *N*,*N*'-di(*n*-hexyl)-2-tri(*n*-butyl)stannylnaphthalene-1,4,5,8-bis(dicarboximide) **2.8** followed a synthetic procedure developed by Polander *et al*.[45] The commercially available naphthalene-1,4,5,8-tetracarboxydianhydride (NDA) was brominated with potassium dibromoisocyanurate to yield product **2.6** (Scheme 2.1) along with undesired unsubstituted and dibrominated products. The dibrominated product was present in the reaction mixture, even where using exactly 1 equivalent of brominating reagent, since the π-donating bromine acts in a manner of ortho/para directing. The brominated dianhydrides **2.7** were then converted to diamides after reaction with hexylamine. Due to the small difference in retention factor (R_f) values of brominated products, the mixture of **2.7** with side products were used as is for the next step. After stannlyation, the desired product **2.8** was purified by column chromatography. This compound has a robust shelf stability of years.

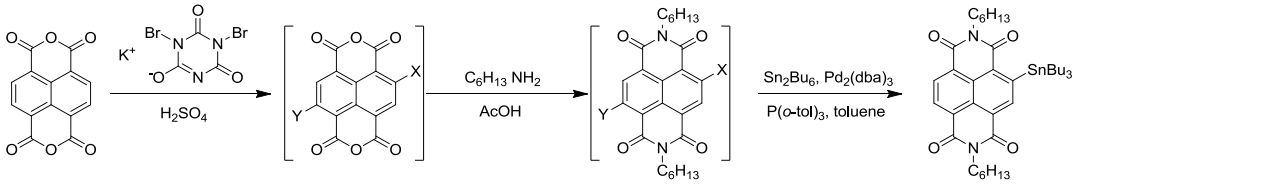

2.6
ZK-I-198 **3.0 g, crude**
XB-I-101 **13.1 g, crude**
XB-I-189 **16.1 g, crude**

2.7
XB-I-91 **3.5 g, crude**
XB-I-102 **15.1 g, crude**
XB-I-190 **14.0 g, crude**
^{1}H NMR

2.8
XB-I-93 **0.8 g**
XB-I-105A **4.8 g, 14% (yield of 3 steps)**
XB-I-193 **7.2 g, 21% (yield of 3 steps)**
^{1}H NMR

Scheme 2.1 Preparation of *N*,*N*'-Di(*n*-hexyl)-2-tri(*n*-butyl)stannylnaphthalene-1,4,5,8-bis(dicarboximide).

Compound **2.9** (3,3'-dibromo-[2,2'-bithiophene]-5,5'-diyl)bis(trimethylsilane) is a common building block for conjugated materials. The traditional method to prepare it is through three-step reaction sequence where the first step is tetrabromination of the dithiophene, followed by reductive dehalogenation of two reactive bromines on α positions of the thiophenes, followed by deprotonation using lithium diisopropylamide (LDA) and quenching with trimethylsilyl chloride.[59, 60] The synthesis of **2.9** here was done by an one-pot base-catalyzed halogen dance reaction developed by Getmanenko *et al.*[61]. The commercially available 2-bromothiophene was lithiated by LDA, followed by quenching with trimethylsilyl chloride. The intermediate was then lithiated again followed by addition of a copper (II) salt to afford product **2.9** (Scheme 2.2), in which the halogen migrated from α to β position of the thiophene, because the negative charges are more stable at α positions. This product can be easily purified by distillation and recrystallization in large scale (~10 g). The purified product was transferred to Rylan Wolfe at Reynolds group for the synthesis of spirobi(dithienogermole) (SDTG) core.

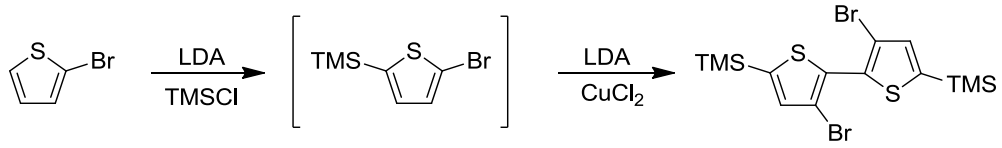

2.9

XB-I-191 **10.2 g, 48%**

^{1}H NMR, GC-MS

Scheme 2.2 Synthesis of (3,3'-dibromo-[2,2'-bithiophene]-5,5'-diyl)bis(trimethylsilane).

The syntheses of 1,1,2,2-tetra(thiophen-2-yl)ethane followed literature procedures for a similar system.[62] 2-Bromothiophene was lithiated and quenched with dimethylcarbamoyl chloride to gives di(thiophene-2-yl)methanone **2.10** (Scheme 2.3), which was then undergoes McMurry coupling to afford the TTE core **2.11**. The yield for this McMurry step is relatively low,

which can be attributed to the decomposition of thiophenes during the reaction, based on observation of strong sulfur odor during the work-up of this reaction. The molecule TTE-Br_4 **2.12** was obtained by bromination of **2.11** using *N*-bromosuccinimide (NBS). The three step syntheses of the TTE core are easy in terms of purification; techniques like recrystallization and washing by small amount of poor solvent were efficient to remove the majority of impurities in these compounds.

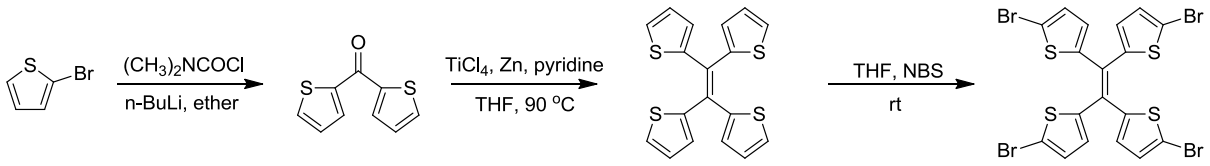

2.10

XB-I-113 **1.44 g, 48%**
XB-I-148 **3.88 g, 65%**
GC-MS

2.11

XB-I-117 **390 mg, 30%**
ZK-II-177 **500 mg, 22%**
GC-MS

2.12

XB-I-120 **130 mg, 18%**
XB-I-201 **870 mg, 92%**
^{1}H and ^{13}C NMR
ESI-MS, EA

Scheme 2.3 Syntheses of 1,1,2,2-tetrakis(5-bromothiophen-2-yl)ethene.

The syntheses of 4,4'-spirobi[cyclopenta[2,1-*b*;3,4-*b*']dithiophene] **2.21** followed a published procedure by Pozzi *et al.*[63]. Product **2.13** (Scheme 4) was synthesized by a Kumada coupling using pre-prepared Grignard reagents. The product was then brominated with different equivalents of NBS to give compounds **2.14** and **2.16**. The TMS groups were incorporated into **2.14** in order to avoid multiple lithium-halogen exchanges in later steps for the synthesis of **2.20**. On the other hand, compound **2.16** undergoes a reductive dehalogenation by using zinc to give product **2.17**, followed by a ring closure of cyclopentadithiophene with ketone group, and was then brominated to afford product **2.19**. The two pieces **2.15** and **2.19** were coupled together by nucleophilic attack of lithiated **2.15** on the ketone group in **2.19**. Before the final ring closure steps to make **2.22**, all α positions on thiophenes were blocked by electron-withdrawing bromine groups to avoid undesired intermolecular reactions during the ring closure step. The Friedel-

Crafts type of ring closure was done by addition of a Lewis acid, $FeCl_3$, at low concentration to minimize competition of intermolecular reactions with intramolecular ring closures. Since the last step needs to be performed in low concentration, the reactions were divided in multiple batches and consistent yields in a range of 43-54% were obtained.

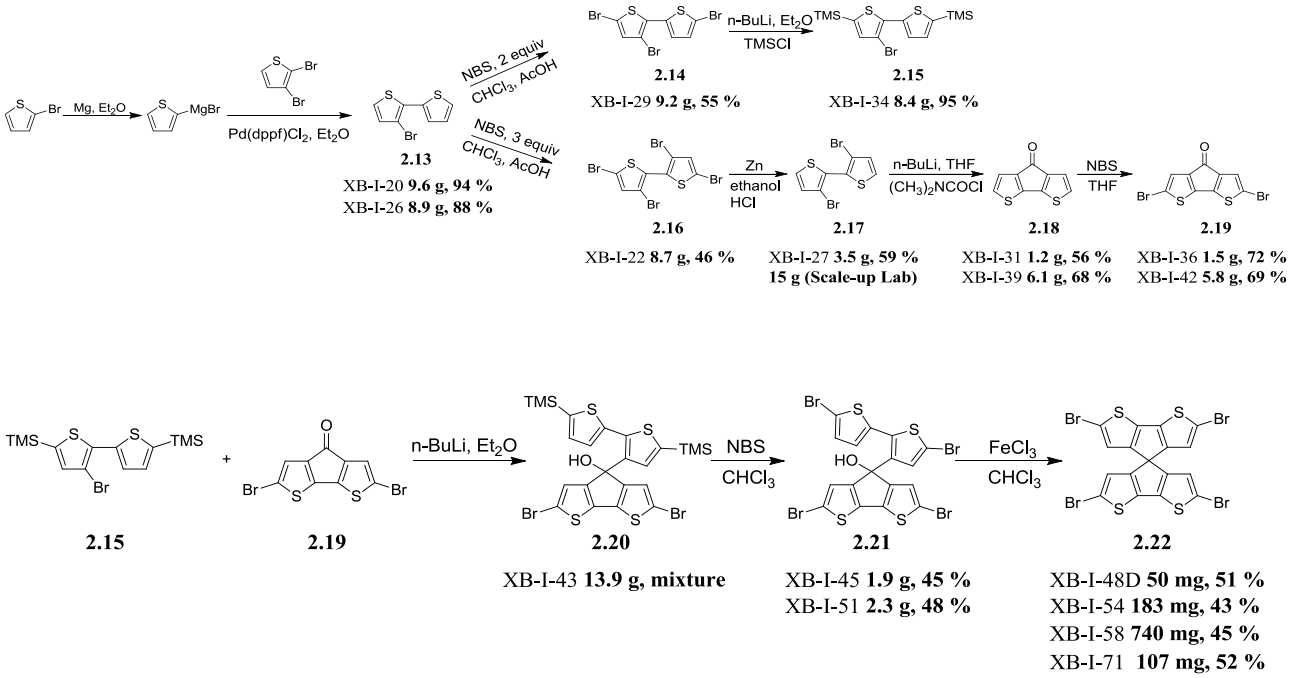

Scheme 2.4 Synthesis of 4, 4'-spirobi[cyclopenta[2,1-*b*;3,4-*b*']dithiophene].

The final non-fullerene acceptors were synthesized via a 4-fold Stille coupling. For synthesis of conjugated systems, the general strategy is to functionalize halogens on electron-poor system (NDIs in this case), and tin/boronic ester groups on the electron rich unit[64]. Because for the first step in cross coupling, oxidative addition, is typically treated as a nucleophilic aromatic substitution reaction, it can be activated by electron withdrawing groups.[64] This synthetic strategy is difficult to apply to these systems because of the difficulty of purifying NDI-Br as mentioned above in the description of synthesis of NDI-$SnBu_3$, and unsuccessful experience of attempting substitution of four stannyl groups on the donor core (four attempts failed on synthesis of SCPDT-$(SnMe_3)_4$). Initial, attempts of this 4-fold Stille coupling reaction

were performed under conventional heating condition for 24 h, but the yield of fully tetra-substituted product was low as determined by thin layer chromatography (TLC). When the reaction conditions were modified by using microwave conditions for 1 h, the tetra-substituted compound was obtained as the major product, with formation of minimal amount of tri-substituted product. The number equivalents of NDI-$SnBu_3$ do not play a huge role for this reaction, since the dehalogenated tri-substituted product was always observed in mass spectrometry results. Due the difficulty of separating tri- and tetra-substituted products (their R_f values were very close, even when eluting with very nonpolar solvents), the desired products were purified by multiple chromatography techniques, for example, silica-gel column chromatography, preparative thin-layer chromatography (prep TLC), and size-exclusion column chromatography (SEC).

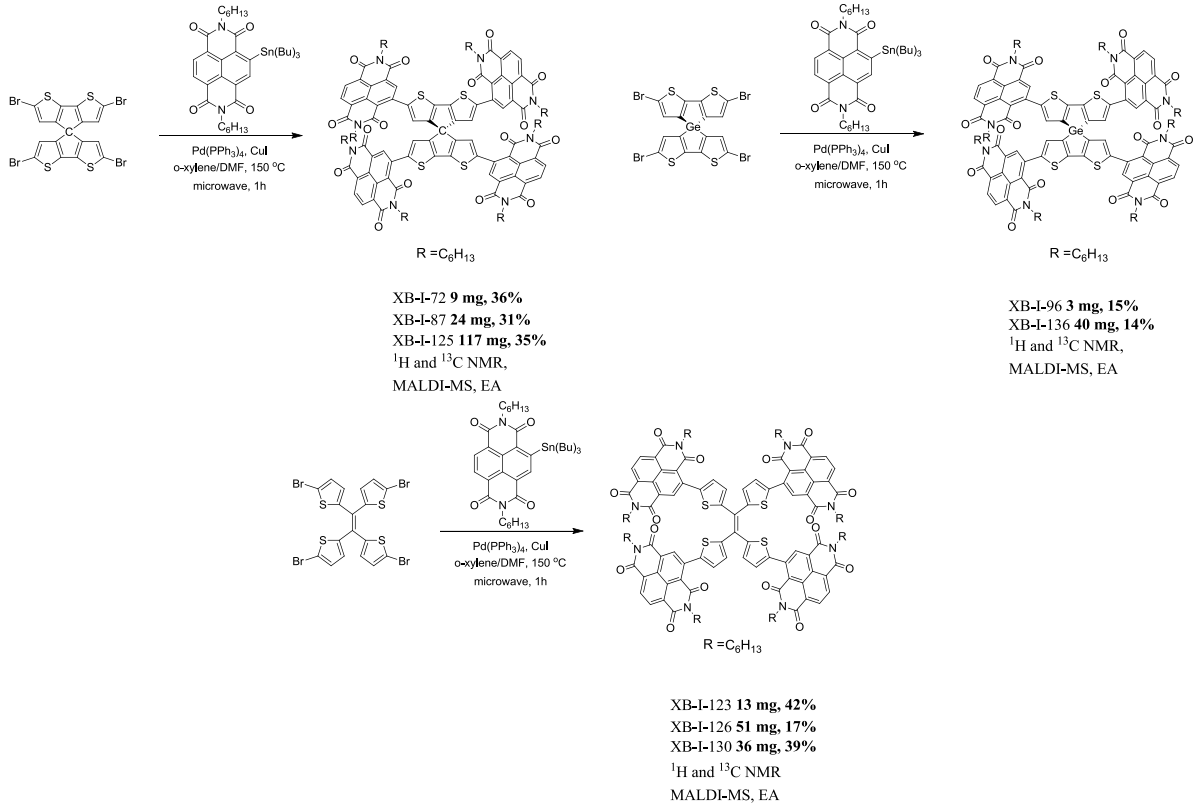

Scheme 2.5 Syntheses of NDI based non-fullerene acceptors.

2.2.3 Optical and electrochemical properties

The optical properties of materials in organic solar cells play an important role in the overall device performance. Parameters include the absorption window of the material, strength of the absorption, optical gap, and degree of aggregation of the material in solid-state; insight into these parameters can be probed by UV-vis absorption spectroscopy. Figure 2.3 below shows solution and solid-state absorption spectra of four NDI-based non-fullerene acceptors. Each non-fullerene acceptor has characteristic absorption peaks from NDI located at the high-energy side of the spectrum, as well as a weaker band on the low-energy side, which is attributed to intramolecular charge transfer (ICT) band from the donor core to acceptor arms.[65, 66] The strongest absorption peaks of these four non-fullerene acceptors are located in the same region (around 362-382 nm), but the ICT band can be tuned by varying the donor core units. SCPDT-NDI_4 and DCPT-NDI_4 have the ICT peaks towards higher wavelength in the visible region (643 nm and 620 nm, respectively), while SDTG-NDI_4 and TTE-NDI_4 have ICT bands are located at 581 nm and 593 nm. Interestingly, the ICT band of SDTG-NDI_4 is blue-shifted compared with SCPDT-NDI_4, which was supported by DFT calculations of larger optical gap of SDTG-NDI_4 than SCPDT-NDI_4. The absorption features of these non-fullerene acceptors are consistent with NDI-based donor-acceptor conjugated systems reported in the literature.[67]

The molar absorptivities of each non-fullerene acceptor were determined and are summarized in Table 2.3. The absorptivity of NDI characteristic peaks approaches 10^5 M^{-1} cm^{-1}. However, this peak does not have much overlap with solar spectra maximum under standard illumination condition. The absorptivities of ICT bands are relatively weak, between 1.5 - 3.2×10^4 $M^{-1}cm^{-1}$. TTE-NDI_4 has the weakest ICT absorption peak among four NDI-based NFAs, but the absorption is broad and consistent with the black color of this material in solution.

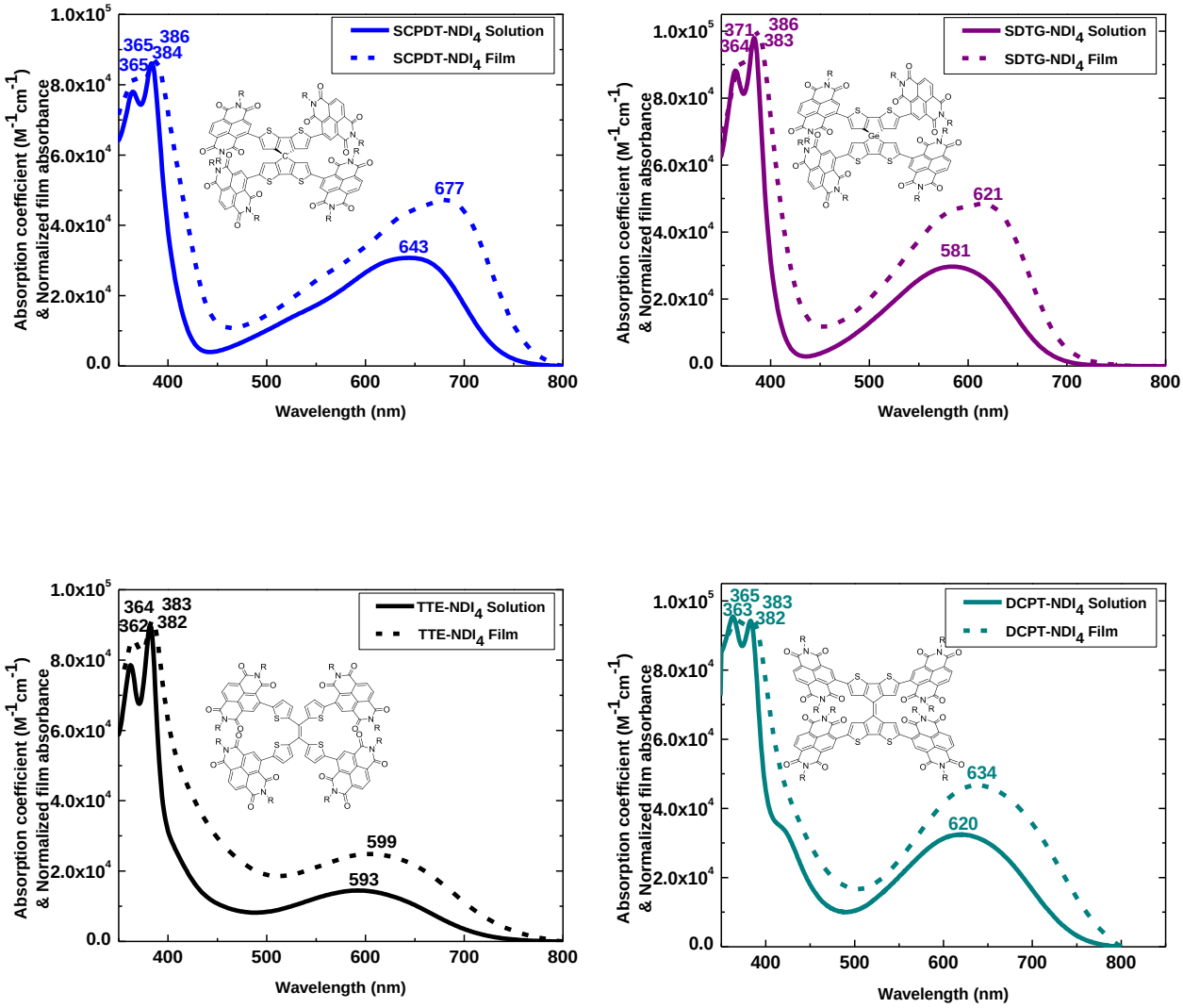

Figure 2.3 UV-vis spectra of NDI based non-fullerene acceptors in solution (chloroform) and film.

Overall, these materials have broader absorption bands, which are significantly stronger compare to fullerenes acceptors (Figure 1.7). In comparing of solution to solid-state spectra, there is no significant shift of NDI peaks, which indicates that there is only weak if any intermolecular interactions of these materials in solid state. In comparison, the absorption spectrum of NDI monomer (Figure 2.4), it is clear that the aggregation behavior of NDI (*i.e.* the

red shifted absorption going from 408 nm in solution to 426 nm in the neat film) is hindered by twisting of the nonplanar cores on these non-fullerene acceptors.

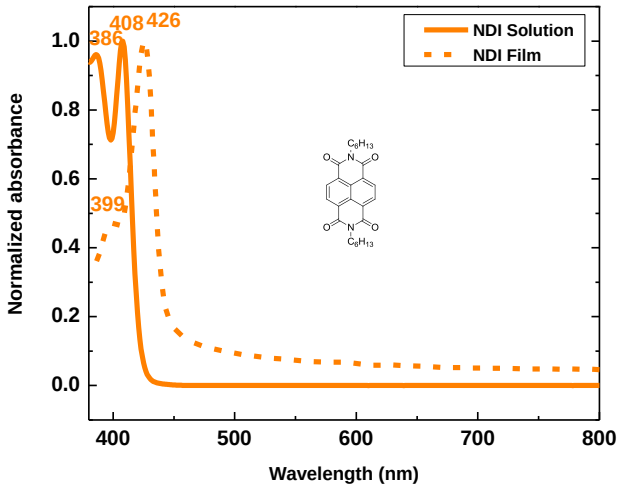

Figure 2.4 UV-vis spectra of monomeric NDI in solution (chloroform) and solid state.

The optical gaps of these materials were estimated by their solution absorption onsets and summarized in Table 2.4. Optical gaps of SCPDT-NDI_4, TTE-NDI_4, and DCPT-NDI_4 are comparable to each other within experimental errors, but SDTG-NDI_4 has about 100 meV larger optical gap than the other three acceptors.

Cyclic voltammetry enable examination of electron-accepting behavior of these non-fullerene acceptors and provides some information about stability of the reduced species, reversibility of the redox process, as well as very rough estimation of electron affinities (EAs) of these acceptors through estimating the reduction potentials (electron affinity is defined as the energy released when an atom or molecule capture an electron in the gas phase or in the solid state), which ignores solvation effects. As expected, all four acceptors have very similar reduction potentials (-1.02 to -1.18 eV versus Fc/Fc^+), as estimated by differential pulse

voltammetry (DPV) of their first reduction potentials (Figure 2.5). The estimated reduction potentials are lower than the reduction potential of $PC_{61}BM$, which is estimated as -0.80 eV by the same method.[68] In addition, all acceptors have two reversible reduction peaks, and the redox processes were stable after multiple cycles. Attempts were made to examine the electrochemical oxidation of these materials, but the oxidized species were not stable, and a decrease of oxidation peak signals was observed after each redox cycle.

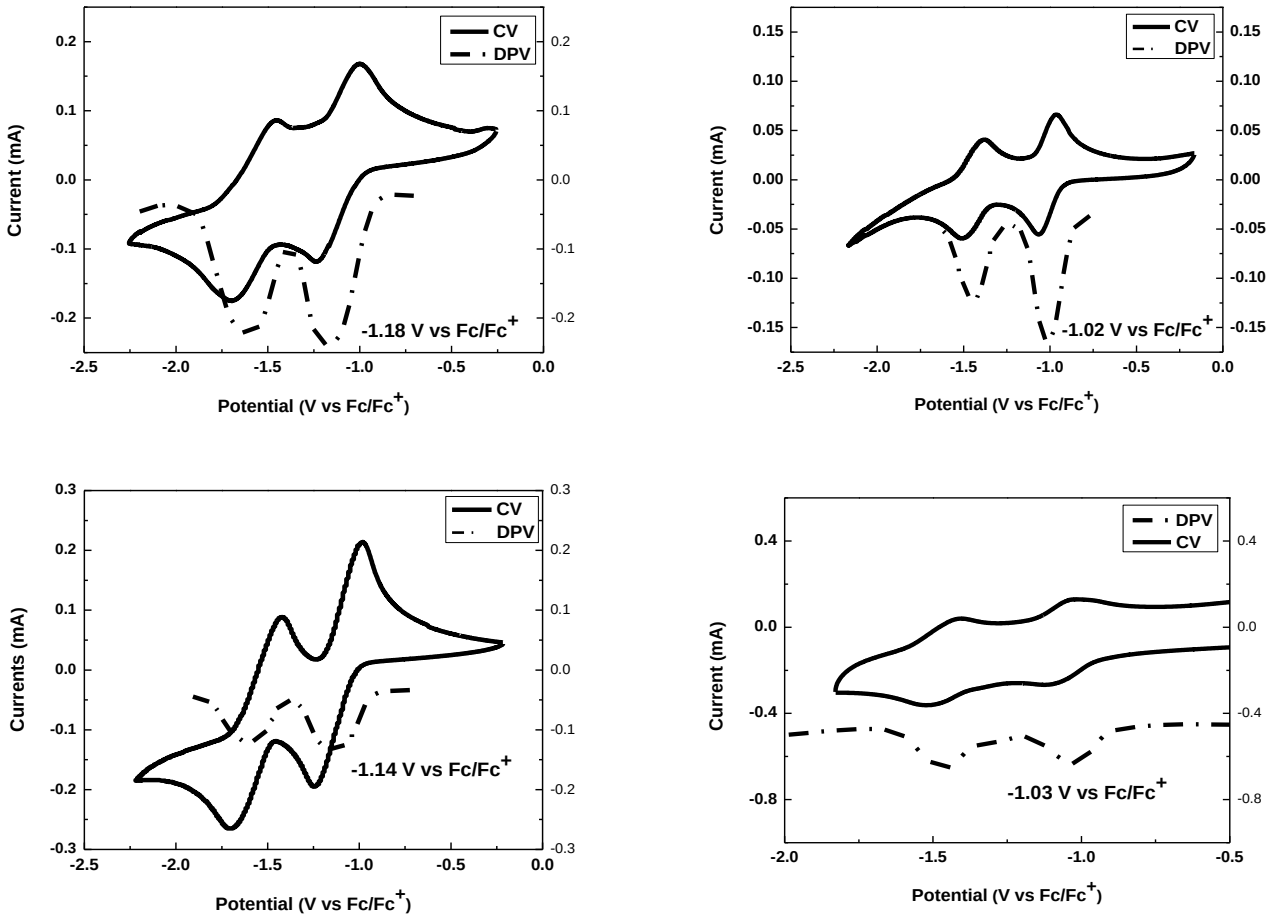

Figure 2.5 CV and DPV voltammograms of SCPDT-NDI_4, SDTG-NDI_4, DCPT-NDI_4 and TTE-NDI_4 (clockwise) in dichloromethane (0.5 M $TBAPF_6$). CVs were recorded at 50 mV s^{-1} scan rate.

In order to quantify the total number of electrons transferred of non-fullerene acceptor in these two reduction processes, bulk electrolysis was employed in order to achieve complete

reduction of the electroactive species. In this potential coulometry measurement, the number total charges that were consumed by the electrode were estimated by tangent line of integrated resulting current, and the numbers of electrons transferred per molecule were then calculated by Faraday's Law:

$$Q=nFVC \qquad \text{Eq.(6)}$$

where Q is charge in C; *n* is the number of electrons transferred per molecule; F is Faraday's constant, 96487 C mol^{-1}; V is the solution volume in L; C is the concentration of electroactive species in mol L^{-1}. The quantitative electrochemistry results are indicated in the following figure:

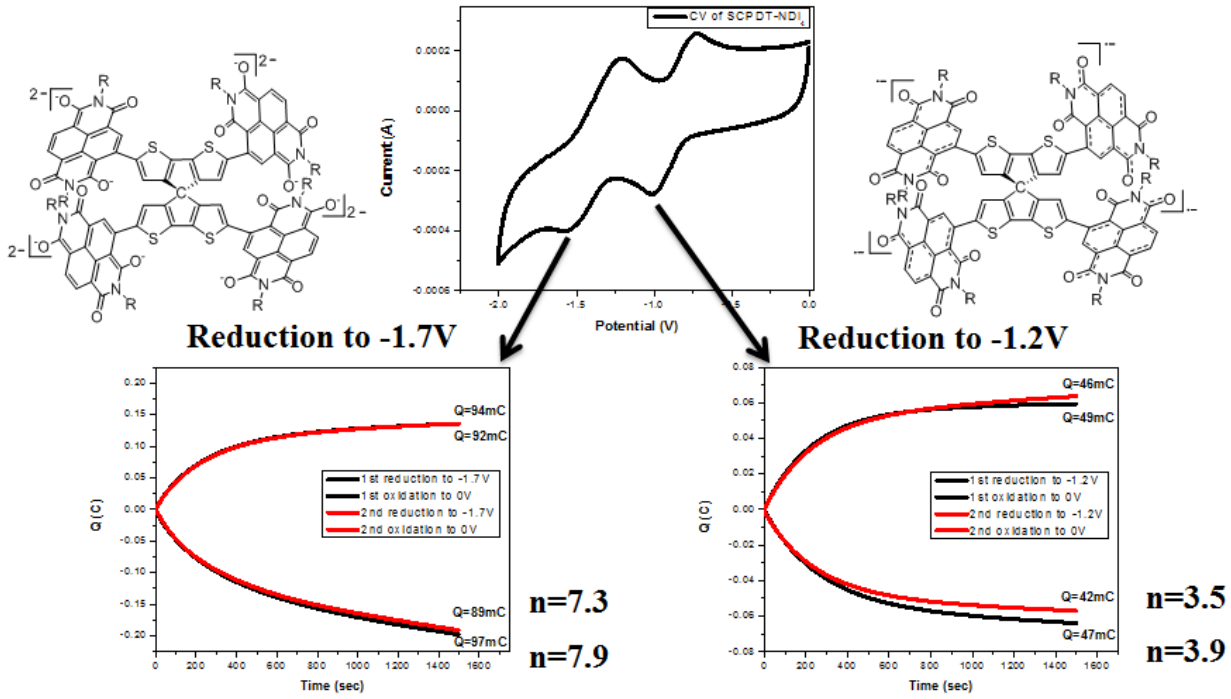

Figure 2.6 Plot of Q(C) vs. Time for the bulk electrolysis of $SCPDT\text{-}NDI_4$ in THF (0.1 M of $TBAPF_6$).

The potential coulometry study demonstrated that each NDI unit of the non-fullerene acceptor was simultaneously reduced to monoanion at -1.2 V resulting in a molecular tetraanion

(n~4), that then undergoes a second reduction at each NDI to give dianions at -1.7 V resulting in a molecular octaanion (n~8). This is consistent with literature reported two-electron successive reduction process of monomeric NDIs, and with negligible NDI-NDI electronic or electrostatic interactions.[67] This result demonstrates that these non-fullerene acceptors have the capability of accepting multiple electrons, which is comparable with fullerene's ability of six-electrons reduction.[69, 70] Table 2.4 summarize the key optoelectronic measurements results in this section:

Table 2.4 Summary of optoelectronic properties of NDI based non-fullerene acceptors.

	λ_{max} (nm)[a]	λ_{onset} (nm)[a]	ε_{max} (10^4 $M^{-1}cm^{-1}$)	reduction potential (V) vs. Fc/Fc^{+}[b]	$E_{g,opt}$ (eV)[c]
SCPDT-NDI_4	384; 643	738	8.6; 3.1	-1.18	1.68
SDTG-NDI_4	383; 581	687	9.8; 2.9	-1.02	1.80
TTE-NDI_4	382; 593	724	9.0; 1.5	-1.14	1.71
DCPT-NDI_4	382; 620	751	9.4; 3.2	-1.03	1.65

[a)]Obtained from solution absorption data; [b)]Estimated by differential pulse voltammetry; [c)]Estimated based on solution absorption onset;

2.2.4 Thermal properties

Since the device fabrication process of OSCs often requires thermal treatment, it is important that organic semiconductors are thermally stable. The decomposition temperatures (estimated by 5% loss of sample weight) of these non-fullerene acceptors were determined by thermogravimetric analysis (TGA), and the results are shown in Figure 2.7. As shown in Figure 2.7, these materials are all thermally stable with decomposition temperatures higher than 320 ^{o}C. The fluctuation of the baselines can be attributed to stepwise weight loss at lower temperature, but no significant decomposition was observed until heating above 320 ^{o}C or higher. This

stepwise weight loss is also observed in other organic compounds in literature.[71] Differential scanning calorimetry (DSC) thermal analysis shown no melting or crystalline peaks on DSC traces (Figure 2.8), which possibly suggests that melting temperatures of these non-fullerene acceptors are higher than their decomposition temperatures.

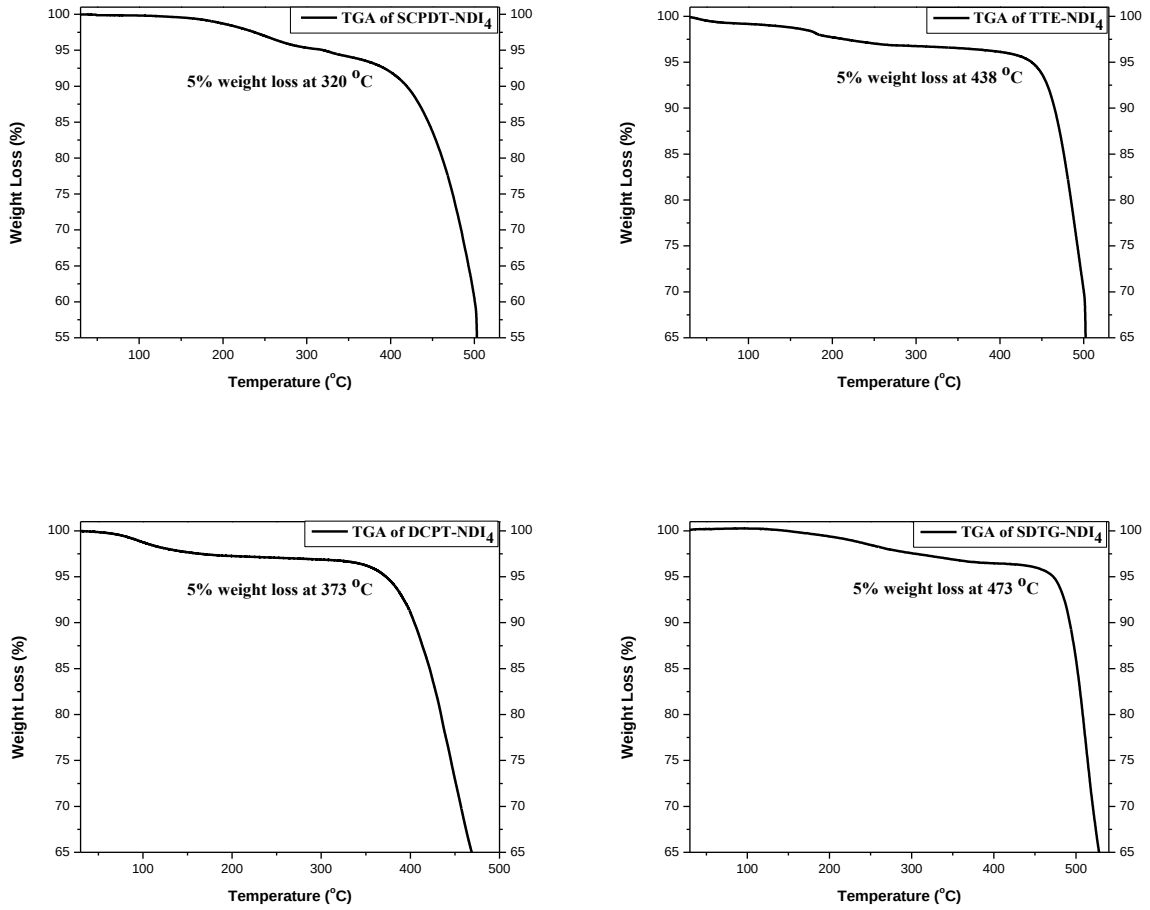

Figure 2.7 TGA of SCPDT-NDI_4, TTE-NDI_4, SDTG-NDI_4 and DCPT-NDI_4 (clockwise) with a heating rate of 10 ^{o}C/min under nitrogen flow.

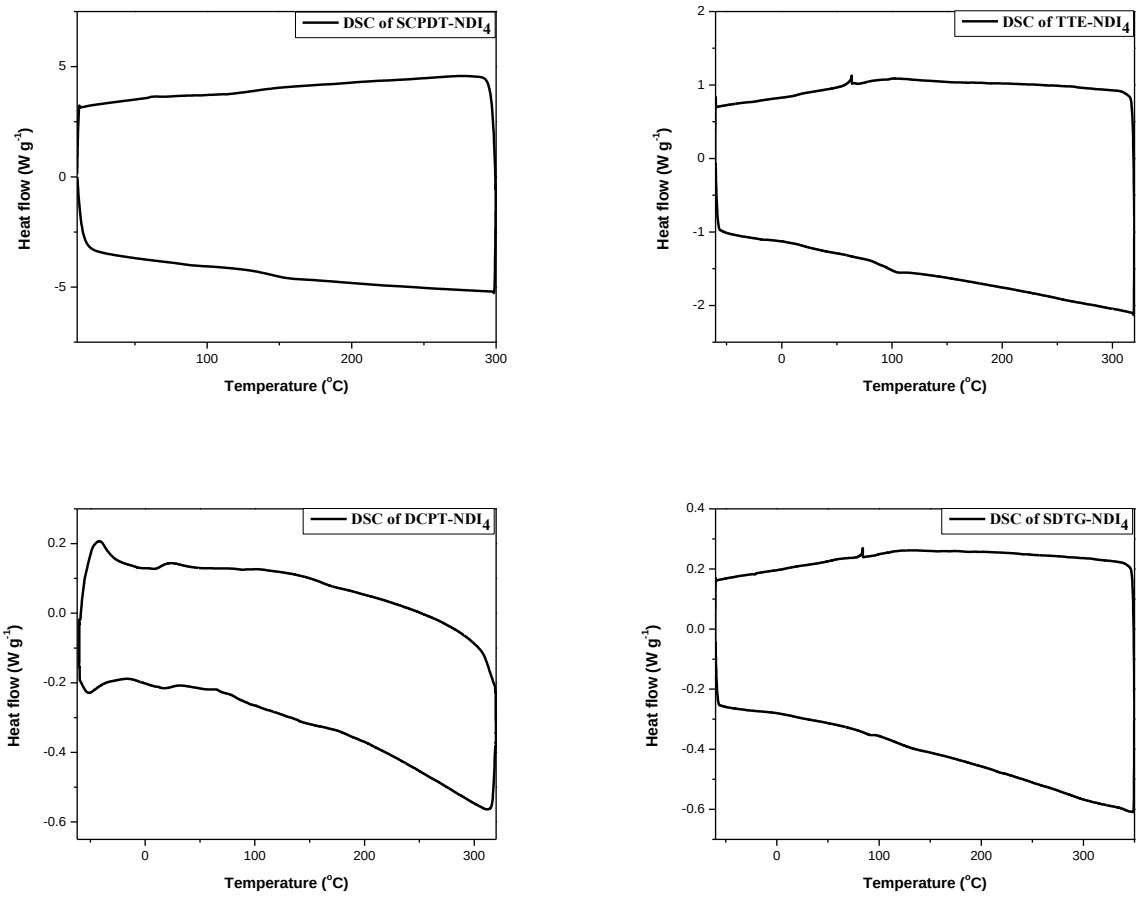

Figure 2.8 DSC thermograms at 10 min^{-1} for SCPDT-NDI_4, TTE-NDI_4, SDTG-NDI_4 and DCPT-NDI_4 (clockwise) in different temperature range.

2.2.5 Photovoltaic measurements (by Shruti Agarkar and Marcel Said)

Organic solar cell devices were fabricated by blending with PCE-11 donor, with an inverted device architecture of ITO/ZnO/PCE-11:non-fullerene acceptor/MoO_3/Ag. PCE-11 (polymer structure of PCE-11 in Figure 2.9) was chosen as the donor component because of its unique feature of morphology control through its temperature-dependent aggregation behavior. During the actual device fabrication, PCE-11:non-fullerene blends were processed at 110 ^oC then allowed to cool and dry during the film-casting process which potentially locks-in the length

scale of the morphology.[72] This process has been reported to enable the formation of reasonably small and pure donor domains of the polymer, and the polymer domains can still maintain high crystallinity.[72]

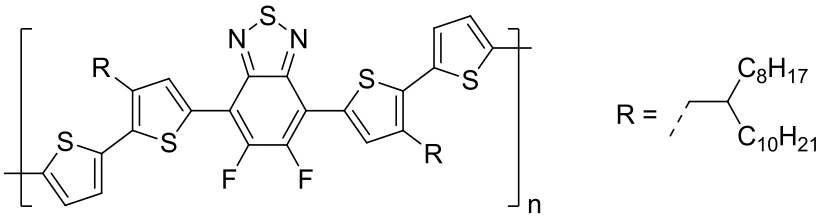

Figure 2.9 Polymer structure of PCE-11 donor.

The corresponding device *J*-*V* curves of NDI-based NFAs are shown in Figure 2.10 and detailed parameters are summarized in Table 2.5. By blending the NFAs with the donor polymer PCE-11, these non-fullerene acceptors have average PCEs between 1.3 to 2.6%. In comparison to the $PC_{61}BM$ based device that fabricated with the same condition, a V_{oc} of 0.70 V and a J_{sc} of 15.6 mA cm^{-2} were achieved. Comparing the four non-fullerene acceptors, TTE-NDI_4 has highest V_{oc}, which can be attributed to its low reduction potential that estimated by electrochemistry measurements, since the upper limit of V_{oc} is believed can be determined by energy differences between the IP of the donor and EA of the acceptor.[73] The germanium cruciform acceptor SDTG-NDI_4 has highest J_{sc}; the blue shifted ICT band of SDTG-NDI_4 (compared with other three non-fullerene acceptors) may possibly result in more complementary absorption with PCE-11, hence higher J_{sc}.

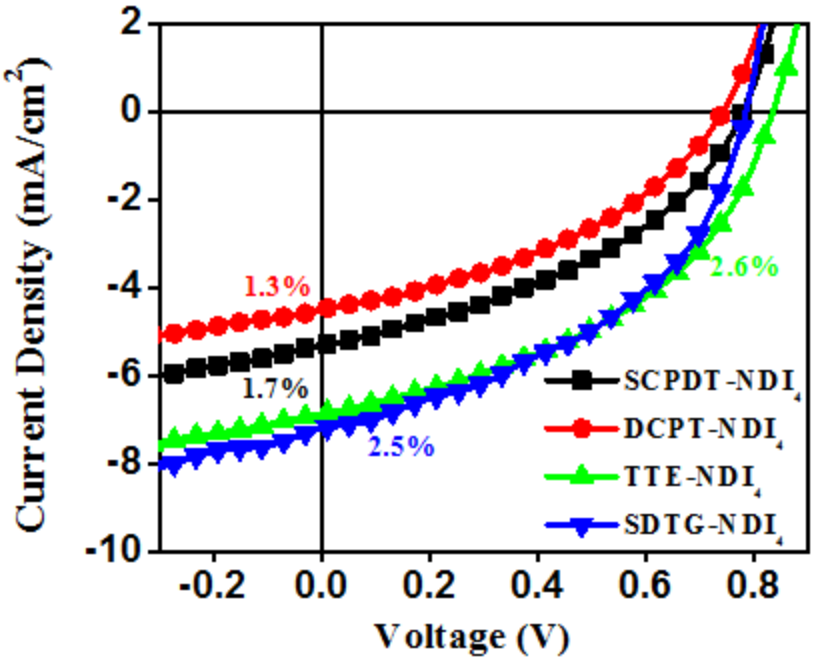

Figure 2.10 J-V curves for optimized PCE-11:SCPDT-NDI$_4$ (black), PCE-11:DCPT-NDI$_4$ (red), PCE-11:TTE-NDI$_4$ (green), and PCE-11:SDTG-NDI$_4$ (blue) devices under AM1.5G illumination.

Table 2.5 summarizes device parameters measured over 15 devices for each NDI-based NFAs (D/A ratio as 1:0.8; film prepared from solution of total concentration 11 mg/mL in 3:1 CD:DCB). Bold PCE in parenthesis are the highest PCE achieved for a single device. The highest V_{oc} achieved by TTE-NDI$_4$ device and highest J_{sc} by SDTG-NDI$_4$ device are highlighted in bold.

Table 2.5 Photovoltaic properties of solar cells for NDI-based non-fullerene acceptors.

Sample	V_{OC} (V)	J_{SC} (mA/cm^2)	FF (%)	PCE (%)
SCPDT-NDI$_4$	0.78 ± 0.03	5.3 ± 0.7	41 ± 2	(**2.0**) 1.7 ± 0.2
DCPT-NDI$_4$	0.74 ± 0.04	4.5 ± 0.2	40 ± 3	(**1.6**) 1.3 ± 0.2
TTE-NDI$_4$	**0.84** ± 0.02	6.9 ± 0.4	44 ± 2	(**2.9**) 2.6 ± 0.2
SDTG-NDI$_4$	0.79 ± 0.02	**7.2** ± 0.2	45 ± 2	(**2.8**) 2.5 ± 0.1

The external quantum efficiency (EQE) is the measurement of the ratio of generated charge carriers to number of photons of a given energy incident on the solar cell.[74] In Figure 2.11, EQE spectral shape shows strong contribution of absorptions from these non-fullerene acceptors (in the region labeled by the arrow in Figure 2.11). By examining EQE spectra of four non-fullerene acceptors, the EQE of SDTG-NDI_4 is the highest, exceeding 40% for a broad wavelength from 500 to 650 nm. Again, this can be partially attributed to the more complementary absorption of ICT band of SDTG-NDI_4 with the absorption of PCE-11 donor.

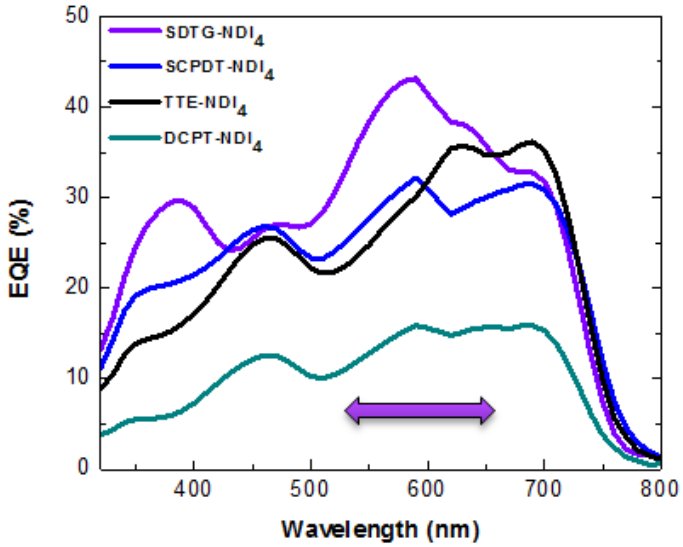

Figure 2.11 External quantum efficiency spectra of the optimized devices based on PCE-11:SCPDT-NDI_4 (blue), PCE-11:DCPT-NDI_4 (green), PCE-11:TTE-NDI_4 (black), and PCE-11:SDTG-NDI_4 (purple).

2.3 SUMMARY AND ON ONGOING WORK

The syntheses of NDI-based NFAs were successful and all new compounds were fully characterized. As a proof of concept, the nonplanar "push-pull" structure extended the absorption of NDI to the visible region by introducing of ICT bands, leading to broader absorptions than those of fullerenes. The main absorption peaks of these NDI-based NFAs are located in the visible region, which does not have great overlap with the solar spectrum maximum. This issue can be solved by substitution of perylene diimide, which have strong and intense absorption in the visible region; this will be covered in next chapter. Electrochemically, these materials are stable under reduction, and multi-electron reductions were observed by potential coulometry study. The estimated reduction potentials of these NDI based NFAs are slightly higher compared to $PC_{61}BM$ (-0.80 V[68]), which is consistent with the observation of high open circuit voltages in the devices. By blending with PCE-11, these materials are electron acceptors and produce average device efficiencies between 1.3-2.6 %. The EQE spectra of these materials indicated contributions of non-fullerene acceptors' absorptions. However, the overall device performances of these non-fullerene acceptors are still not comparable with fullerene; low J_{sc} is a common shortcoming for these four acceptors. Since J_{sc} is closely related to optical properties of the active layer, the weak absorption of NDI-based non-fullerene acceptor in the visible region or possibly inappropriate morphology of the active layer could be possible reasons for the low currents. A charge separation study by photoluminescence quenching and a transistor mobility measurement are still ongoing.

2.4 EXPERIMENTAL SECTION

2.4.1 Synthetic procedures and structural characterizations

Commercially available starting materials and reagents were purchased and used without further purification unless otherwise specified. PffBT4T-2OD (PCE-11) donor polymer was a gift from 1-Material. For water-sensitive reactions, commercially acquired anhydrous *o*-xylene and *N*,*N*-dimethylformamide were used. Diethyl ether and tetrahydrofuran were dried by distillation from sodium benzophenone ketyl after obtaining from a MBRAUN solvent purification system (MBRAUN-SPS). ^{1}H and $^{13}C\{^{1}H\}$ NMR spectra were recorded on a Bruker AMX 400 MHz spectrometer with chemical shift reference using the residual solvent resonance peak or internal standard tetramethylsilane (TMS, 0.0 ppm). Mass spectra were measured on an Applied Biosystems 4700 Proteomics Analyzer from Georgia Tech Mass Spectrometry Facility. Elemental analyses were carried out by Atlantic Microlab using a LECO 932 CHNS elemental analyzer. Chromatographic separations were performed with standard flash column chromatography methods using silica gel purchased from Sorbent Technologies (60 Å, 32-63 μm). For separation of final compounds, size exclusion column chromatography was performed with S-X1 resin purchased from Bio-Beads (molecular weight exclusion limits range from 400 to 14000).

2.6-2.8

A solution of naphthalene dianhydride (NDA) (13 g, 48.5 mmol) was suspended in concentrated sulfuric acid (500 mL) and was then heated to 55 ºC. In a separate flask, potassium dibromoisocyanurate (15.6 g, 48.5 mmol) was dissolved in concentrated sulfuric acid (280 mL) while stirring at room temperature for 1 h. Once dissolved, the solution was added to the reaction

flask and the mixture was allowed to stir at 85 ºC for 48 h. The mixture was poured into ice water (2.5 L) with care and stirred for another 2 h, while being allow to warm to room temperature. The resulting yellow precipitate was collected by filtration, washed with methanol, dried under vacuum (crude yield 13.1, used without purification). A mixture of brominated NDAs from previous step (13.11 g, crude), acetic acid (450 mL), and hexylamine (25.83 mL, 156.43 mmol) was refluxed for 2 h, then allowed to cool overnight, and poured into methanol (0.5 L) and filtered. Instead of purifying the brominated NDIs by column chromatography, the mixture was boiled in dichloromethane, followed by a hot filtration to remove small quantity of dark yellow solid, then concentrated and cooled down to allow recrystallization overnight. The solid was removed by filtration, and the filtrate was concentrated under reduced pressure to yield a pink solid (crude yield 13.6 g, used without purification).

A mixture of brominated NDIs from synthesis of **2.7** (14 g, crude), bis(tributyltin) (20.7 mL, 40.9 mmol), tri-*o*-tolylphosphine (1.66 g, 5.45 mmol), and dry toluene (300 mL) was deoxygenated with nitrogen for 5 min. $Pd_2(dba)_3$ (1.25 g, 1.36 mmol) was then added and the reaction was heated to 90 ^oC for 24 h. After cooling, the mixture was precipitated in methanol (500 mL), the solid was removed by filtration, and the solvent was concentrated under reduced pressure and collected. The final product NDI-$SnBu_3$ was purified by trimethylamine treated column chromatography (silica, 10% dichloromethane in hexane) by dry loading to afford an orange solid (4.8 g, yield 14% for three steps). ^1H NMR (400 MHz, $CDCl_3$) δ 8.97 (s, 1H), 8.74 (d, J = 7.6 Hz, 1H), 8.71 (d, J = 7.6 Hz, 1H), 4.22 (t, J = 8.0 Hz, 2H), 4.18 (t, J = 8.0 Hz, 2H), 1.76-1.69 (m, 4H), 1.57-1.51 (m, 6H), 1.44-1.32 (m, 18H), 1.28-1.20 (t, J = 8.2 Hz, 6H), 0.91-0.86 (m, 15H). The ^1H NMR spectrum of **2.8** was in agreement with the spectrum reported in the literature.[45]

2.9

2-Bromothiophene (14.7 g, 0.09 mol) was dissolved in 200 mL of anhydrous THF and the colorless solution was cooled to -78 ^{o}C. Freshly opened LDA (2.0 M in heptane/THF/ethylbenzene, 45 mL, 0.09 mol) was added dropwise and the mixture was stirred for 1 h. TMSCl (9.8 g, 0.09 mol) was added dropwise, stirred for 1 h and the formation of intermediate was checked by GC-MS (M.W.: 235 g/mol). LDA (55 mL, 0.11 mol) was then added dropwise to the mixture again over 0.5 h, and stir for another 0.5 h until suspension formed. GC-MS was checked again before addition of anhydrous $CuCl_2$ (14.8 g, 0.11 mol) in one portion. The dark green mixture was then allowed to stir at room temperature overnight. Hexanes and water were be added after the reaction was deemed to be complete, and organic phase was removed. The aqueous phase was extracted with hexane 3 times, combined with previous organic phase, dried over $MgSO_4$ and concentrated under reduced pressure. The crude product was dissolved in hexanes and filtered through a silica gel plug. The product was purified by distillation, during the purification by distillation, a white oil (impurity) was collected at a head temperature about 150 ^{o}C at 1 torr, then the desired product distilled at a head temperature at 165 ^{o}C as a yellow oil, which was then recrystallized in ethanol to afford a white bulk crystal (10.2 g, 48%). The purity of this compound was checked by GC-MS and the data is in agreement with spectrum reported in the literature.[61]

2.10-2.12

In a three-necked round bottom flask, 2-bromothiophene (5.9 mL, 61 mmol) and distilled ether (300 mL) was stirred and cooled to -78 ^{o}C, a solution of n-BuLi (2.5 M in hexane, 24.5 mL, 61 mmol) was added slowly to the mixture. The reaction mixture was stirred for 2 h at -78 ^{o}C, followed by dropwise addition of dimethylcarbamyl chloride (2.8 mL, 31 mmol) at -78 ^{o}C, and

the reaction mixture was allowed to warm up to room temperature overnight. The reaction mixture was quenched with water, extracted with ether 3 times, washed with water 2 times, then dried over $MgSO_4$, and concentrated under reduced pressure. This crude product **2.10** was purified by recrystallization in ether to afford needle like off-white crystals (3.88 g, 65%). ^{1}H NMR (400 MHz, $CDCl_3$) δ 7.91 (dd, J = 3.6 and 1.2 Hz, 2H), 7.71 (dd, J = 4.8 and 1.2 Hz, 2H), 7.19 (dd, J = 4.8 and 3.6 Hz, 2H). The ^{1}H NMR spectrum of **2.10** was in agreement with the spectrum reported in the literature.[62]

Titanium tetrachloride ($TiCl_4$) (14.1 mL, 129 mmol) was carefully added in distilled THF (165 mL) at 0 ^{o}C. Zinc dust (16.8 g, 257 mmol) was then added in after the solution was stirred at 0 ^{o}C for 30 min. The reaction mixture was refluxed at 85 ^{o}C for 2h. Then pyridine (10.4 mL, 129 mmol) was added, and the mixture was refluxed for another 1h. After cooling to room temperature, a solution of **2.10** (5.0 g, 26 mmol) in dry THF (45 mL) was added and the reaction mixture was refluxed at 90 ^{o}C for 3 days. The crude product was obtained by removing THF under reduced pressure, followed by treatment of 0.5 M HCl. The acidic mixture was extracted with toluene and dried over $MgSO_4$, and then filtered through an alumina pad with hot toluene. The filtrate was collected and washed by small amount of methanol to afford compound **2.11** as a red powder (500 mg, 22%). The physical data of **2.11** was in agreement with those reported in the literature.[62]

To a solution of 1,1,2,2-tetra(thiophen-2-yl)ethene **2.11** (0.5 g, 1.4 mmol) in THF (60 mL) was added *N*-bromosuccinimide (1.5 g, 8.5 mmol) in portions at 0 ^{o}C with shielding from the light. After 24 h, color of the mixture turned from deep red to light orange, with yellow precipitates forming at the bottom of the flask. The mixture was stirred for additional 12 h and concentrated, re-dissolved in dichloromethane, then washed with water. After drying over

$MgSO_4$, the collected solid was washed by ethanol to afford pale yellow powder **2.12** (0.87 g, 92%). ^{1}H NMR (400 MHz, $CDCl_3$) δ 6.92 (d, J = 4.0 Hz, 4H), 6.66 (d, J = 4.0 Hz, 4H); ^{13}C{^{1}H} NMR (100 MHz, $CDCl_3$) δ 143.94, 131.12, 130.00, 126.89, 115.91. HRMS (ESI) *m/z* calculated for $C_{18}H_8Br_4S_4$ (M^+), 667.6237; found, 667.6239. Anal. Calc. for $C_{18}H_8Br_4S_4$: C, 32.17; H, 1.20. Found: C, 32.45; H, 1.32.

2.13

A Grignard solution of 2-bromothiophene (4.80 mL, 49.60 mmol) and Mg (2.01 g, 82.7 mmol) in 60 mL of distilled ether was refluxed for 45 min under N_2. The Grignard solution was added dropwise under nitrogen over 1 h to a stirred and cooled suspension of 0.34 g Pd(dppf)Cl_2 DCM (0.34 mL, 0.41 mmol), and 2,3-dibromothiophene (4.68 mL, 41.3 mmol) in dry ether (40 mL). After stirring at 0 ^{o}C for 3 h, methanol (4 mL) was added and the mixture was filtered through a Na_2SO_4/silica gel double layer pad (~3 cm). The layer was further eluted with 20 ml dry ether, combined, and dried under reduced pressure. The residual oil was purified by silica gel chromatography with hexane/CCl_4 (98:2) to yield a green oil (9.6 g, 95%). ^{1}H NMR (400 MHz, $CDCl_3$) δ 7.42 (dd, J = 3.6 and 1.2 Hz, 1H), 7.36 (dd, J = 3.6 and 1.2 Hz, 1H), 7.20 (d, J = 5.2 Hz, 1H), 7.09 (q, J = 4.8 Hz, 1H), 7.02 (d, J = 5.2 Hz, 1H). The ^{1}H NMR spectrum of **2.13** was in agreement with the spectrum reported in the literature.[63]

2.14

N-bromosuccinimide (14.34 g, 80.59 mmol) was added at once to a solution of 3-bromo-2,2'-bithiophene (10.13 g, 41.33 mmol) in $CHCl_3$/AcOH (85 mL/ 65 mL) at room temperature. The mixture was stirred for 24 h, and the solvents were removed under reduced pressure. The residue was dissolved in DCM and washed with H_2O, 5% aqueous $NaHCO_3$, H_2O, brine and

dried over $MgSO_4$. The solution was concentrated under reduced pressure to afford a white solid (9.2 g, 55%). ^{1}H NMR (400MHz, $CDCl_3$) δ 7.42 (m, 2H), 7.36 (s, 1H). The ^{1}H NMR spectrum of **2.14** was in agreement with the spectrum reported in the literature.[63]

2.15

To a stirred solution of **2.14** (9.16 g, 22.7 mmol) in dry ether (150 mL) at -78 ^{o}C, n-BuLi (2.2 M in hexane, 20.7 mL, 45.5 mmol) was added dropwise over 15 min. The reaction mixture was stirred for 30 min at -78 ^{o}C, then slowly warmed up to -10 ^{o}C and stirred for another 5 h. Chlorotrimethylsilane (5.80 mL, 45.5 mmol) was added by syringe, and the mixture was stirred for 12 h at room temperature, and quenched with water. The crude product was extracted with ether and the organic layer was washed with water, brine, then dried over $MgSO_4$, and concentrated under reduced pressure. Purification using silica gel column chromatography in hexane afforded the product as a deep green oil (8.41 g, 95%). ^{1}H NMR (400 MHz, $CDCl_3$) δ 7.51 (d, J = 2.4 Hz, 1H), 7.20 (d, J = 2.4 Hz, 1H), 7.10 (s, 1H), 0.35 (s, 9H), 0.33 (s, 9H). The ^{1}H NMR spectrum of **2.15** was in agreement with the spectrum reported in the literature.[63]

2.16

N-Bromosuccinimide (17.42 g, 78.32 mmol) was added at once to a solution of 3-bromo-2,2'-bithiophene (9.60 g, 39.16 mmol) in $CHCl_3$/AcOH (85 mL/ 66 mL) at room temperature. The mixture was stirred for 24 h then the solvents were removed under reduced pressure. The residue was dissolved in DCM and washed with H_2O, 5% aqueous $NaHCO_3$, H_2O, brine and dried over $MgSO_4$. The solution was concentrated under reduced pressure to afford a white solid (8.7 g, 46%). ^{1}H NMR (400 MHz, $CDCl_3$) δ 7.05 (s, 2H). The ^{1}H NMR spectrum of **2.16** was in agreement with the spectrum reported in the literature.[63]

2.17

To a vigorously stirred refluxing mixture of **2.16** (8.74 g, 18.1 mmol) in 45 mL of ethanol with additional 4.5 mL of water, 11 mL of glacial acetic acid, and 1 mL of 3 M HCl aqueous solution, Zn powder (3.56 g, 54.4 mmol) was added in portions. After refluxing for 2 h, the mixture was filtered hot, followed by cooling down to 0 ^{o}C. The yellow crystals were collected. The crystals were then dissolved in ether, and washed three times with 25 mL of water and once with 10 mL of brine, then dried over $MgSO_4$ and concentrated under reduced pressure to yield a pink solid (3.5 g, 59%). ^{1}H NMR (400 MHz, $CDCl_3$) δ 7.41 (d, J = 5.2 Hz, 2H), 7.09 (d, J = 5.2 Hz, 2H). The ^{1}H NMR spectrum of **2.17** was in agreement with the spectrum reported in the literature.[63]

2.18

In a round bottom flask, **2.17** (3.50 g, 10.8 mmol) in ether (250 mL) was stirred and cooled at -78 ^{o}C; a solution of n-BuLi in hexane (2.2 M in hexane, 10.06 mL, 22.1 mmol) was added slowly. The reaction mixture was stirred for 2 h, and dimethylcarbamyl chloride (1.00 mL, 10.8 mmol) was added dropwise at -78 ^{o}C, and the reaction mixture was allowed to warm up to room temperature overnight. The reaction mixture was quenched with ice water, and extracted with ether 3 times and washed with water 2 times, then dried and concentrated under reduced pressure to afford a dark red residue. This raw material can be purified using column chromatography to afford a red solid (1.2 g, 56%). ^{1}H NMR (400 MHz, $CDCl_3$) δ 7.04 (d, J = 4.8 Hz, 2H), 6.99 (d, J = 4.8 Hz, 2H). The ^{1}H NMR spectrum of **2.18** was in agreement with the spectrum reported in the literature.[63]

2.19

2.18 (1.16 g, 5.91 mmol) was dissolved in 20 mL of THF and cooled to 0 ^{o}C, followed by addition of NBS (2.16 g, 12.1 mmol). The mixture was stirred for 45 min at 0 ^{o}C, and 3 h at room temperature. The reaction mixture was washed twice with water and brine, dried over $MgSO_4$ and concentrated under reduced pressure to afford a dark solid. The dark solid was boiled in methanol (10 mL) for 1 H. The residue was filtered on a Buchner funnel after cooled to room temperature to afford final product as dark-violet flakes (1.5 g, 72%). ^{1}H NMR (400 MHz, $CDCl_3$) δ 7.00 (s, 2H). The ^{1}H NMR spectrum of **2.19** was in agreement with the spectrum reported in the literature.[63]

2.20

To a stirred solution of **2.15** (8.41 g, 21.6 mmol) at -78 ^{o}C under nitrogen, n-BuLi in hexane (2.2 M, 9.58 mL, 21.0 mmol) was added dropwise. The reaction mixture was then warmed to -30 ^{o}C and stirred for an additional hour. The **2.19** (7.37 g, 21.06 mmol) was added at once and the reaction mixture was stirred for an additional 30 min at -30 ^{o}C. After 6 h, aqueous NH_4Cl was added. The organic layer was separated and washed with water, brine, dried over $MgSO_4$, and concentrated under reduced pressure. The residue was purified using column chromatography (hexane/DCM 5/4) affording an off-white foam, which was used without furthur purification for next step (13.9 g). ^{1}H NMR (400MHz, $CDCl_3$) δ 7.58 (s, 1H), 6.87 (d, 1H), 6.80 (s, 2H), 6.42 (d, 1H), 2.44 (s, 1H), 0.33 (s, 9H), 0.30 (s, 9H). The ^{1}H NMR spectrum of **2.20** was in agreement with the spectrum reported in the literature.[63]

2.21

The carbinol **2.20** (4.07 g, 6.16 mmol) in $CHCl_3$ (100 mL) was cooled to -78 ^{o}C under nitrogen. NBS (2.52 g, 14.20 mmol) was added at once. The reaction was stirred at -30 ^{o}C for 2 h

and slowly warmed to room temperature. Aqueous $Na_2S_2O_3$ and DCM were added. The organic layer was washed with water, brine, then dried over $MgSO_4$ and concentrated under reduced pressure. The crude product was purified on silica gel column chromatography (hexane/DCM, 1/1) to afford an off-white foam (1.9 g, 45%). ^{1}H NMR (400 MHz, $CDCl_3$) δ 7.35 (s, 1H), 6.84 (s, 2H), 6.76 (d, J = 3.6 Hz, 1H), 6.24 (d, J = 3.6 Hz, 1H), 2.40 (s, 1H). The ^{1}H NMR spectrum of **2.21** was in agreement with the spectrum reported in the literature.[63]

2.22

To a boiling solution of **2.21** (100 mg, 0.15 mmol) in chloroform (200 mL), $FeCl_3$ (6 mg, 0.04 mmol) was added under nitrogen. The mixture was boiled for 20 min and quickly cooled to room temperature. The residue solvent was removed and the solid was purified using silica gel column chromatography (hexane/DCM, 1/1) followed by size exclusion column chromatography (THF) to afford an off-white solid (50 mg, 51%). ^{1}H NMR (400 MHz, $CDCl_3$) δ 6.55 (s, 4H); ^{13}C{^{1}H} NMR (100 MHz, $CDCl_3$) δ 147.0, 138.9, 124.3, 112.7, 53.6. The ^{1}H and ^{13}C NMR spectrum of **2.22** was in agreement with the spectrum reported in the literature.[63]

SCPDT-NDI$_4$, TTE-NDI$_4$, and SDTG-NDI$_4$

General procedure for syntheses of naphthalene diimides (NDIs) based non-fullerene acceptors: SCPDT-Br_4 (45 mg, 0.07 mmol), NDI-$SnBu_3$ (298 mg, 0.41 mmol), and CuI (1 mg) were added into a microwave vial with a mixture of anhydrous o-xylene/DMF (8:1, v/v, 4.5 mL). Nitrogen was passed through the mixture for 15 min with stirring, followed by addition of $Pd(PPh_3)_4$ (16 mg, 0.01 mmol). The vial was then sealed and reacted in the CEM Discover MW reactor system at 250 W, 150 ^{o}C for 1 h. After cooling to room temperature, the crude product was participated into methanol (25 mL) and filtered. The crude product was purified by silica gel

column chromatography (DCM/hexane, 8/2) twice, and then further purified by preparative thin layer chromatography (in DCM) two times to afford final product as deep blue solid (14-42%).

SCPDT-NDI$_4$. Deep blue solid (yield 31-36%). ^{1}H NMR (400 MHz, $CDCl_3$) δ 8.74 (m, 12H) 7.22 (s, 4H), 4.14 (m, 16H), 1.67 (m, 16H), 1.30 (m, 48H), 0.82 (m, 24H); $^{13}C\{^1H\}$ NMR (100 MHz, $CDCl_3$) δ 162.90, 162.55, 162.41, 150.83, 143.29, 140.27, 136.51, 131.54, 130.46, 128.25, 126.76, 126.58, 126.07, 125.45, 124.51, 122.21, 41.19, 31.60, 28.12, 26.82, 22.52, 13.98. HRMS (MALDI) *m/z* calculated for $C_{121}H_{121}N_8O_{16}S_4$ (M^+H), 2069.7849; found, 2069.7783. Anal. Calc. for $C_{121}H_{120}N_8O_{16}S_4$: C, 70.19; H, 5.84; N, 5.41. Found: C, 69.99; H, 6.06; N, 5.19.

TTE-NDI$_4$. Dark green solid (yield 17-42%). ^{1}H NMR (400 MHz, $CDCl_3$) δ 8.79 (d, J = 7.6 Hz, 4H), 8.73 (d, J = 7.6 Hz, 4H), 8.66 (s, 4H), 7.31 (d, J = 4.0 Hz, 4H), 7.28 (d, J = 4.0 Hz, 4H) 4.07 (t, J = 7.6 Hz, 8H), 3.97 (t, J = 7.6 Hz, 8H), 1.62-1.56 (m, 16H), 1.37-1.17 (m, 48H), 0.86 (t, J = 6.6 Hz, 12H), 0.77 (t, J = 6.6 Hz, 12H); $^{13}C\{^1H\}$ NMR (100 MHz, $CDCl_3$) δ 162.85, 162.58, 162.54, 161.99, 145.58, 144.36, 140.28, 136.35, 131.63, 131.36, 130.65, 128.60, 128.12, 128.07, 127.09, 126.58, 126.36, 125.27, 123.56, 41.11, 41.03, 31.58, 31.55, 29.81, 28.07, 28.02, 26.81, 26.65, 22.63, 14.16, 14.11. HRMS (MALDI) *m/z* calculated for $C_{122}H_{124}N_8O_{16}S_4$ (M^+), 2084.7937; found, 2084.8018. Anal. Calc. for $C_{122}H_{124}N_8O_{16}S_4$: C, 70.22; H, 5.99; N, 5.37. Found: C, 70.51; H, 6.13; N, 5.18.

SDTG-NDI$_4$. Dark purple solid (yield 14-15%). ^{1}H NMR (400 MHz, $CDCl_3$) δ 8.81 (d, J = 7.6 Hz, 4H), 8.79 (s, 4H), 8.74 (d, J = 7.6 Hz, 4H), 7.46 (s, 4H), 4.20-4.14 (m, 16H), 1.76-1.69 (m, 16H), 1.41-1.25 (m, 48H), 0.87 (t, J = 7.2 Hz, 12H), 0.83 (t, J = 7.2 Hz, 12H); $^{13}C\{^1H\}$ NMR (100 MHz, $CDCl_3$) δ 162.91, 162.58, 162.52, 162.31, 151.63, 143.40, 139.91, 136.55, 136.45, 132.16, 131.61, 130.66, 128.14, 126.91, 126.69, 126.39, 125.57, 122.85, 41.39, 41.09, 31.61,

31.60, 29.82, 28.13, 28.11, 26.90, 26.82, 22.69, 22.64, 14.16. HRMS (MALDI) *m/z* calculated for $C_{120}H_{120}N_8O_{16}S_4Ge$ (M^+), 2130.6816; found, 2130.6917. Anal. Calc. for $C_{120}H_{120}N_8O_{16}S_4Ge$: C, 67.63; H, 5.68; N, 5.26. Found: C, 67.61; H, 5.87; N, 5.07.

2.4.2 Optical and electrochemical measurements

UV-Vis-NIR spectroscopic data were collected in chloroform (spectroscopic grade) on an Agilent Cary 5000 spectrometer in 1 cm quartz cuvette. Film absorption spectra were measured on spin coated 1''×1'' glass slides. Electrochemical measurements were carried out inside nitrogen filled glove box in dry deoxygenated dichloromethane solution containing 0.5 M tetrabutylammonium hexafluorophosphate ($TBAPF_6$) as electrolyte, using an EG&G Princeton Applied Research model 273A potentiostat-galvanostat. The electrochemical cell had an Ag/Ag^+ electrode as the reference electrode (inner solution of 10 m M of $AgNO_3$ in 0.5 M $TBAPF_6$-ACN; outer solution of 0.5 M $TBAPF_6$-ACN), a platinum coil as the counter electrode, and working electrode of platinum disk electrode (0.02 cm^2). The electrochemical calibration was done by measuring the oxidation potential of ferrocene/ferrocenium (Fc/Fc^+) in electrolyte solution versus Ag/Ag^+ electrode. EAs were estimated as EA ≈ E_{red} (vs. Fc/Fc^+) + 4.8 eV.

2.4.3 Bulk electrolysis

Bulk electrolysis cell was purchased from BASi, included a 75 mL glass cell with Teflon cap, counter electrode chamber, port plug, and reticulated vitreous carbon working electrode. The counter and reference electrodes are a platinum coil and an Ag/Ag^+ electrode as the reference electrode (inner solution of 10 mM of $AgNO_3$ in 0.5 M $TBAPF_6$-ACN; outer solution of 0.5 M $TBAPF_6$-ACN). Anhydrous tetrahydrofuran was freeze-pump-thaw three times before

transfer into the glove box. The total charge consumed by the electrode was estimated by tangent line of integrated resulting current, after subtraction of background charges.

CHAPTER 3 PERYLENE DIIMIDE-BASED NON-FULLERENE ACCEPTORS WITH TETRATHIENYLETHYLENE (TTE) CORE

3.1 INTRODUCTION

Perylene diimide (PDI) based non-fullerene acceptors have achieved high power conversion efficiencies up to ~9% in recent published literature.[75-77] For example, a structure of a BDT-Th core substituted with four PDI units that was reported to give a PCE of 8.47% by Luping Yu group (**3.1**)[77], which was the first literature example of 3D shaped non-fullerene acceptor with a thiophene-based donor core unit. PDI has its maximum absorption peak located in the visible region (about 530 nm), a decent electron affinity of 3.91 eV (compared to 3.90 eV for NDI). In addition, the larger molecular surface area of PDI favors π-packing, which might facilitate the formation of suitable morphology with appropriate selection of donor materials. Another PDI derivative, PDIS, was recently reported by Wang and coworkers.[78] PDIS has a sulfur bridge that links two bay positions of the PDI, and the dimer of PDIS (**3.2**) has shown superior device performance compare to regular PDI dimer.[78] Comparing the differences in properties between PDI and PDIS, the PDIS dimer has a more twisted molecular conformation that might facilitate more efficient intermolecular π-packing.[78] It also has lower estimated electron affinity than the PDI dimer, which may increase the upper limit of the obtainable V_{oc}. PDIS dimer has a blue shifted absorption in comparison to PDI dimer and as such, the PDIS absorption is more complementary to those of low optical gap polymers donors such as PCE-11.[78] However, device parameters and characterizations of the differences between these PDI and PDIS dimers were not included in the work by Wang and co-workers, and the reason why PDIS NFAs perform better than analogous PDI NFAs is still unclear. In this chapter, both PDI and PDIS were attached to the tetrathienylethylene core, and the optoelectronic properties of these materials will be compared and discussed.

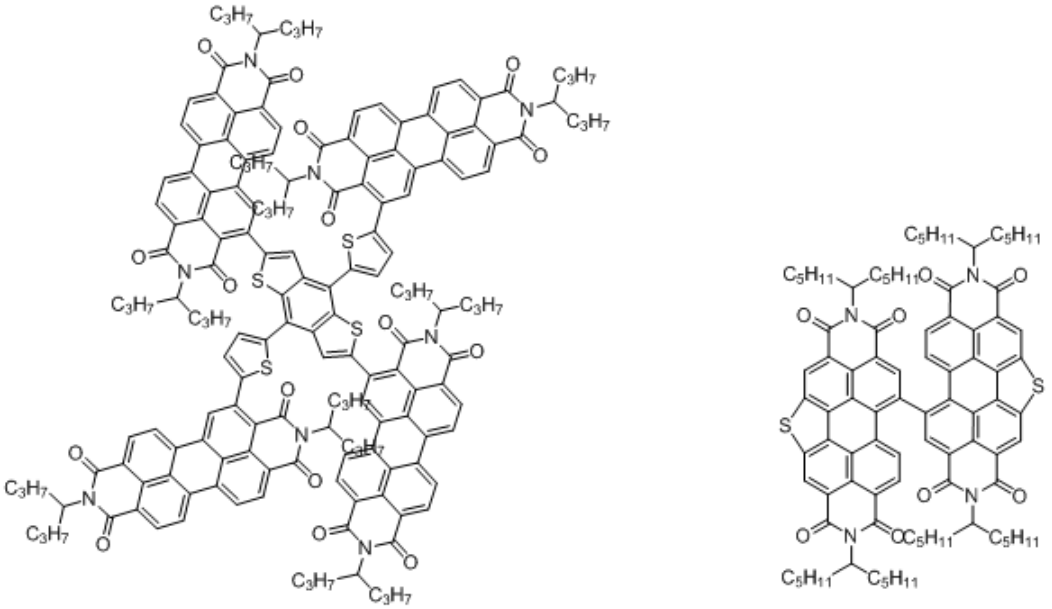

Figure 3.1 Perylene diimide-based non-fullerene acceptors in recent literature.

Tetrathienylethylene (TTE) was chosen as the core unit since it achieved the highest device performance compared to other three cores (carbon and germanium spiro cores and the fulvalene core) for NDI based non-fullerene acceptors. In addition, TTE-Br_4 can be easily synthesized on appreciable scale in three steps without the laborious purification processes required for other cores. The next section will cover the synthesis and optoelectronic properties, as well as initial device results of TTE-PDI_4 and TTE-$PDIS_4$.

3.2 RESULTS AND DISCUSSION

3.2.1 Material syntheses

The preparation of PDI based non-fullerene acceptors (Scheme 3.1) were assembled in the opposite manner as those described in the previous chapter, where the Sn groups are on NDI and halogens are on the cores. Due to the high reactivity of *bay* position of PDI, stannylation or

borylation of the PDI *bay* position are still challenging (PDI homocoupling was observed as major reaction when dibromo-PDI is subjected to stannylation conditions[79a]). Therefore, attempts were made for 4-fold stannylation or borylation of the TTE core. Borylation was first attempted under standard conditions, but multiple TLC spots were observed with no presence of major product (according to the area of each spot on TLC). Instead of separating the borylated mixtures, the stannylation was attempted and gave that desired tetrasubstituted TTE-$(SnMe_3)_4$ **3.1** in excellent yields (83-87%). TTE-PDI_4 and TTE-$PDIS_4$ were then synthesized by Stille coupling reaction under microwave conditions as for syntheses of NDI-based NFAs in chapter 2. The same problem of obtaining both the tri-substituted and tetra-substituted compounds was observed for the PDI NFA, which was previously described for analogous NDI-based NFA, as observed by mass spectrometry. Furthermore, the chromatographic separation of the tri-substituted product from the tetra-substituted product was problematic because many of the fractions containing the tetra-substituted product were contaminated with the tri-substituted product. The final compounds were purified by utilizing multiple chromatography techniques such as silica gel column chromatography, preparative thin layer chromatography, and size-exclusion chromatography.

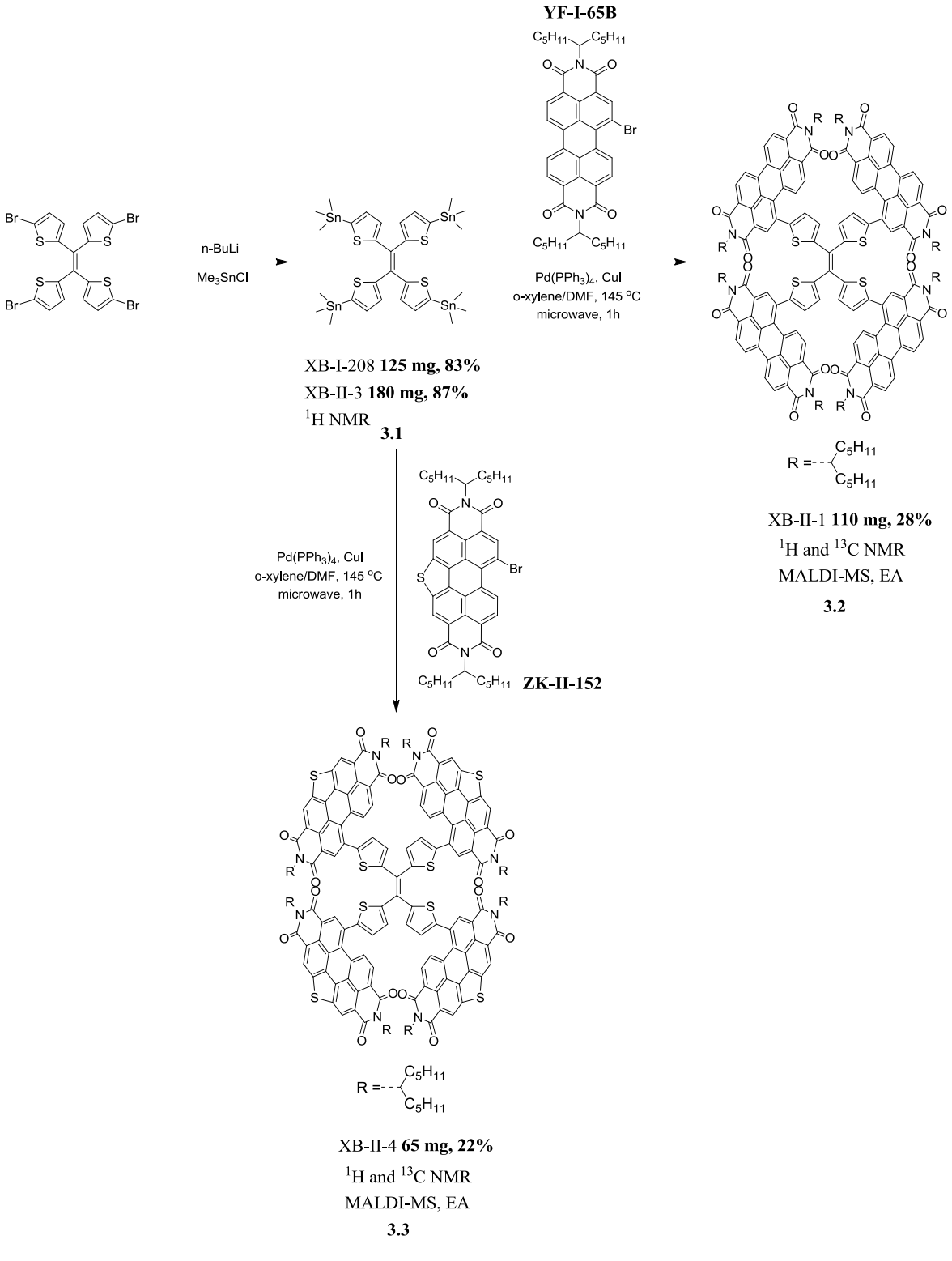

Scheme 3.1 Synthesis of PDI based non-fullerene acceptors TTE-PDI_4 and TTE-$PDIS_4$.

3.2.2 Optical and electrochemical properties

In comparison with TTE-NDI_4, the PDI-based NFAs have broader and stronger absorption bands in the visible region of the spectrum (Figure 3.2). In solution, the spectrum of TTE-PDI_4 has an absorption maximum at 526 nm, and TTE-$PDIS_4$ has its maximum at 503 nm, with possible overlap of ICT bands on the high wavelength side of the spectra. This ICT band feature is consistent with absorptions of PDI containing donor-acceptor conjugated systems in literature.[79b] It is also consistent with literature that PDIS based compounds have blue shifted absorptions relative to PDI based compounds. The blue shifted of TTE-$PDIS_4$ absorption could result in more complementary absorption with low optical gap polymers such as PCE-11. In addition, by comparing absorption spectra in solution and in films, similar peak positions suggest weak aggregation of these compounds in the solid state.

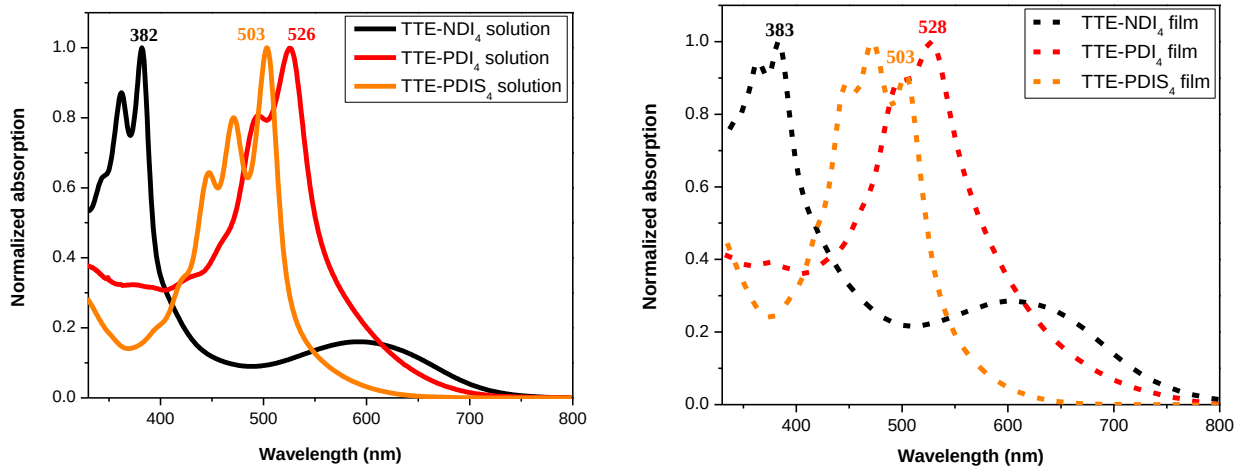

Figure 3.2 UV-vis spectra of three TTE core non-fullerene acceptors, solution absorptions were taken in chloroform.

Upon going from solution to a film, the TTE-PDI_4 main absorption peak barely shifted (from 526 nm to 528 nm), TTE-$PDIS_4$ has an absorption peak at the same position at 503 nm, but a change in vibronic structures. The molar absorptivities of three TTE core acceptors are

summarized in Table 3.1, the strength of TTE-PDIS$_4$ (1.1×10^5 $M^{-1}cm^{-1}$) absorption is comparable with that of TTE-PDIS$_4$ (1.2×10^5 $M^{-1}cm^{-1}$), which is inconsistent with literature reported dramatic increase of extinction coefficients of PDIS dimer in comparison with that of the PDI dimer.[78] To determine whether the sample solutions were pre-aggregated, temperature dependent UV-vis measurements were performed. In this experiment, spectra were collected as the temperatures were increased from 25 to 85 ^oC in 10 ^oC increments. As shown in Figure 3.3, there are no significant shifts of peak positions of these three acceptors' solution absorptions. The same observations were also made in concentration-dependent absorption experiments.

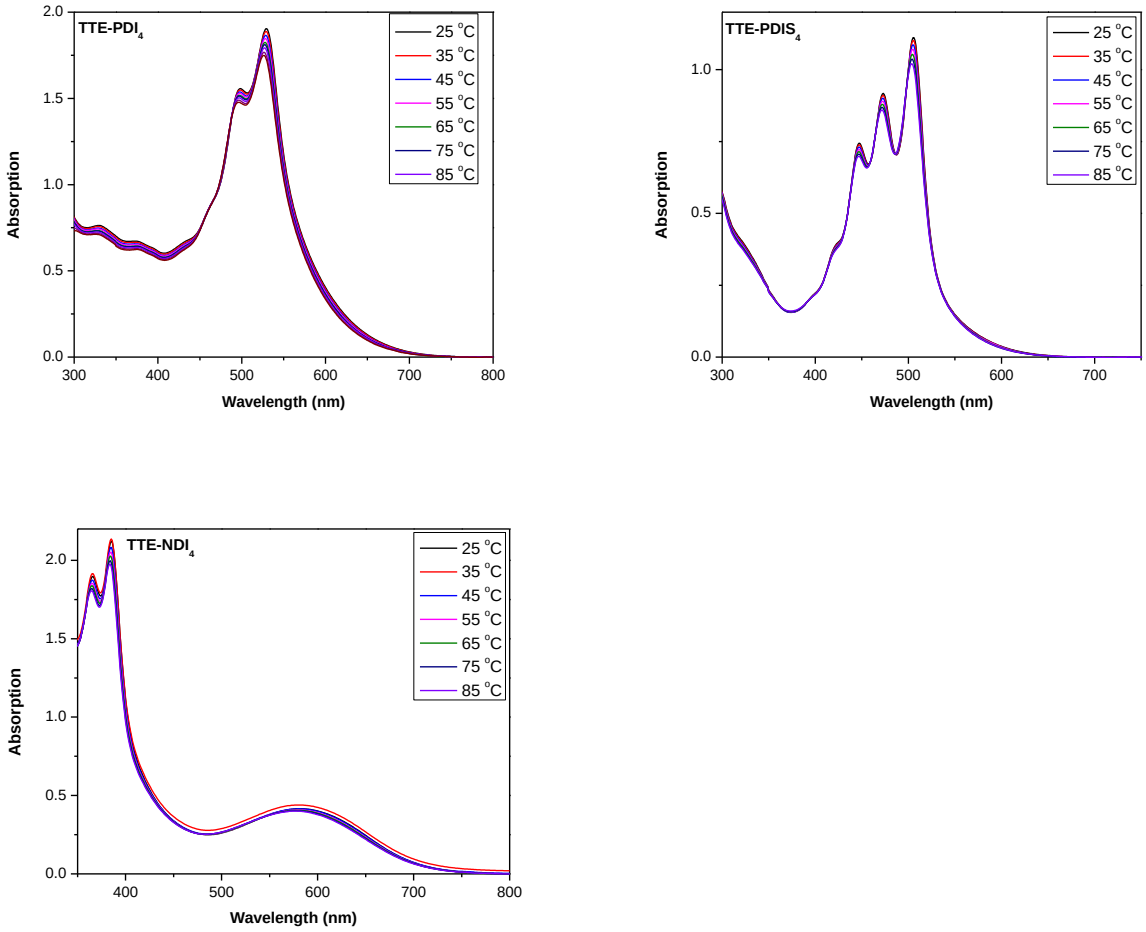

Figure 3.3 Temperature dependent UV-vis spectra of TTE core non-fullerene acceptors in chloroform.

The cyclic voltammograms of the three TTE core non-fullerene acceptors are plotted in Figure 3.4. All three compounds showed reversible multiple-electron reduction processes. It is not surprising that both TTE-NDI_4 and TTE-PDI_4 have eight-electron reductions since each NDI and PDI are able accept two electrons, as supported the quantitative electrochemistry result in Chapter 2. By comparing reduction potentials of three materials, PDI based NFAs are estimated to have very similar reduction potentials (-1.03 and -1.09 eV) in comparison to their NDI analog (-1.14 eV), which is consistent with quantum chemical calculations values from the literature.[80] TTE-$PDIS_4$ has a slightly deeper larger reduction potential compared to that of TTE-PDI_4; this can be attributed to LUMO destabilization by increased electron density of incorporating sulfur bridges.

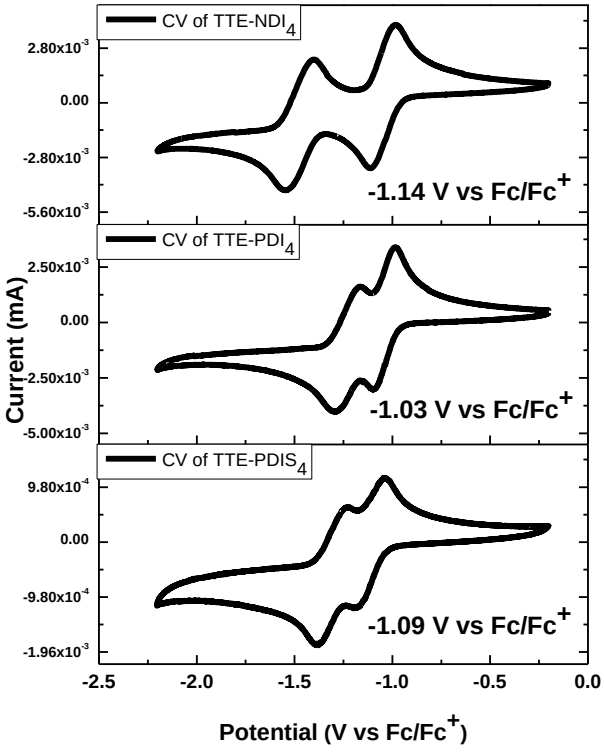

Figure 3.4 Cyclic voltammograms of TTE core non-fullerene acceptors in dichloromethane (0.5 M $TBAPF_6$), at 50 mV/s scan rate.

Table 3.1 Summary of optoelectronic properties of TTE core non-fullerene acceptors.

	λ_{max} (nm)[a]	λ_{onset} (nm)[a]	ε_{max} ($M^{-1}cm^{-1}$)	Reduction potential (V) vs. Fc/Fc^{+}[b]	$E_{g,opt}$ (eV)[c]
TTE-PDI_4	526	873	1.1×10^5	-1.03	1.42
TTE-$PDIS_4$	503	805	1.2×10^5	-1.09	1.54
TTE-NDI_4	382; 593	724	9.0×10^4;1.5×10^4	-1.14	1.71

[a)]Obtained from solution absorption data; [b)]Estimated by differential pulse voltammetry; [c)]Estimated based on solution absorption onset for TTE-NDI_4, electrochemical gap from TTE-PDI_4 and TTE-$PDIS_4$ (due to the difficulty of estimating optical gap from solution absorption onsets).

3.2.3 Initial photovoltaic characterizations (by Shruti Agarkar)

Organic solar cell devices were fabricated by blending TTE core NFAs with PCE-11 donor, with an inverted device architecture of ITO/ZnO/PCE-11: NFA/MoO_3/Ag. PCE-11 was chosen again for device performance comparisons with the NDI analog. In addition, there is literature evidence of high performance (PCE ~ 6%) of PDI-based 3D-shaped NFAs with PCE-11 donor.[81] Figure 3.5 has plots of absorptions of three TTE core NFAs with PCE-11, the complementary absorptions of TTE-PDI_4 and TTE-$PDIS_4$ with the donor polymer might lead to improved light harvesting.

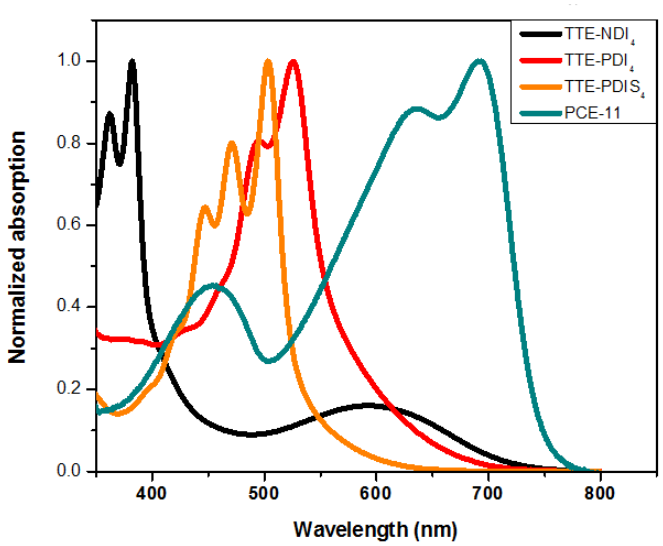

Figure 3.5 Overlap of absorptions PCE-11 donor and TTE core acceptors.

As expected, the TTE-PDI_4 device achieved a high V_{oc} of 0.83 V (Table 3.2) compare to $PC_{61}BM$ device fabricated under the same condition (V_{oc} of 0.70 V obtained), because of the large reduction potential (-1.03 V) of TTE-PDI_4. This device result is still very preliminary, and many of parameters such as spin speed, donor/acceptor ratio, and spin rates can still be further optimized. At this stage, not too many comments can be made for comparing the device results with NDI analogs.

Table 3.2 Initial device result for TTE-PDI_4:PCE-11 device.

	J_{sc} (mA/cm^2)	V_{oc} (V)	FF (%)	Efficiency (%)
TTE-PDI_4	4.2±0.5	0.83± 0.5	39 ±1	1.4 ±0.1

3.3 SUMMARY AND ONGOING WORK

Two perylene diimides based non-fullerene acceptors TTE-PDI_4 and TTE-$PDIS_4$ were synthesized and optoelectronic properties were compared with TTE-NDI_4. As expected, by incorporating PDI units, the absorptions of TTE-PDI_4 and TTE-$PDIS_4$ are mainly located in the visible region with possible overlap of ICT bands. The absorption of TTE-$PDIS_4$ blue shifted compared to that of TTE-PDI_4. The estimated reduction potentials of three TTE core NFAs are not significantly different. Initial device results do not indicate superior performance of PDI acceptors over NDIs, but the many device fabrication conditions are still being optimized, and there is still large room for improvement.

3.4 EXPERIMENTAL SECTION

3.4.1 Synthetic procedures and structural characterizations

Commercially available starting materials and reagents were purchased and used without further purification unless otherwise specified. PffBT4T-2OD (PCE-11) donor polymer was a gift from 1-Material. For water-sensitive reactions, commercially acquired anhydrous *o*-xylene and *N*,*N*-dimethylformamide were used. Diethyl ether and tetrahydrofuran were dried by distillation from sodium benzophenone ketyl after obtaining from an MBRAUN solvent purification system (MBRAUN-SPS). ^{1}H and $^{13}C\{^{1}H\}$ NMR spectra were recorded on a Bruker AMX 400 MHz spectrometer with chemical shift reference using the residual solvent resonance peak or internal standard tetramethylsilane (TMS, 0.0 ppm). Mass spectra were measured on an Applied Biosystems 4700 Proteomics Analyzer from Georgia Tech Mass Spectrometry Facility. Elemental analyses were carried out by Atlantic Microlab using a LECO 932 CHNS elemental analyzer. Chromatographic separations were performed with standard flash column chromatography methods using silica gel purchased from Sorbent Technologies (60 Å, 32-63 μm). For separation of final compounds, size exclusion column chromatography was performed with S-X1 resin purchased from Bio-Beads (molecular weight exclusion limits range from 400 to 14000).

PDIS-Br was synthesized by Kostiantyn Ziabrev (Marder group), and PDI-Br was obtained from Yali Fan (Marder group). The synthetic routes and detailed experimental procedures of these two compounds will not be included in this thesis.

3.1

n-BuLi (2.6 M in hexane, 0.52 mL, 0.44 mmol) was added dropwise to a solution of TTE-Br_4 (150 mg, 0.07 mmol) in THF (10 mL) at -80 °C. The resulting solution was stirred for 1.5 h at -80 °C followed by addition of $(CH_3)_3SnCl$ (1.0 M solution in hexane, 2.23 mL, 0.74 mmol) in one portion. The reaction mixture was stirred for 1 h at -80 °C and then warmed slowly to room temperature for 2 h. After the reaction was deemed to be complete by TLC, the mixture was poured into cold water and extracted with diethyl ether three times. The organic extracts were combined and dried over $MgSO_4$ and solvent was removed under reduced pressure to afford a deep green solid (125 mg, 83%). Due to the potential instability of this compound, it was quickly characterized by proton NMR and used as is immediately for the next step without any further purification. ^{1}H NMR (400MHz, $CDCl_3$) δ 7.02 (d, J = 3.6 Hz, 4H), 6.92 (d, J = 3.6 Hz, 4H), 0.32 (s, 36H).

3.2 (TTE-PDI_4)

TTE-$(SnMe_3)_4$ (65 mg, 0.06 mmol), PDI-Br (251 mg, 0.32 mmol) and CuI (1 mg) were loaded into a microwave vial followed by a mixture of o-xylene/DMF 8/1 (3.6 mL). Argon was passed through the reaction mixture for 15-20 min followed by addition of $Pd(PPh_3)_4$ (15 mg, 0.01 mmol). The reaction vial was sealed and heated in the CEM Discover MW reactor system at 250 W, 150 ^{o}C for 1 h. This reaction was monitored by TLC. Another batch of 65 mg of starting materials was prepared in the same method and combined before purifications. After completion of the reaction, the crude product was poured into 25 mL of methanol, filtered, dried under reduced pressure. The crude product was purified using silica gel column chromatography (hexane/ethyl acetate, 9/1) to remove most impurities. The product was further purified using size exclusion column chromatography (in THF) to give a dark red solid (110 mg, 28%). ^{1}H NMR (400 MHz, $CDCl_3$) δ 8.61-8.58 (m, 20H), 8.30 (d, J = 8.4 Hz, 4H), 8.05 (d, J = 5.6 Hz,

4H), 7.37 (d, J = 3.2 Hz, 4H), 7.26 (d, J = 3.2 Hz, 4H), 5.01 (m, 8H), 2.41-1.79 (m, 32H), 1.25-0.72 (m, 144H); $^{13}C\{^{1}H\}$ NMR (100 MHz, $CDCl_3$) δ 163.80, 147.05, 135.13, 134.40, 133.97, 133.03, 132.47, 129.63, 129.22, 129.19, 128.22, 127.62, 127.13, 123.72, 122.95, 32.38, 32.17, 31.83, 31.70, 29.85, 26.70, 26.58, 22.64, 22.58, 14.14, 14.11. HRMS (MALDI) *m/z* calculated for $C_{202}H_{220}N_8O_{16}S_4Na$ $(M^+Na)^+$, 3164.5245; found, 3164.5428. Anal. Calc. for $C_{202}H_{220}N_8O_{16}S_4$: C, 77.16; H, 7.05; N, 3.56. Found: C, 77.37; H, 7.43; N, 3.41.

3.3 (TTE-PDIS$_4$)

TTE-$(SnMe_3)_4$ (65 mg, 0.06 mmol), PDIS-Br (261 mg, 0.32 mmol) and CuI (1 mg) were loaded into the microwave vial followed by a mixture of o-xylene/DMF 8/1 (3.6 mL). Argon was passed through the reaction mixture for 15-20 min followed by addition of $Pd(PPh_3)_4$ (15 mg, 0.01 mmol). The reaction vial was sealed and heated in the CEM Discover MW reactor system at 250 W, 150 ^{o}C for 1 h. This reaction was monitored by TLC. After completion of the reaction, the crude product was poured into 25 mL of methanol, filtered, dried under reduced pressure. The crude product was purified using silica-gel column chromatography (dichloromethane/hexane, 2/1) to remove most impurities. The product was further purified using size exclusion column chromatography (THF) to give a dark red solid (65 mg, 22%). ^{1}H NMR (400 MHz, $CDCl_3$) δ 9.34 (d, J = 17.6 Hz, 4H), 9.12 (s, 4H), 8.89 (d, J = 20.8 Hz, 4H), 8.61 (d, $J_{app}{}^{a}$ = 7.6 Hz, 4H), 8.13 (s, 4H), 7.68 (s, 4H), 7.37 (s, 4H), 5.25-4.78 (m, 8H), 2.26-1.12 (m, 128H), 0.79-0.72 (m, 48H). $^{13}C\{^{1}H\}$ NMR (100 MHz, $CDCl_3$) δ 163.93, 147.20, 145.55, 138.36, 137.82, 133.57, 133.43, 132.74, 132.74, 132.30, 131.74, 131.43, 128.63, 127.25, 126.58, 125.83, 124.05, 122.72, 55.16, 54.86, 32.51, 31.90, 31.72, 26.76, 22.68, 22.62, 14.15, 14.08. Anal. Calc. for $C_{202}H_{212}N_8O_{16}S_8$: C, 74.32; H, 6.55; N, 3.43. Found: C, 74.33; H, 6.71; N, 3.34.

Due to the low intensity of $(M^+)^+$ signal in HRMS MALDI spectrum, accurate mass analysis cannot be performed on this compound.

[a] This coupling is consistent with literature ^{1}H NMR spectrum of PDIS dimer.[78]

3.4.2 Optical and electrochemical measurements

UV-Vis-NIR spectroscopic data were collected in chloroform (spectroscopic grade) on an Agilent Cary 5000 spectrometer in 1 cm quartz cuvette. Film absorption spectra were measured on spin coated 1''×1'' glass slides. Electrochemical measurements were carried out inside nitrogen filled glove box in dry deoxygenated dichloromethane solution containing 0.5 M tetrabutylammonium hexafluorophosphate ($TBAPF_6$) as electrolyte, using an EG&G Princeton Applied Research model 273A potentiostat-galvanostat. The electrochemical cell had an Ag/Ag^+ electrode as the reference electrode (inner solution of 10 m M of $AgNO_3$ in 0.5 M $TBAPF_6$-ACN; outer solution of 0.5 M $TBAPF_6$-ACN), a platinum coil as the counter electrode, and working electrode of platinum disk electrode (0.02 cm^2). The electrochemical calibration was done by measuring the oxidation potential of ferrocene/ferrocenium (Fc/Fc^+) in electrolyte solution versus Ag/Ag^+ electrode. EAs were estimated as EA ≈ E_{red} (vs. Fc/Fc^+) + 4.8 eV.

CONCLUSION AND OUTLOOK

This thesis covers design and synthesis of 3D shaped non-fullerene acceptors based on naphthalene and perylene diimides. By examining their optical properties, these acceptors have broader and more intense absorption compare to typical fullerenes, and the absorptions are overlapped better with the solar spectrum maxima. Electrochemically, these acceptors have larger reduction potentials in comparison to $PC_{61}BM$ (-0.80 V[68]), which might increase the upper limits of the obtainable V_{oc}. This is consistent with the OSC device results in Chapter 2, optimized NDI based acceptors have high V_{oc} range from 0.74 to 0.84 V. However, the overall device performance of these non-fullerene acceptors are still not comparable with fullerene, low J_{sc} is a common problem observed for these devices. Since J_{sc} is closely related to optical properties of the active layer[82], the relatively weak absorptions of NDI based non-fullerene acceptors at the visible region could be one possible reason for such low currents. In addition, it is well-known that morphology of the active layer plays an important role for exciton splitting and charge-carrier transport. High performance polymer-fullerene bulk heterojunction (BHJ) organic solar cells contain three-phase morphology, which includes pure polymer domain, pure fullerene domain, and mixed polymer/fullerene domain.[83] Possible inappropriate morphologies of the blend of these non-fullerene acceptors with PCE-11 may another reason for low performances.

As the non-fullerene acceptor field is rapidly moving forward, there are more literature examples investigating appropriate donor selection and tailor-made donors for fullerene free solar cell. Yan and co-workers pointed out state-of-art donor used in fullerene solar cells may not perform as well as with non-fullerene acceptors, since PCE-11 yielded 10.8% PCE with fullerene, but it only gives PCE of 4% with small molecule NFA ITIC.[4] In their recent work, Yan group re-

designed the state-of-art donor polymer PCE-11, by introducing a less symmetric monomer unit *para* difluorinated benzene to lower the crystallinity of the polymer. As the results, this new tailor-made donor polymer yield > 10% with non-fullerene acceptor ITIC, and only yield 6.5% of PCE with fullerene acceptor.[84]

These observations do not appear to be an exception. Back to the early days of non-fullerene acceptors, the bay-linked PDI dimer (PCE ~ 6%) is popularly recognized to perform better compare to hydrazine-linked PDI dimer (PCE < 5%) in combination of a variety of donors.[85,86] Jen and co-workers recently reported device results of these materials with PTB7-Th. As suggested by Jen, hydrazine-linked PDI dimer with more rigid structures can provide more suitable percolation pathways for charge transport hence higher device performance (PCE of 6.41%) compare with bay-linked PDI dimer, when PTB7-Th is used.[87] The more twisted bay-linked PDI dimer was found to disrupt the π-π stacking of PTB7-Th.[87] This work demonstrated the importance of pairing NFAs with appropriate donor materials.

Since a variety of different types of NFAs have been designed and synthesized, and in fact majority of donor polymers in this field now were designed for fullerene solar cells and such they may not be optimal for NFAs. The next step for research in this field may be to design tailor-made donor materials to complement with these NFAs, by tuning the energy level, the absorption window, and blend morphologies. Ultimately this may lead to a deeper understanding of the morphology of active layer, and establish new design rules for donor: NFA pairs.

APPENDIX

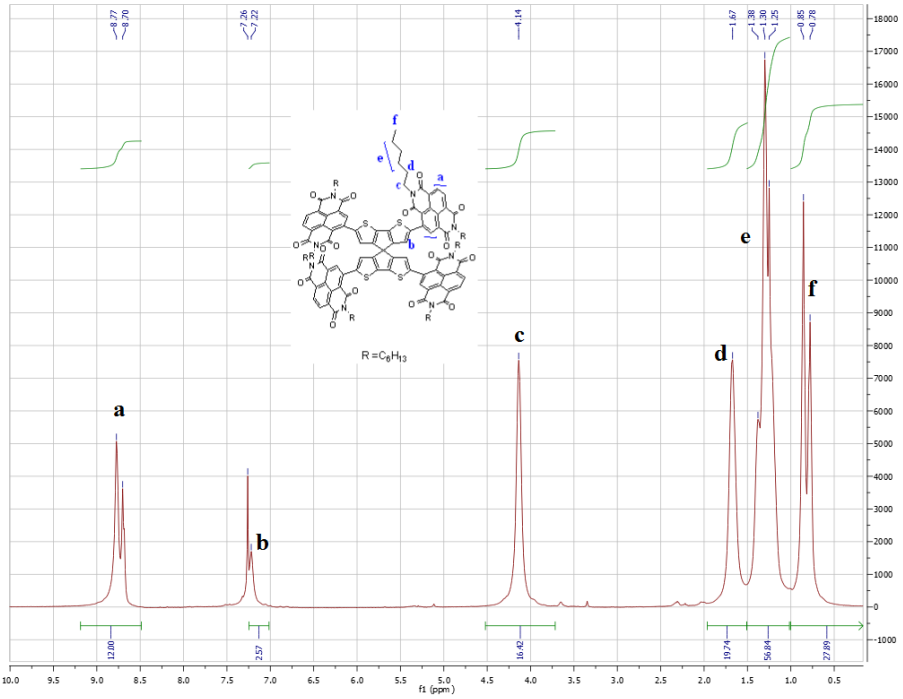

Figure A.1 ^{1}H NMR spectrum of SCPDT-NDI_4 in $CDCl_3$.

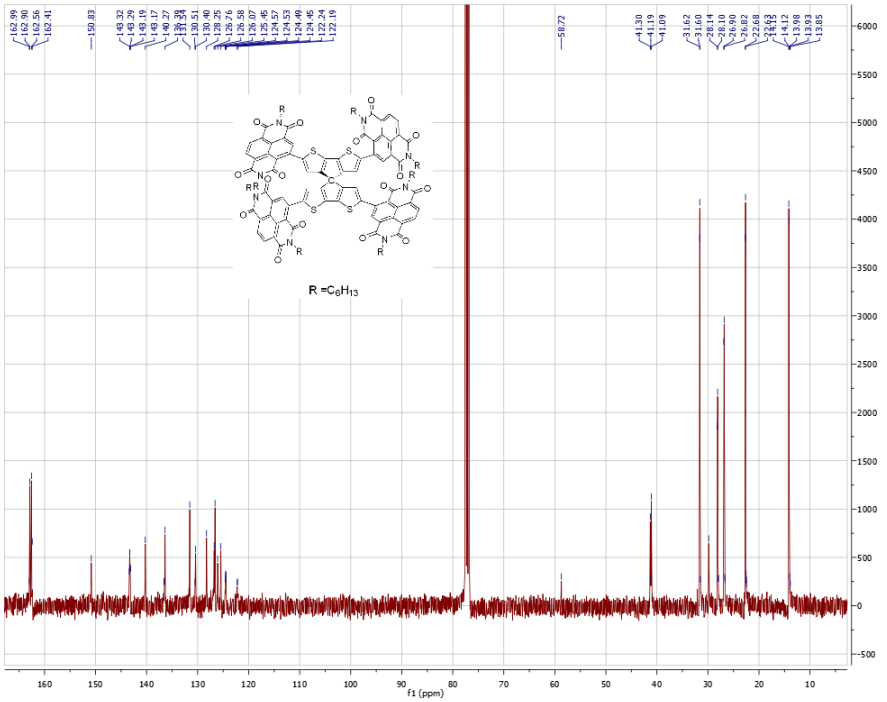

Figure A.2 $^{13}C\{^{1}H\}$ NMR spectrum of SCPDT-NDI_4 in $CDCl_3$.

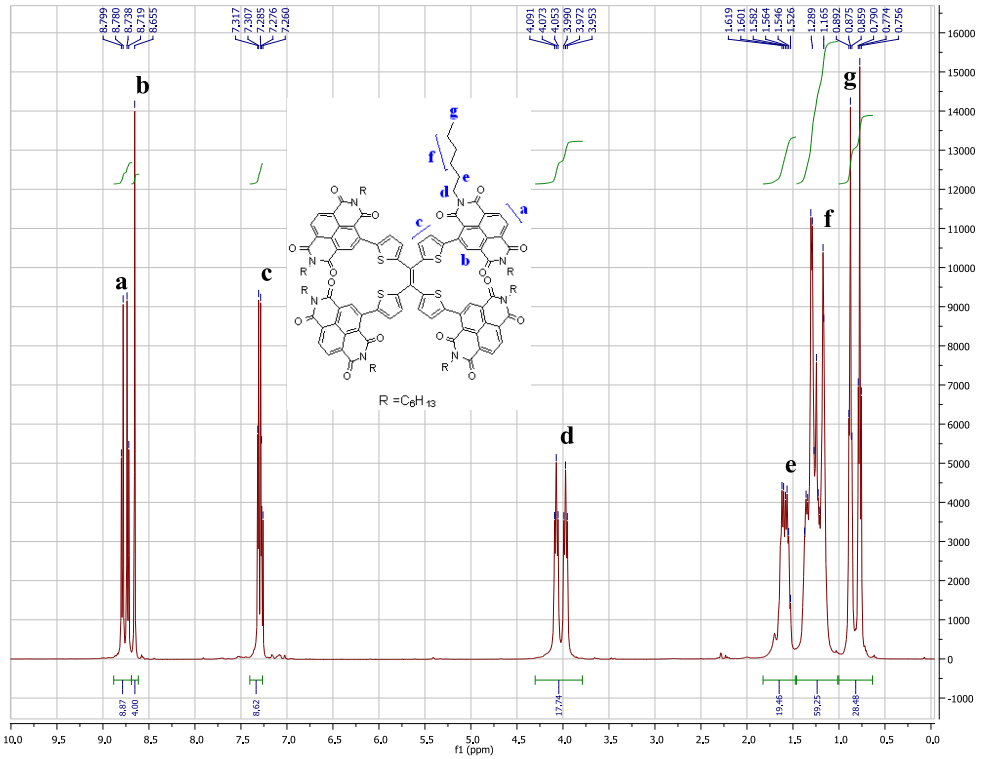

Figure A.3 ^{1}H NMR spectrum of TTE-NDI_4 in $CDCl_3$.

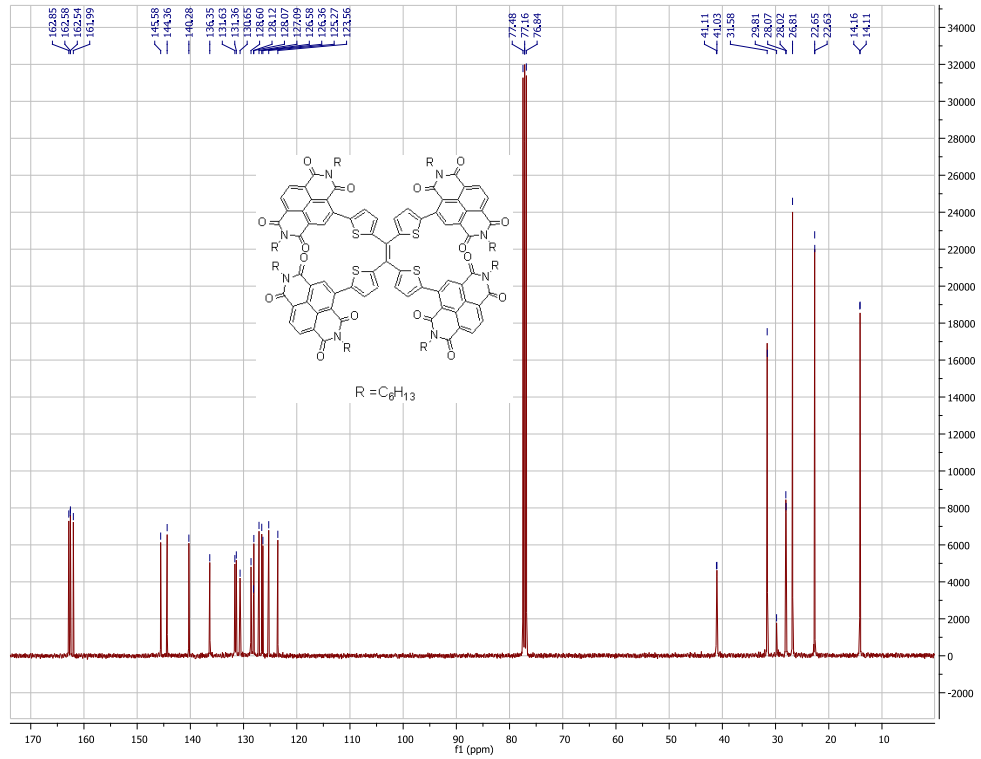

Figure A.4 $^{13}C\{^{1}H\}$ NMR spectrum of TTE-NDI_4 in $CDCl_3$.

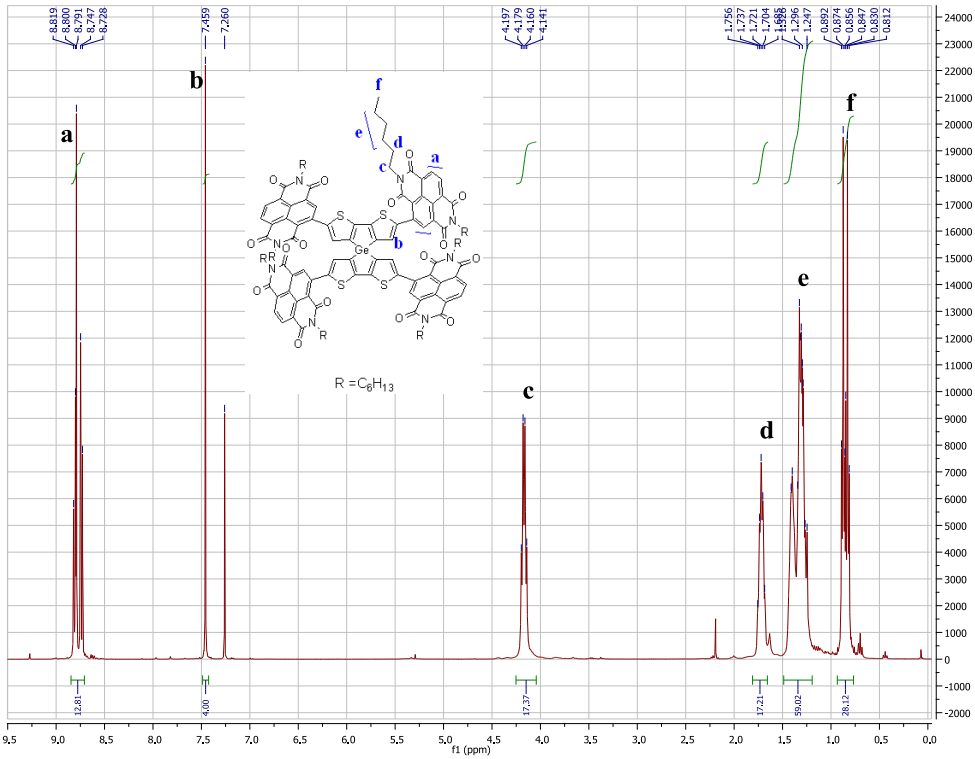

Figure A.5 ^{1}H NMR spectrum of SDTG-NDI_4 in $CDCl_3$.

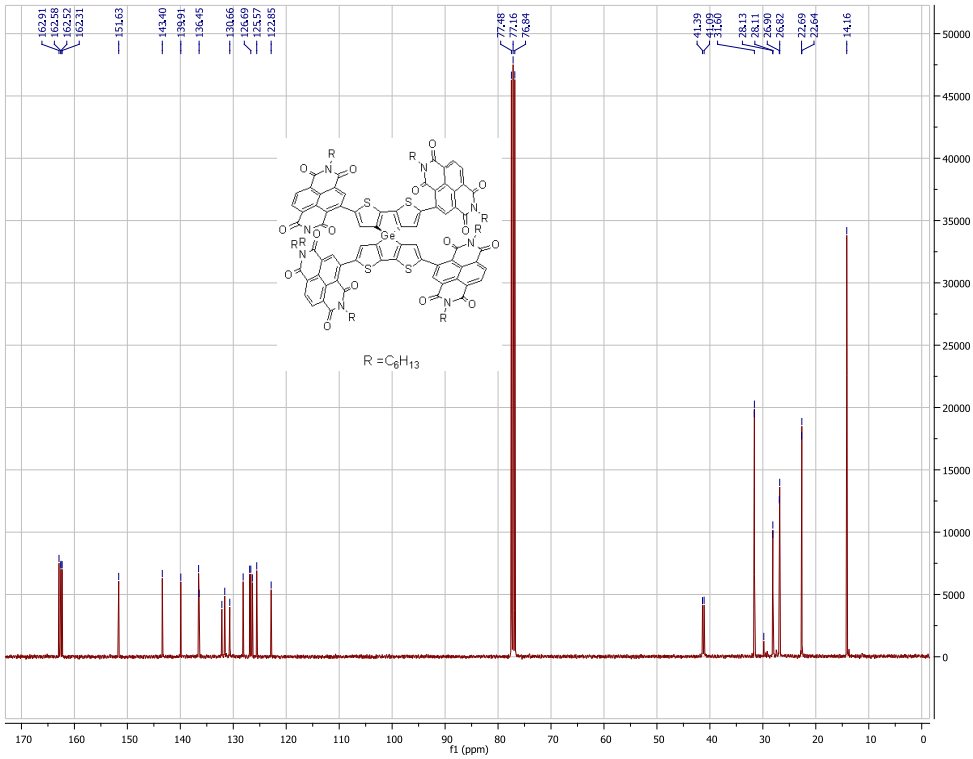

Figure A.6 $^{13}C\{^{1}H\}$ NMR spectrum of SDTG-NDI_4 in $CDCl_3$.

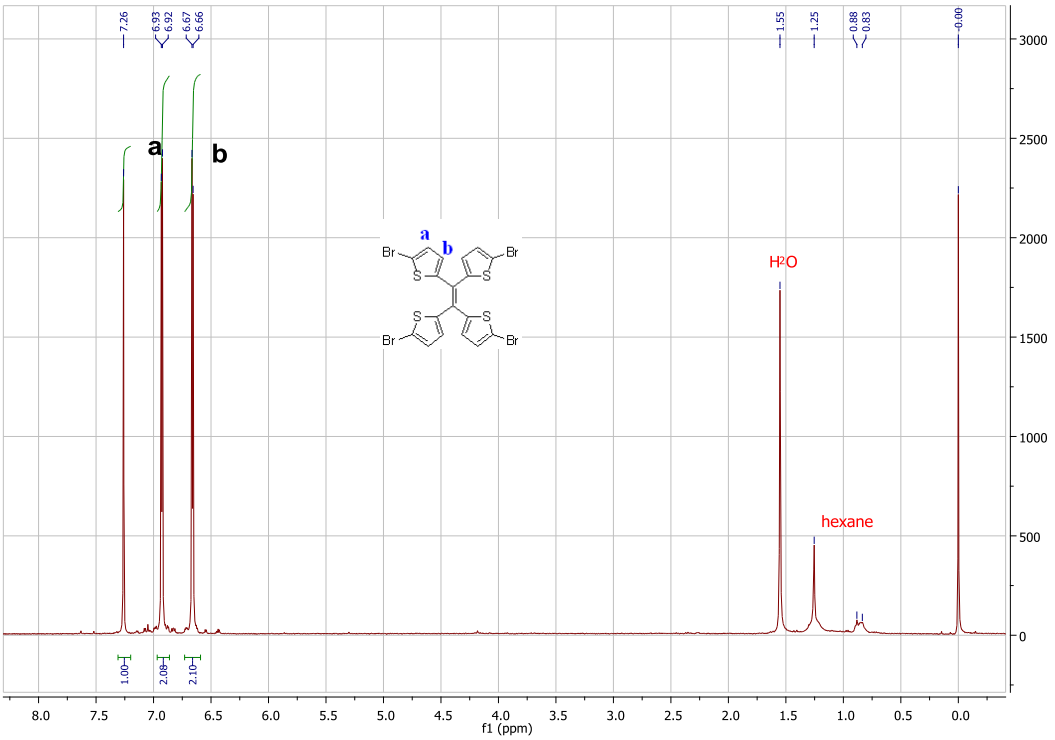

Figure A.7 ^{1}H NMR spectrum of TTE-Br_4 in $CDCl_3$.

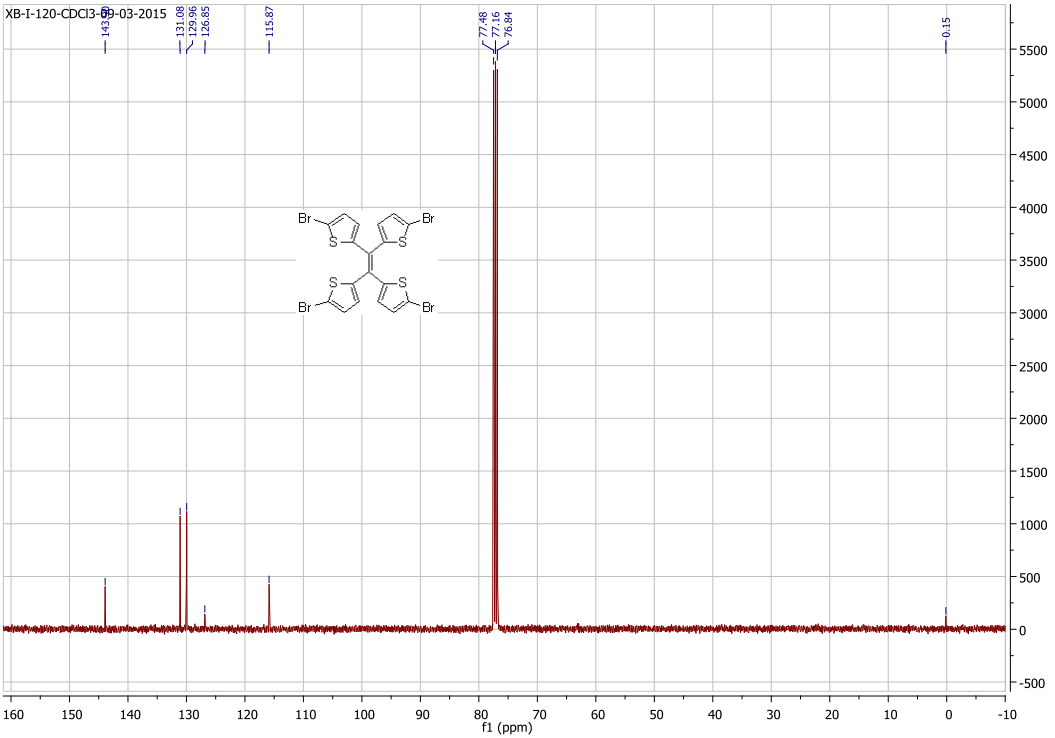

Figure A.8 $^{13}C\{^{1}H\}$ NMR spectrum of TTE-Br_4 in $CDCl_3$.

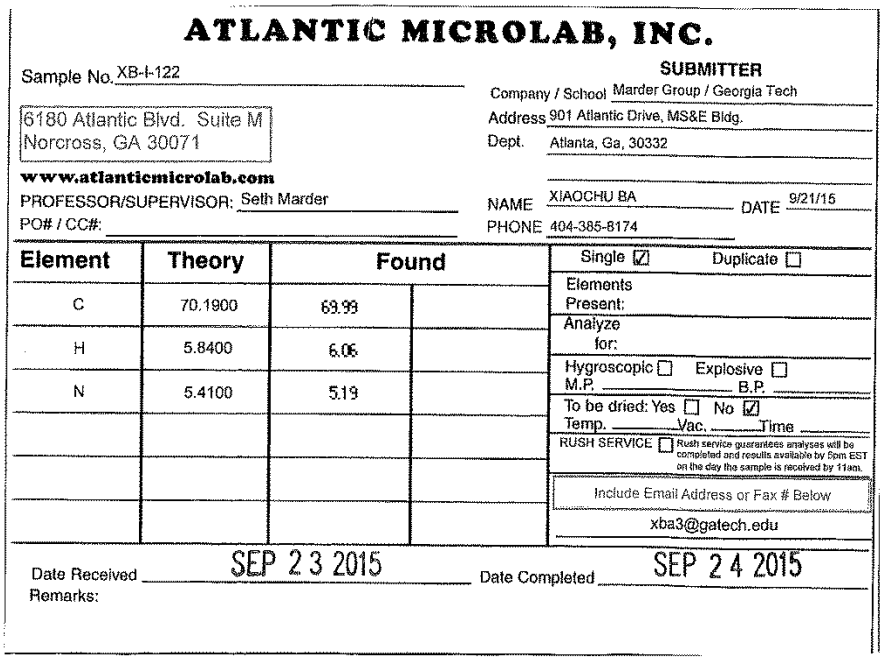

ATLANTIC MICROLAB, INC.

Sample No. XB-I-122

6180 Atlantic Blvd. Suite M
Norcross, GA 30071

www.atlanticmicrolab.com

PROFESSOR/SUPERVISOR: Seth Marder

PO# / CC#:

SUBMITTER

Company / School: Marder Group / Georgia Tech

Address: 901 Atlantic Drive, MS&E Bldg.

Dept.: Atlanta, Ga, 30332

NAME: XIAOCHU BA DATE: 9/21/15

PHONE: 404-385-8174

Element	Theory	Found	
C	70.1900	69.99	
H	5.8400	6.06	
N	5.4100	5.19	

Single ☑ Duplicate ☐

Elements Present:

Analyze for:

Hygroscopic ☐ Explosive ☐

M.P. B.P.

To be dried: Yes ☐ No ☑

Temp. Vac. Time

RUSH SERVICE ☐ Rush service guarantees analyses will be completed and results available by 5pm EST on the day the sample is received by 11am.

Include Email Address or Fax # Below

xba3@gatech.edu

Date Received SEP 23 2015 Date Completed SEP 24 2015

Remarks:

Figure A.9 Elemental analysis results of SCPDT-NDI_4.

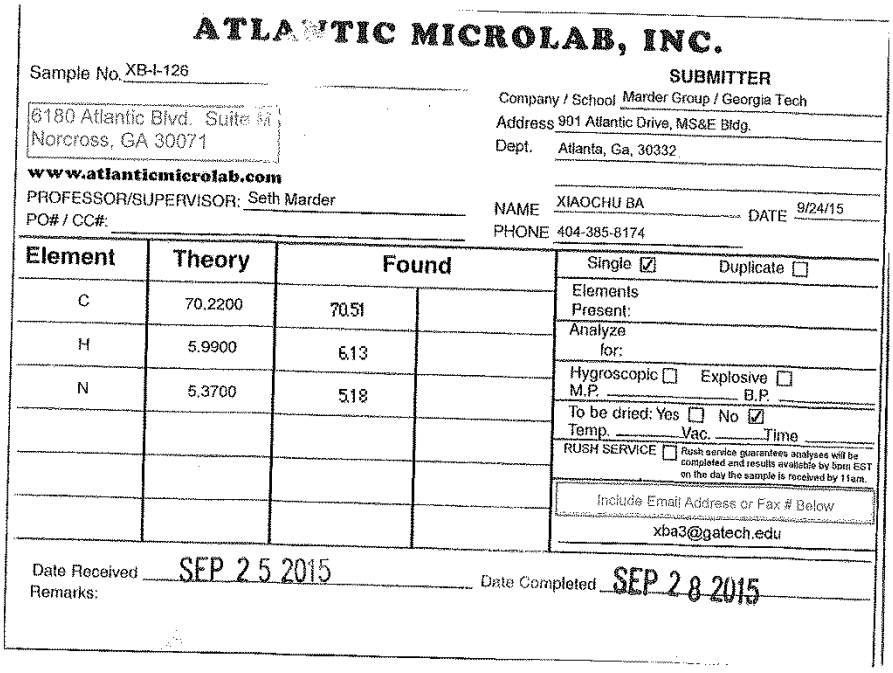

ATLANTIC MICROLAB, INC.

Sample No. XB-I-126

6180 Atlantic Blvd. Suite M
Norcross, GA 30071

www.atlanticmicrolab.com

PROFESSOR/SUPERVISOR: Seth Marder

PO# / CC#:

SUBMITTER

Company / School: Marder Group / Georgia Tech

Address: 901 Atlantic Drive, MS&E Bldg.

Dept.: Atlanta, Ga, 30332

NAME: XIAOCHU BA DATE: 9/24/15

PHONE: 404-385-8174

Element	Theory	Found	
C	70.2200	70.51	
H	5.9900	6.13	
N	5.3700	5.18	

Single ☑ Duplicate ☐

Elements Present:

Analyze for:

Hygroscopic ☐ Explosive ☐

M.P. B.P.

To be dried: Yes ☐ No ☑

Temp. Vac. Time

RUSH SERVICE ☐ Rush service guarantees analyses will be completed and results available by 5pm EST on the day the sample is received by 11am.

Include Email Address or Fax # Below

xba3@gatech.edu

Date Received SEP 25 2015 Date Completed SEP 28 2015

Remarks:

Figure A.10 Elemental analysis results of TTE-NDI_4.

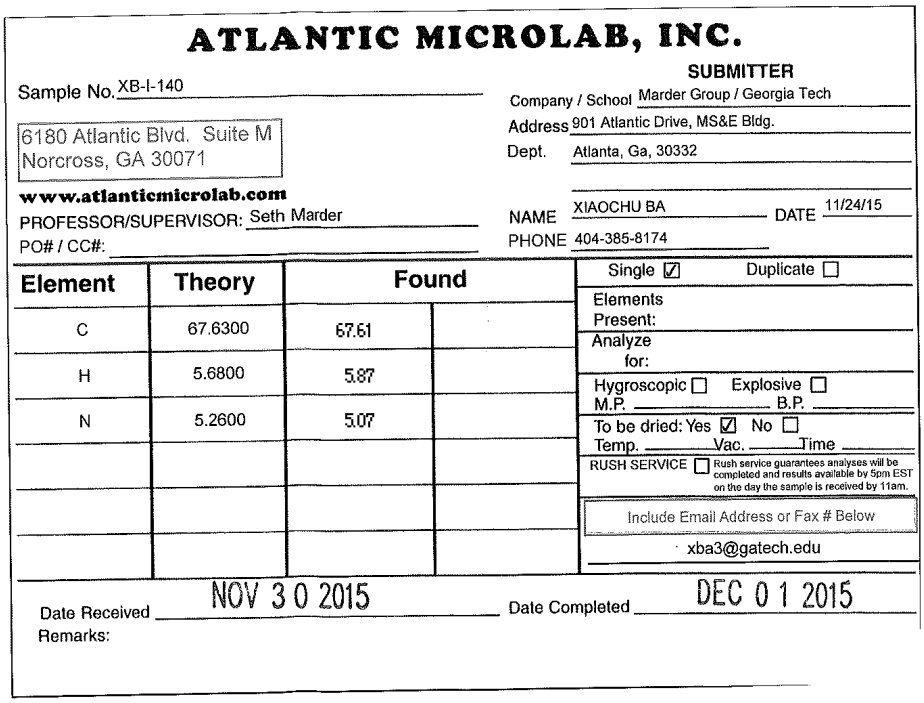

ATLANTIC MICROLAB, INC.

Sample No. XB-I-140

6180 Atlantic Blvd. Suite M
Norcross, GA 30071

www.atlanticmicrolab.com

PROFESSOR/SUPERVISOR: Seth Marder

PO# / CC#:

SUBMITTER

Company / School: Marder Group / Georgia Tech

Address: 901 Atlantic Drive, MS&E Bldg.

Dept. Atlanta, Ga, 30332

NAME: XIAOCHU BA DATE: 11/24/15

PHONE: 404-385-8174

Element	Theory	Found	
C	67.6300	67.61	
H	5.6800	5.87	
N	5.2600	5.07	

Single ☑ Duplicate ☐

Elements Present:

Analyze for:

Hygroscopic ☐ Explosive ☐

M.P. _____ B.P. _____

To be dried: Yes ☑ No ☐

Temp. _____ Vac. _____ Time _____

RUSH SERVICE ☐ Rush service guarantees analyses will be completed and results available by 5pm EST on the day the sample is received by 11am.

Include Email Address or Fax # Below

xba3@gatech.edu

Date Received NOV 3 0 2015 Date Completed DEC 0 1 2015

Remarks:

Figure A.11 Elemental analysis results of SDTG-NDI$_4$.

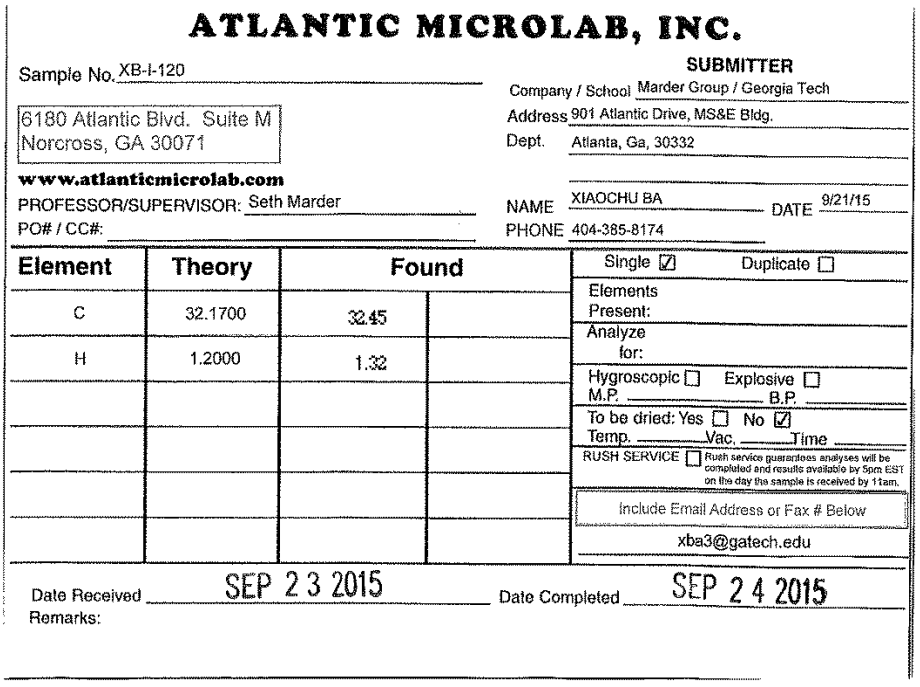

ATLANTIC MICROLAB, INC.

Sample No. XB-I-120

6180 Atlantic Blvd. Suite M
Norcross, GA 30071

www.atlanticmicrolab.com

PROFESSOR/SUPERVISOR: Seth Marder

PO# / CC#:

SUBMITTER

Company / School: Marder Group / Georgia Tech

Address: 901 Atlantic Drive, MS&E Bldg.

Dept. Atlanta, Ga, 30332

NAME: XIAOCHU BA DATE: 9/21/15

PHONE: 404-385-8174

Element	Theory	Found	
C	32.1700	32.45	
H	1.2000	1.32	

Single ☑ Duplicate ☐

Elements Present:

Analyze for:

Hygroscopic ☐ Explosive ☐

M.P. _____ B.P. _____

To be dried: Yes ☐ No ☑

Temp. _____ Vac. _____ Time _____

RUSH SERVICE ☐ Rush service guarantees analyses will be completed and results available by 5pm EST on the day the sample is received by 11am.

Include Email Address or Fax # Below

xba3@gatech.edu

Date Received SEP 2 3 2015 Date Completed SEP 2 4 2015

Remarks:

Figure A.12 Elemental analysis results of TTE-Br$_4$.

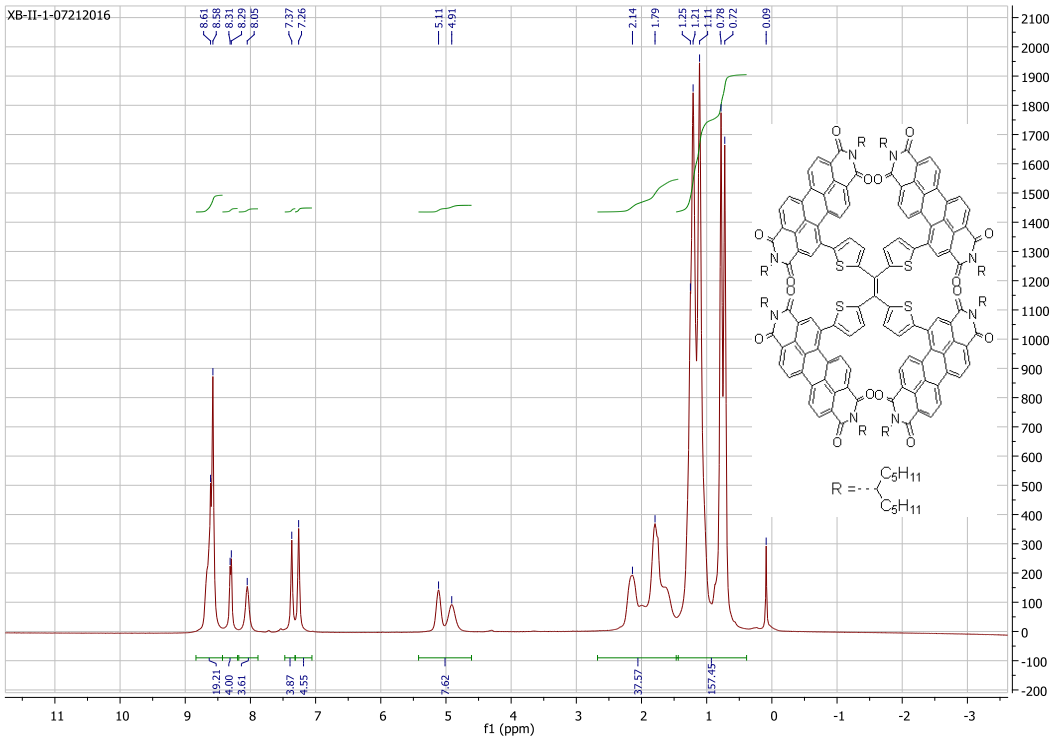

Figure A.13 ^{1}H NMR spectrum of TTE-PDI$_4$ in $CDCl_3$.

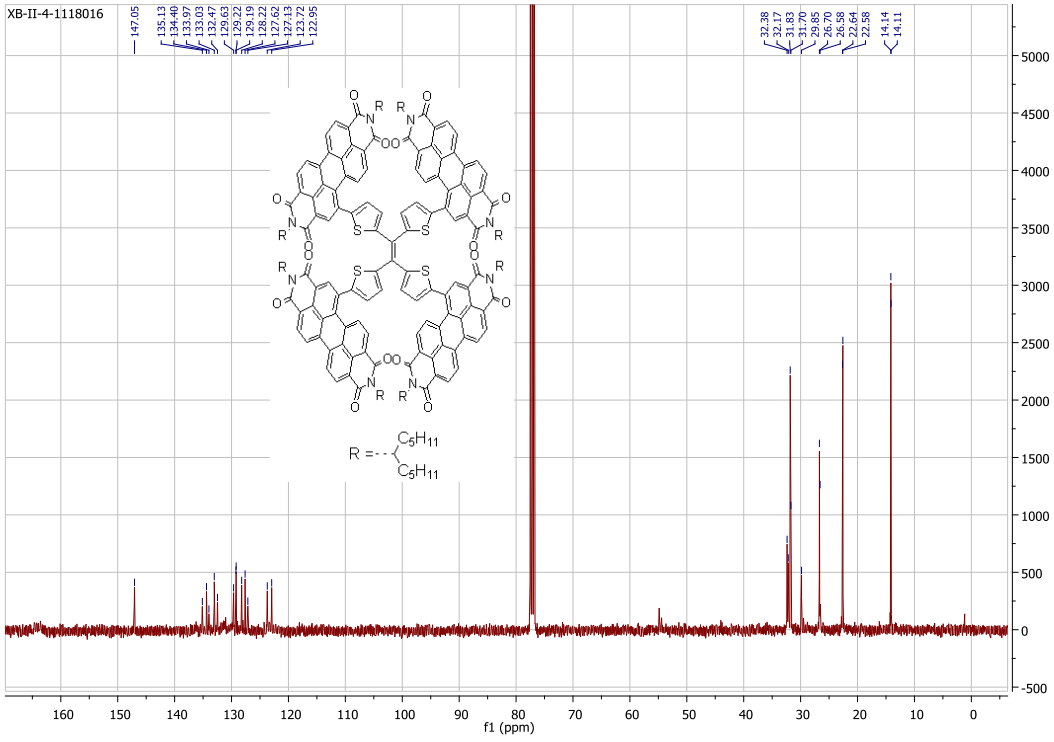

Figure A.14 $^{13}C\{^{1}H\}$ NMR spectrum of TTE-PDI$_4$ in $CDCl_3$.

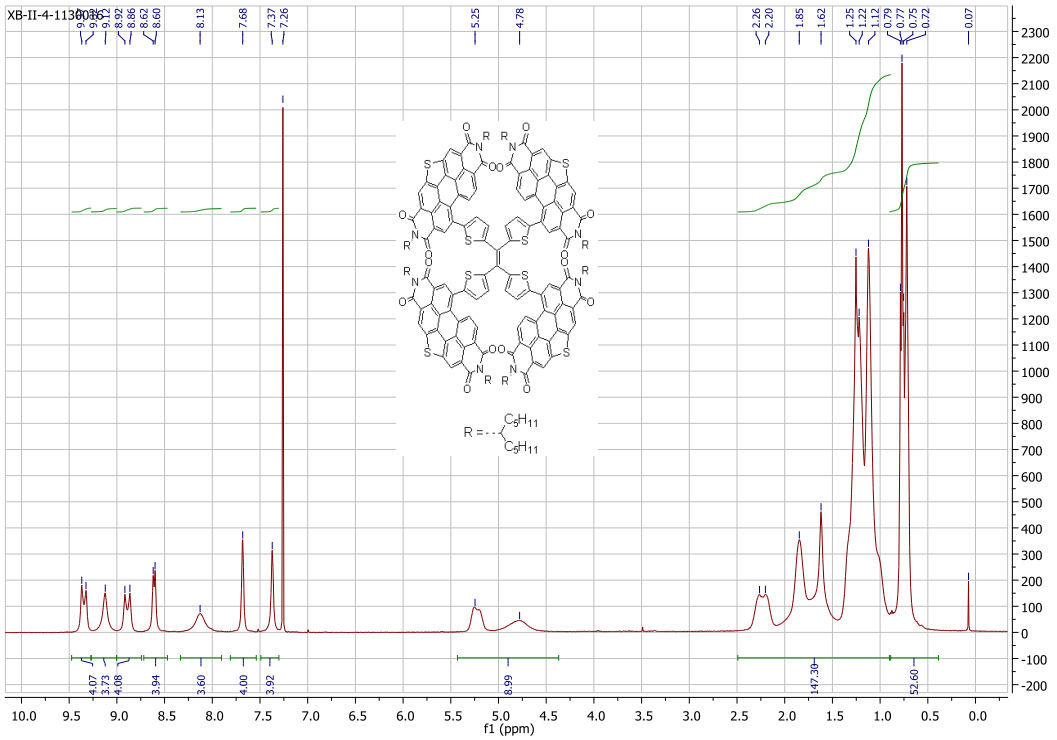

Figure A.15 ^{1}H NMR spectrum of TTE-PDIS$_4$ in $CDCl_3$.

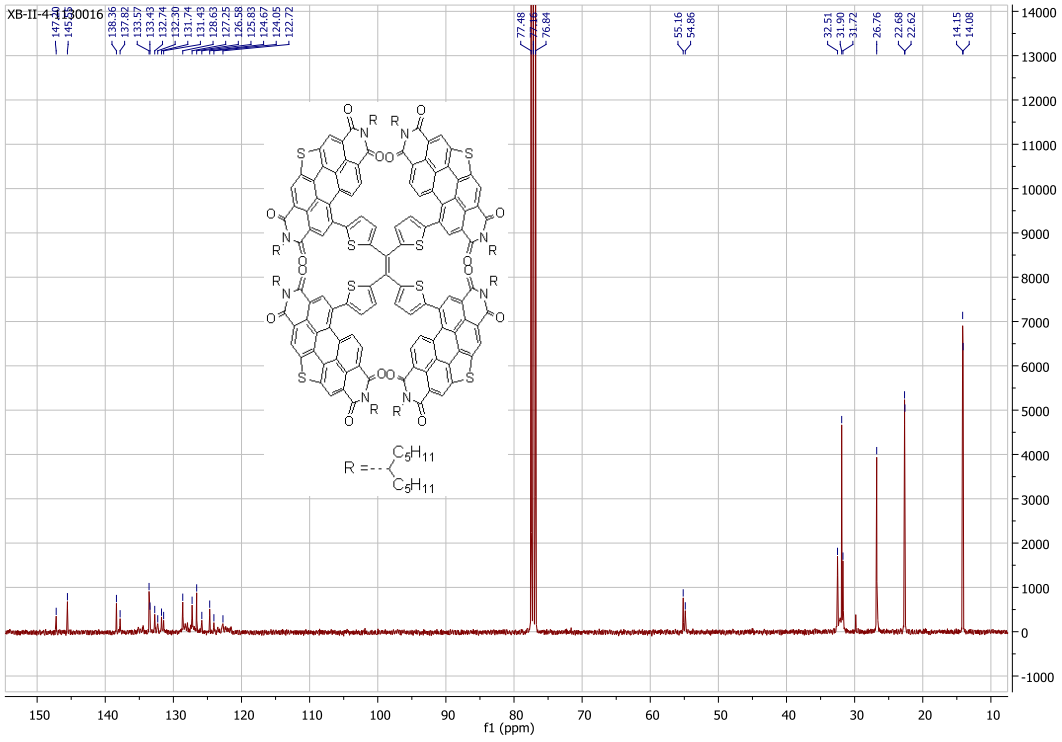

Figure A.16 $^{13}C\{^{1}H\}$ NMR spectrum of TTE-PDIS$_4$ in $CDCl_3$.

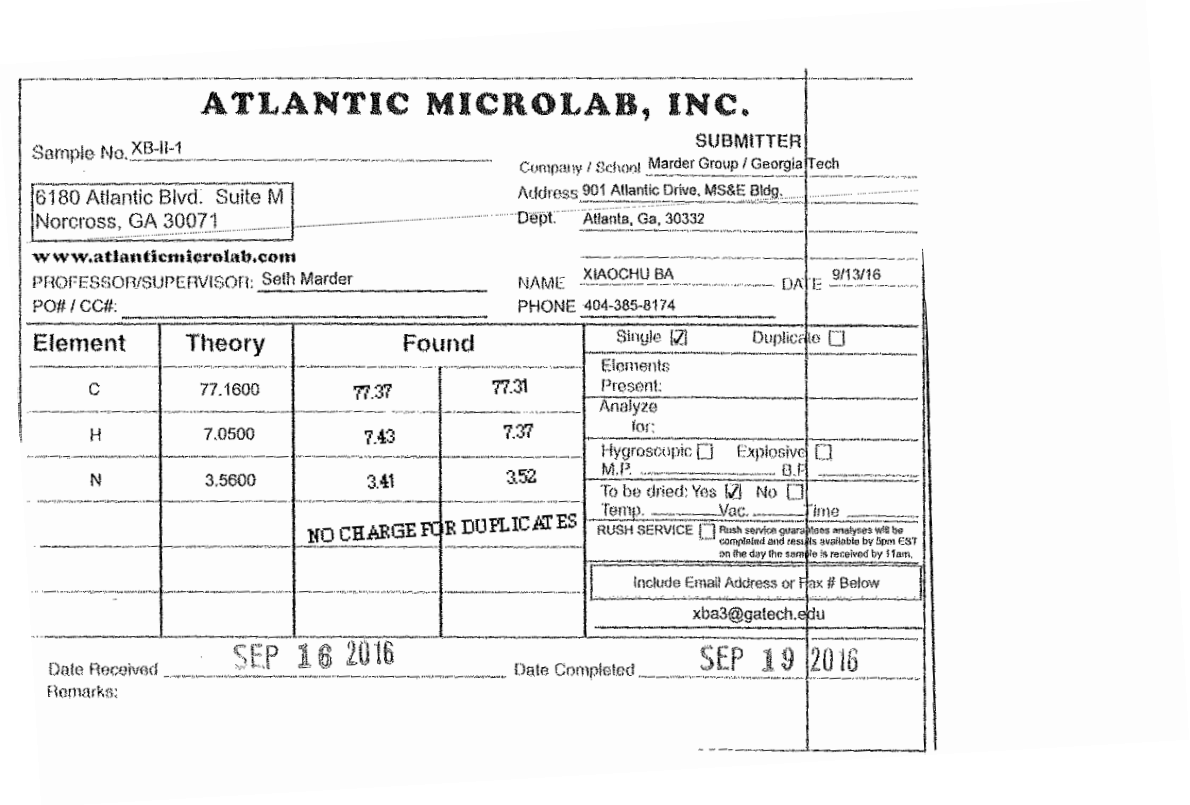

ATLANTIC MICROLAB, INC.

Sample No. XB-II-1

6180 Atlantic Blvd. Suite M
Norcross, GA 30071

www.atlanticmicrolab.com

PROFESSOR/SUPERVISOR: Seth Marder

PO# / CC#:

SUBMITTER

Company / School: Marder Group / Georgia Tech

Address: 901 Atlantic Drive, MS&E Bldg.

Dept.: Atlanta, Ga, 30332

NAME: XIAOCHU BA DATE: 9/13/16

PHONE: 404-385-8174

Element	Theory	Found	
C	77.1600	77.37	77.31
H	7.0500	7.43	7.37
N	3.5600	3.41	3.52
		NO CHARGE FOR DUPLICATES	

Single ☑ Duplicate ☐

Elements Present:

Analyze for:

Hygroscopic ☐ Explosive ☐

M.P. B.P.

To be dried: Yes ☑ No ☐

Temp. Vac. Time

RUSH SERVICE ☐ Rush service guarantees analyses will be completed and results available by 5pm EST on the day the sample is received by 11am.

Include Email Address or Fax # Below

xba3@gatech.edu

Date Received: SEP 16 2016 Date Completed: SEP 19 2016

Remarks:

Figure A.17 Elemental analysis results of TTE-PDI_4.

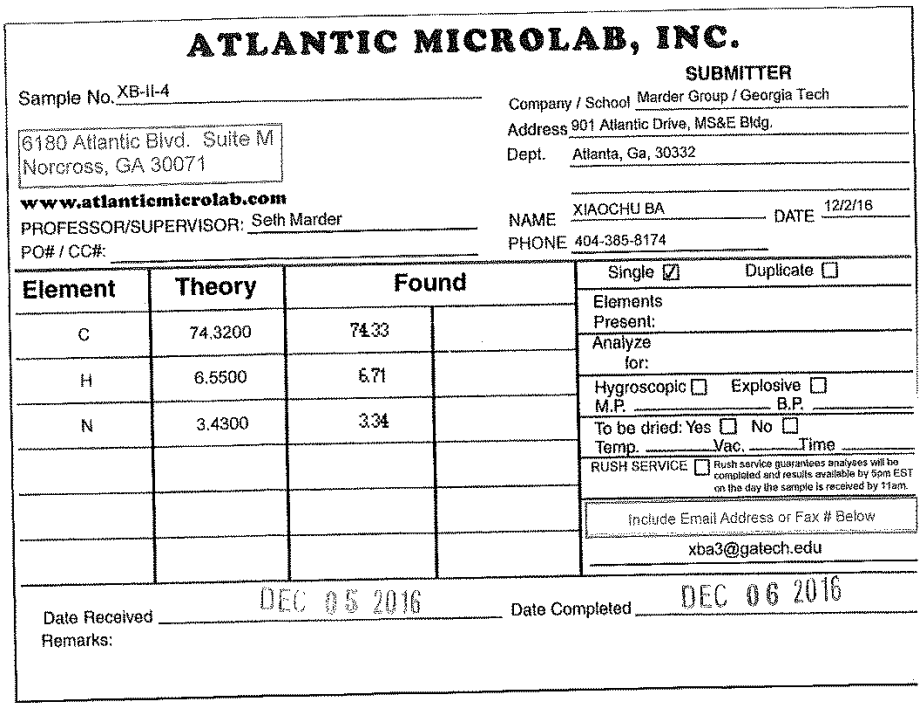

ATLANTIC MICROLAB, INC.

Sample No. XB-II-4

6180 Atlantic Blvd. Suite M
Norcross, GA 30071

www.atlanticmicrolab.com

PROFESSOR/SUPERVISOR: Seth Marder

PO# / CC#:

SUBMITTER

Company / School: Marder Group / Georgia Tech

Address: 901 Atlantic Drive, MS&E Bldg.

Dept.: Atlanta, Ga, 30332

NAME: XIAOCHU BA DATE: 12/2/16

PHONE: 404-385-8174

Element	Theory	Found	
C	74.3200	74.33	
H	6.5500	6.71	
N	3.4300	3.34	

Single ☑ Duplicate ☐

Elements Present:

Analyze for:

Hygroscopic ☐ Explosive ☐

M.P. B.P.

To be dried: Yes ☐ No ☐

Temp. Vac. Time

RUSH SERVICE ☐ Rush service guarantees analyses will be completed and results available by 5pm EST on the day the sample is received by 11am.

Include Email Address or Fax # Below

xba3@gatech.edu

Date Received: DEC 05 2016 Date Completed: DEC 06 2016

Remarks:

Figure A.18 Elemental analysis results of TTE-$PDIS_4$.

REFERENCES

1. Brédas, J. -L.; Norton, J. E.; Cornil, J.; Coropceanu, V. *Acc. Chem. Res*. **2009**, 4*2*, 1691.
2. Kippelen, B.; Brédas, J. -L. *Energy Environ. Sci*. **2009**, *2*, 251.
3. Morteani, A. C.; Sreearunothai, P.; Herz, L. M.; Friend, R. H.; Silva, C. *Phys. Rev. Lett*. **2004**, *104*, 247402.
4. Yu, G.; Gao, J.; Hummelen, J. C.; Wudl, F.; Heeger, A. J. *Science*. **1995**, *70*, 1789.
5. Scharber, M. C.; Sariciftci, N. S. *Prog. Polym. Sci.* **2013**, *38*, 1929.
6. Photovoltaic Education Network. http:// http://pveducation.org (accessed Sep 18, 2016).
7. National Instruments. Part II – Photovoltaic Cell I-V Characterization Theory and LabVIEW Analysis Code. http://www.ni.com/white-paper/7230/en (accessed Sep 18, 2016).
8. Lu, L.; Zheng, T.; Wu, Q.; Schneider, A. M.; Zhao, D.; Yu, L. *Chem. Rev*. **2015**, *115*, 12666.
9. Tang, C. W. *Appl. Phys. Lett*. **1986**, *48*, 183.
10. Nunzi, J. –M. *C. R. Phys*. **2002**, *3*, 523.
11. Son, H. J.; He, F.; Carsten, B.; Yu, L. *J. Mater. Chem*. **2011**, *21*, 18934.
12. Thompson, B. C.; Kim, Y. –G.; McCarley, T. D.; Reynolds, J. R. *J. Am. Chem. Soc*. **2006**, *128*, 12714.
13. Holliday, S.; Ashraf, R. S.; Wadsworth, A.; Baran, D.; Yousaf, S. A.; Nielsen, C. B.; Tan, C. –H.; Dimitrov, S. D.; Shang, Z.; Gasparini, N.; Alamoudi, M.; Laquai, F.; Brabec, C. J.; Salleo, A.; Durrant, J. R.; Nelson, J.; McCulloch, I. *Nat. Commun*. **2016**, *7*, 11585.
14. Kim, J. Y.; Kim, S. H.; Lee, H. H.; Lee, K.; Ma, W.; Gong, X.; Heeger, A. J. *Adv. Mater.* **2006**, *18*, 572.
15. Aernouts, T.; Aleksandrov, T.; Girotto, C.; Genoe, J.; Poortmans, J. *Appl. Phys. Lett.* **2008**, *92*, 033306.

16. Hoth, C. N.; Steim, R.; Schilinsky, P.; Choulis, S. A.; Tedde, S. F.; Hayden, O.; Brabec, C. J. *Org. Electron*. **2009**, *10*, 587.

17. Roncali, J. *Macromol. Rapid Commun*. **2007**, *28*, 1761.

18. Zhao, G.; He, Y.; Li, Y. *Adv. Mater*. **2010**, *22*, 4355.

19. Amb, C. M.; Chen, S.; Graham, K. R.; Subbiah, J.; Small, C. E.; So, F.; Reynolds, J. R. *J. Am. Chem. Soc*. **2011**, *133*, 10062.

20. Gupta, V.; Lai, L. F.; Datt, R.; Chand, S.; Heeger, A. J.; Bazan, G. C.; Singh, S. P. *Chem. Commun*. **2016**, *52*, 8596.

21. Liang, Y.; Feng, D.; Wu, Y.; Tsai, S. –T.; Li, G.; Ray, C.; Yu, L. *J. Am. Chem. Soc*. **2009**, *131*, 7792.

22. Chen, H. –Y.; Hou, J.; Zhang, S.; Liang, Y.; Yang, G.; Yang, Y.; Yu, L.; Wu, Y.; Li, G. *Nat. Photonics* **2009**, *3*, 649.

23. Guo, J.; Liang, Y.; Szarko, J.; Lee, B.; Son, H. J.; Rolczynski, B. S.; Yu, L.; Chen, L. X. *J. Phys. Chem. B* **2010**, *114*, 742.

24. Yu, L.; Liang, Y.; He, F. Semiconducting polymers. Google Patents: 2013; p WO2013116643A1.

25. Liu, Y.; Zhao, J.; Li, Z.; Mu, C.; Ma, W.; Hu, H.; Jiang, K.; Lin, H.; Ade, H.; Yan, H. *Nat. Commun*. **2014**, *5*, 5293.

26. Liu, X.; Sun, Y.; Perez, L. A.; Wen, W.; Toney, M. F.; Heeger, A. J.; Bazan, G. C. *J. Am. Chem. Soc*. **2012**, *134*, 20609.

27. Sariciftci, N. S.; Smilowitz, L.; Heeger, A. J.; Wudl, F. *Science*. **1992**, *258*, 1474.

28. Wong, H. C.; Li, Z.; Tan, C. H.; Zhong, H.; Huang, Z.; Bronstein, H.; McCulloch, I.; Cabral, J. T.; Durrant, J. R. *ACS Nano*. **2014**, *8(2)*, 1297.

29. Thompson, B. C. PhD. Dissertation, University of Florida, 2005.

30. Chochos, C. L.; Tagmatarchis, N.; Gregoriou, V. G. *RSC Adv*. **2013**, *3*, 7160.

31. Popesce, L. M.; Van Hof, P.; Sieval, A. B.; Jonkman, H. T.; Hummelen, J. C. *Appl. Phys. Lett*. **2006**, *89*, 213507.

32. Zhang, Y.; Yip, H. –L.; Acton, O.; Hau, S. K.; Huang, F. Jen, A. K. -Y. *Chem. Mater*. **2009**, *21*, 2598.

33. Meng, X.; Zhang, W.; Tan, Z.;; Du, C.; Li, C.; Bo, Z.; Li, Y.; Yang, X.; Zhen, M.; Jiang, F.; Zheng, J.; Wang, T.; Jiang, L.; Shu, C.; Wang, C. *Chem. Commun*, **2012**, *48*, 425.

34. Zhao, W.; Qian, D.; Zhang, S.; Li, S.; Inganäs, O.; Gao, F.; Hou, J. *Adv*. *Mater*. **2016**, *28*, 4734.

35. Meng, D.; Fu, H.; Xiao, C.; Meng, X.; Winands, T.; Ma, W.; Wei, W.; Fan, B.; Huo, L.; Doltsinis, N. L.; Li, Y.; Sun, Y.; Wang, Z. *J*. *Am*. *Chem*. *Soc*. DOI: 10.1021/jacs.6b04368.

36. Lin, Y.; He, Q.; Zhao, F.; Huo, L.; Mai, J.; Lu, X.; Su, C-J.; Li, T.; Wang, J.; Zhu, J.; Sun, Y.; Wang, C.; Zhan, X. *J*. *Am*. *Chem*. *Soc*. **2016**, *138*, 2973.

37. Zhong, Y.; Trinh, M. T.; Chen, R.; Purdum, G. E.; Khlyabich, P. P.; Sezen, M.; Oh, S.; Zhu, H.; Fowler, B.; Zhang, B.; Wang, W.; Nam, C. Y.; Sfeir, M. Y.; Black, C. T.; Steigerwald, M. L.; Loo, Y. L.; Ng, F.; Zhu, X. –Y.; Nuckolls, C. *Nat*. *Commun*. **2015**, *6*, 8242.

38. Lin, Y.; Wang, J.; Zhang, Z. G.; Bai, H.; Li, Y,; Zhu, D.; Zhan, X. *Adv*. *Mater*. **2015**, *27*, 1170.

39. Holliday, S.; Ashraf, R. S.; Wadsworth, A.; Baran, D.; Nielsen, C. B.; Yousaf, A.; Tan, C. –H.; Dimitrov, S. D.; Shang, Z.; Gasparini, N.; Brabec, C. J.; Salleo, A.; Durrant, J. R.; McCulloch, I. *Nat*. *Commun*. **2016**, *7*, 11585.

40. Douglas, J. D.; Chen, M. S.; Niskala, J. R.; Lee, O. P.; Yiu, A. T.; Young, E. P.; Fréchet, J. M. J. *Adv*. *Mater*. **2014**, *26*, 4313.

41. Jiang, W.; Ye, L.; Li, X.; Xiao, C.; Tan, F.; Zhao, W.; Hou, J.; Wang, Z. *Chem*. *Commun*. **2014**, *50*, 1024.

42. Zhong, Y.; Trinh, M. T.; Chen, R.; Purdum, G. E.; Khlyabich, P. P.; Sezen, M.; Oh, S.; Zhu, H.; Fowler, B.; Zhang, B.; Wang, W.; Nam, C. Y.; Sfeir, M. Y.; Black, C. T.; Steigerwald, M. L.; Loo, Y. L.; Ng, F.; Zhu, X. –Y.; Nuckolls, C. *Nat*. *Commun*. **2015**, *6*, 8242.

43. Anthony, J. E.; Facchetti, A.; Heeney, M.; Marder, S. R.; Zhan, X. *Adv. Mater.* 2010, *22*, 3876.

44. Yue, W.; Lv, A.; Gao, J.; Jiang, W.; Hao, L.; Li, C.; Li, Y.; Polander, L. E.; Barlow, S.; Hu, W.; Motta, S. D.; Negri, F.; Marder, S. R.; Wang, Z. *J. Am. Chem. Soc*. **2012**, *134*, 5770.

45. Polander, L. E.; Romanov, A. S.; Barlow, S.; Hwang, D. K.; Kippelen, B.; Timofeeva, T. V.; Marder, S. R. *Org*. *Lett*. **2012**, *14*, 918.

46. Hubner, C. G.; Ksenofontov, V.; Nolde, F.; Müllen, K.; Basché, T. *J*. *Chem*. *Phys*. **2004**, *120*, 10867.

47. Dittmer, J. J.; Marseglia, E. A.; Friend, R. H. *Adv*. *Mater*. **2000**, *12*, 1270.

48. Liu, Y.; Zhang, L.; Lee, H.; Wang, H-W.; Santala, A.; Liu, F.; Diao, Y.; Briseno, A. L.; Russell, T. P. *Adv*. *Energy Mater*. **2015**, *5*, 1500195.

49. Lee, J.; Singh, R.; Sin, D. H.; Kim, H. G.; Song, K. C.; Cho, K. *Adv*. *Mater*. **2016**, *28*, 69.

50. Liu, Y.; Mu, C.; Jiang, K.; Zhao, J.; Li, Y.; Zhang, L.; Li, Z.; Lai, J. Y. L.; Hu, H.; Ma, T.; Hu, R.; Yu, D.; Huang, X.; Tang, B. Z.; Yan, H. *Adv*. *Mater*. **2016**, *27*, 1015.

51. Liu, S-Y.; Wu, C-H.; Li, C-Z.; Liu, S-Q.; Wei, K-H.; Chen, H-Z.; Jen, A. K. –Y. *Adv*. *Sci*. **2015**, *2*, 1500014.

52. Amb, C. M.; Chen, S.; Graham, K. R.; Subbiah, J.; Small, C. E.; So, F.; Reynolds, J. R. *J. Am. Chem. Soc.* **2011**, *133*, 10062.

53. Gupta, V.; Lai, L. F.; Datt, R.; Chand, S.; Heeger, A. J.; Bazan, G. C.; Singh, S. P. *Chem. Commun*. **2016**, *52*, 8596.

54. Simmons, H. E.; Fukunaga, T. *J. Am. Chem. Soc*. **1967**, *89*, 5280.

55. Sweetnam, S.; Graham, K. R.; Ngongang Ndjawa, G. O.; Heumüller, T.; Bartelt, J. A.; Burke, T. M.; Li, W.; You, W.; Amassian, A.; McGehee, M. D. *J. Am. Chem. Soc*. **2014**, *136(40)*, 14078.

56. Zhong, H.; Wu, C-H.; Li, C-Z.; Carpenter, J.; Chueh, C-C.; Chen, J-Y.; Ade, H.; Jen, A. K.-Y. *Adv. Mater*. **2016**, *28*, 951.

57. He, Y.; Li, Y. *Phys. Chem. Chem. Phys*. **2011**, *13*, 1970.

58. Coropceanu, V.; Cornil, J.; da Silva Filho, D. A.; Olivier, Y.; Silbey, R.; Brédas, J. –L. *Chem. Rev*. **2007**, *107*, 926.

59. Liao, L.; Dai, L. M.; Smith, A.; Durstock, M.; Lu, J. P.; Ding, J. F.; Tao, Y. *Macromolecules* **2007**, *40*, 9406.

60. Usta, H.; Lu, G.; Facchetti, A.; Marks, T. J. *J. Am. Chem. Soc*. **2006**, *128*, 9034.

61. Getmanenko, Y. A.; Tongwa, P.; Timofeeva, T. V.; Marder, S. R. *Org. Lett*. **2010**, *12*, 2137.

62. Wu, T.; Shi, J.; Li, C.; Song, J.; Xu, L.; Wang, H. *Org. Lett*. **2013**, *15*, 354.

63. Pozzi, G.; Orlandi, S.; Cavazzini, M.; Minudri, D.; Macor, L.; Otero, L.; Fungo, F. *Org. Lett*. **2013**, *15*, 4642.

64. Parker, T. and Marder, S. *Synthetic Methods in Organic Electronic and Photonic Materials: A Practical Guide*, 1st ed.; The Royal Society of Chemistry, Thomas Graham House, Science Park, Milton Road: Cambridge, 2015.

65. Roquet, S.; Cravino, A.; Leriche, P.; Alévêque, O.; Frère, P.; Roncali, J. *J. Am. Chem. Soc.* **2006**, *128*, 3459.

66. Roncali, J. *Chem. Rev.* **1997**, *97*, 173.

67. Polander, L. E.; Tiwari, S. P.; Pandey, L.; Seifried, B. M.; Zhang, Q.; Barlow, S.; Risko, C.; Brédas, J-L.; Kippelen, B.; Marder, S. R. *Chem. Mater.* **2011**, *23*, 3408.

68. He, Y.; Li, Y. *Phys. Chem. Chem. Phys.* **2011**, *13*, 1970.

69. Xie, Q.; Perez-Cordero, E.; Echegoyen, L. *J. Am. Chem. Soc.* **1992**, *114*, 3978.

70. Allemand, P. M.; Koch, A.; Wudl, F.; Rubin, Y.; Diederich, F.; Alvarez, M. M.; Anz, S. J.; Whetten, R. L. *J. Am. Chem. Soc.* **1991**, *113*, 1050.

71. Lin, Y.; Wang, J.; Zhang, Z. G.; Bai, H.; Li, Y,; Zhu, D.; Zhan, X. *Adv. Mater.* **2015**, *27*, 1170.

72. Liu, Y.; Zhao, J.; Li, Z.; Mu, C.; Ma, W.; Hu, H.; Jiang, K.; Lin, H.; Ade, H.; Yan, H. *Nat. Commun.* **2014**, *5*, 5293.

73. Solanki, C. S. *Solar Photovoltaics: Fundamentals, Technologies And Applications*, 3rd ed.; PHI Learning Private Limited: Delhi, 2015.

74. Photovoltaic Education Network. http:// http://pveducation.org (accessed Sep 26, 2016).

75. Zhong, Y.; Trinh, M. T.; Chen, R.; Purdum, G. E.; Khlyabich, P. P.; Sezen, M.; Oh, S.; Zhu, H.; Fowler, B.; Zhang, B.; Wang, W.; Nam, C. Y.; Sfeir, M. Y.; Black, C. T.; Steigerwald, M. L.; Loo, Y. L.; Ng, F.; Zhu, X. –Y.; Nuckolls, C. *Nat. Commun.* **2015**, *6*, 8242.

76. Meng, D.; Fu, H.; Xiao, C.; Meng, X.; Winands, T.; Ma, W.; Wei, W.; Fan, B.; Huo, L.; Doltsinis, N. L.; Li, Y.; Sun, Y.; Wang, Z. *J. Am. Chem. Soc.* DOI: 10.1021/jacs.6b04368.

77. Wu, Q.; Zhao, D.; Schneider, A. M.; Chen, W.; Yu, L. *J. Am. Chem. Soc.* **2016**, *138*, 7248.

78. Sun, D.; Meng, D.; Cai, Y.; Fan, B.; Li, Y.; Jiang, W.; Huo, L.; Sun, Y.; Wang, Z. *J. Am.*

Chem. *Soc*. **2016**, *137*, 11156.

79. (a) Polander, L. E.; Getmanenko, Y. A.; Dasari, R. R.; Marder, S.; Hwang, D. K.; Kippelen, B.; Singh, S.; Shi, Q. Stannyl derivatives of naphthalene diimides and related compositions and methods. WO 2013096915 A1, June 27, 2013. (b) Huang, C.; Barlow, S.; Marder, S. R.; *J. Org. Chem. Soc*. **2011**, *76*, 2386.
80. Yue, W.; Lv, A.; Gao, J.; Jiang, W.; Hao, L.; Li, C.; Li, Y.; Polander, L. E.; Barlow, S.; Hu, W.; Motta, S. D.; Negri, F.; Marder, S. R.; Wang, Z. *J. Am. Chem. Soc*. **2012**, *134*, 5770.
81. Lee, J.; Singh, R.; Sin, D. H.; Kim, H. G.; Song, K. C.; Cho, K. *Adv*. *Mater*. **2016**, *28*, 69.
82. Photovoltaic Education Network. http:// http://pveducation.org (accessed Sep 18, 2016).
83. Sweetnam, S.; Graham, K. R.; Ngongang Ndjawa, G. O.; Heumüller, T.; Bartelt, J. A.; Burke, T. M.; Li, W.; You, W.; Amassian, A.; McGehee, M. D. *J*. *Am*. *Chem*. *Soc*. **2014**, *136(40)*, 14078.
84. Li, Z.; Jiang, K.; Yang, G.; Lai, J. Y. L.; Ma, T.; Zhao, J.; Ma, W.; Yan, H. *Nat*. *Commun*. **2016**, *7*, 13094.
85. Zang, Y.; Li, C. Z.; Chueh, C. C.; Williams, S. T.; Jiang, W.; Wang, Z. H.; Yu, J. S.; Jen, A. K. Y. *Adv*. *Mater*. **2014**, *26*, 5708.
86. Lee, C.; Kang, H.; Lee, W.; Kim, T.; Kim, K. H.; Woo, H. Y.; Wang, C.; Kim, B. J. *Adv*. *Mater*. **2015**, *27*, 2466.
87. Wu, C. H.; Chueh, C. C.; Xi, Y. Y.; Zhong, H. L.; Gao, G. P.; Wang, Z. H.; Pozzo, L. D.; Wen, T. C.; Jen, A. K. Y. *Adv*. *Funct*. *Mater*. **2015**, *25*, 5326.